Theoretical and Experimental Investigations of the Kerr Effect and Cotton-Mouton Effect

BY

ANGELA LOUISE JANSE VAN RENSBURG
B Sc Hons (UKZN)

Submitted in partial fulfilment of the requirements for the degree of Master of Science in the School of Physics University of KwaZulu-Natal

PIETERMARITZBURG
AUGUST 2008

Acknowledgements

I wish to express my sincere gratitude and appreciation to all those people who have assisted and supported me throughout this work. I would like to make special mention of the following people:

My supervisor, Dr V. W. Couling, for his constant assistance and encouragement. For all the extra time and effort he took in helping and guiding me during this work.

The staff of the Electronics Centre, in particular Mr G. Dewar, Mr A. Cullis and Mr J. Woodley for their endless assistance in maintaining, repairing and building the electronic apparatus used in this work.

The staff of the Mechanical Instrument Workshop for repairing and constructing components used in the experimental part of this work.

Mr K. Penzhorn and Mr R. Sivraman of the Physics Technical Staff for their help in accessing tools from the Physics Workshop. Also from the Physics Technical Staff, Mr A. Zulu for helping me move dewars of liquid nitrogen from the School of Chemistry to the School of Physics.

The National Laser Centre for providing a new laser for the experimental aspect of this work and for their interest in my work.

Mr N. Chetty, a fellow postgraduate student, for assisting in my learning of HP-Basic and Latex.

Finally, my family, my parents for financing all of my studies and for their constant support and encouragement. My husband, for always taking an interest in my work and for his encouraging support.

Declaration

This dissertation describes the work undertaken at the School of Physics, University of KwaZulu-Natal(Pietermaritzburg), under the supervision of Dr V. W. Couling between January 2006 and January 2008.

I declare the work reported in this dissertation to be my own research, unless specifically indicated to the contrary in the text. This thesis has not been submitted in any form for any degree or examination to any other university.

Signed: A Ronsborg.

On this 22nd day of December 2008

I hereby certify that this statement is correct

V. W. Couling

Dr V. W. Couling
(SUPERVISOR)

Abstract

Mr T. J. Sono, an MSc student during the period January 2001 to January 2003, developed an apparatus to measure the pressure and temperature dependence of the electric-field induced birefringence (or electro-optic Kerr effect) in gases. Mr Sono obtained experimental results for dimethyl ether at a wavelength of 632.8 nm resulting in polarizability tensor components, first and second Kerr hyperpolarizabilities, and second Kerr-effect virial coefficients for this particular molecular species.

One of the primary concerns of this thesis has been to obtain new measured Kerr-effect data for dimethyl ether and for trifluoromethane over a range of temperature. The cell has been calibrated using hydrogen as a primary standard, and has been carefully aligned to avoid multiple reflections of the incident laser beam off the closely-spaced electrode surfaces. The data has been analyzed to extract values of the polarizability anisotropy and the second Kerr hyperpolarizability for these molecules. In addition, precise values for the second Kerr-effect virial coefficients have been obtained from measurements of the Kerr effect a function of pressure.

The molecular-tensor theory of the second Kerr-effect virial coefficient B_K is reviewed. This theory describes the effects of intermolecular interactions on the molar Kerr constant, and it has been used to compute B_K for dimethyl ether and trifluoromethane over the experimental temperature range. Agreement between experiment and theory is generally good. B_K for ammonia has also been calculated, and compared to recent measured data found in the literature.

The theory of the Cotton-Mouton effect (the magnetic analogue of the Kerr-effect) in a dilute gas is reviewed, and a new molecular-tensor theory describing the effects of molecular pair-interactions is developed. Calculations for a test molecule, namely chloromethane, indicate that density-dependent effects for this molecule are extremely tiny (of the order of 1% for typical experimental pressures). This new theory could be profitably used in selecting molecules which might demonstrate a larger effect which might be more readily measured in the laboratory.

Contents

Chapter 1

Introduction and Aims

1.1 Introduction and the aims of this work

Molecular Optics has as its goals the experimental and theoretical determination of the electromagnetic properties of individual molecules. This can be achieved by experimentally investigating how light interacts with macroscopic samples of matter, and coupling such measurements with suitable molecular-tensor theories to relate the macroscopic observables to the property tensors of molecules in the sample.

Measurements of the electro-optic Kerr effect are an important tool in determining the electric properties of molecules (such as the polarizability and hyperpolarizabity tensors) which provide insight into the structure and charge distribution of molecules. It needs to be noted that in a gas sample the molecules cannot be treated as though they are independent systems as the presence of molecular interactions affect the bulk properties of the sample, modifying them from that of an ideal gas. Since these properties play an important role in the understanding of the intimate workings of molecules, the Kerr electro-optic effect is a useful technique in the fields of physics, chemistry and biology. The effects in gases are very small in comparison to those in liquids and solids and are difficult to measure with accuracy. This has led to a scarcity in experimental data in the case of gases.

The work described in this thesis was undertaken using the Kerr effect apparatus built during the MSc project of Mr T. Sono.[1] Ms A. Singh in her MSc

thesis verified the reproducibility of the measurements on the gas, dimethyl ether[2], as reported in Sono's thesis. Our aim has been to obtain new measurements for trifluoromethane in the temperature range 303 K to 473 K, as well as to study dimethyl ether over a temperature range extending down to 260K where previous measurements have failed[2]. In the event higher temperatures were also studied.

Our initial measurements for the gas dimethyl ether were not in good agreement with those of Sono[1] and Singh[2]. Changes in the calibration constants of any one or more of the following: the high-voltage power supply, the pressure transducer, the platinum thermistors or the Faraday cell could have resulted in the discrepancies in our measurements. Only once reproducibility was established were we able to move onto the study of trifluoromethane over a range of temperatures, and of dimethyl ether at a temperature of 260 K.

The investigation into the measurements of dimethyl ether at a temperature of 260 K took a significant amount of time since cooling the cell down to this temperature proved to be a challenging task. In addition, sample vapour pressures were so low that the measurable effect was small and unstable.

We now turn to a review of birefringence in the Kerr and Cotton-Mouton effects.

1.2 References

1. T. J. Sono, MSc thesis, University of Natal, 2003.

2. A. Singh, MSc thesis, University of KwaZulu-Natal, 2005.

Chapter 2

Review: Birefringence in the Kerr and Cotton-Mouton Effects

2.1 Introduction

Materials that are optically anisotropic have an index of refraction that varies with the propagation direction in the material.[1] These materials are referred to as being birefringent. The term birefringence defines the difference between refractive indices for two directions of light propagation and/or light polarization. Birefringences, also known as optical anisotropies, can occur when radiation impinges on matter in the presence of external electromagnetic fields.[2] An isolated isotropic medium without external fields does not exhibit birefringence. There are many different types of birefringence that can be observed; these depend on the state of polarization of the light, geometrical setup, symmetry of the sample subject to radiation and the type of external field.[2] The most common example of birefringence is linear birefringence. Linear birefringence occurs when polarized light interacts with a sample in the presence of an external electric field with a component perpendicular to the direction of propagation.[2] This is known as the Kerr effect. Birefringence is not only useful for the manipulation of polarized light but in the design of optical modulators and the use of nonlinear optics for harmonic generation.[1] The mathematics used to describe birefringence makes use of tensors.[1] This will be developed in the following chapters.

2.2 History of Birefringence

The first recorded observation of birefringence was made by Erasmus Bartholinus in 1669 with calcite. He believed that this phenomenon was a special case of refraction and therefore called the effect *double refraction.*[1]

In 1690 Huygens discovered that light passing through calcite could be extinguished by passing it through a second, specifically oriented, piece of calcite. He was however unable to explain the origin of these observations.[1]

It was accidentally that Ètienne Louis Malus in 1808 observed that two images of the sun produced by a piece of calcite would dim and brighten as the crystal was rotated. He termed this property of light *polarization*, relating the orientation of the preferred direction of light to the earth's poles. In 1817 Young suggested that light propagates as a transverse wave. Maxwell's theory was the final step in understanding the polarization properties of light.[1]

2.3 Induced Linear Birefringence

Induced Linear birefringence occurs when a static electric field E (Kerr effect) or a magnetic field H (Cotton-Mouton effect) or an electric field gradient ∇E (Buckingham effect) is applied with a component perpendicular to the direction of propagation of a probe beam. The difference between the refractive index for linearly polarized monochromatic light with polarization vector parallel ($n_{\|}$) and perpendicular ($n_{\perp}$) to the direction of the external field (or field gradient) is given as follows:[2]

$$\Delta n = n_{\|} - n_{\perp}. \tag{2.1}$$

The three different types of linear birefringence, namely the Kerr effect, Cotton-Mouton effect and Buckingham effect, are illustrated in figure 1. The externally applied field is represented by a bold arrow, whose direction in this case forms an angle θ with that of the polarization direction of the light beam. The directions defining $n_{\|}$ and $n_{\perp}$ are indicated.[2]

Linear birefringences can be estimated by measuring the ellipticity acquired by the polarized beam after passing through the sample. The anisotropy

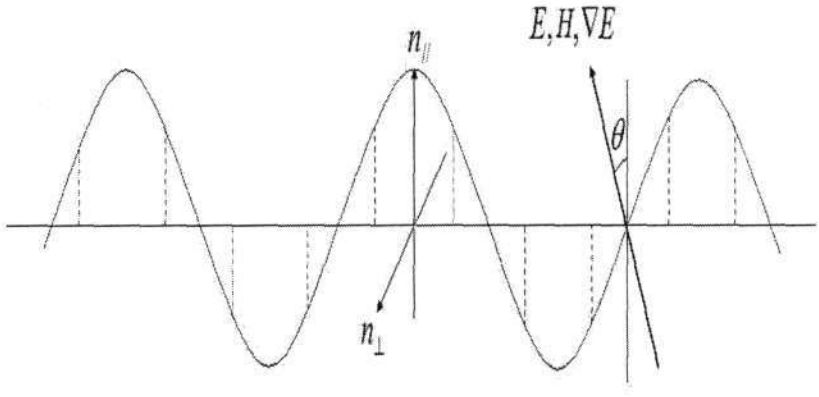

Figure 2.1: This diagram is reproduced from Birefringences: A Challenge for Both Theory and Experiment by Antonio Rizzo and Sonia Coriani, page 146[2]

of the refractive index induces a phase difference (ϕ) between the two perpendicular components of the polarization vector. This phase difference is given as follows:[2]

$$\phi = 2\pi \frac{l}{\lambda} \Delta n \sin 2\theta, \tag{2.2}$$

where l is the optical path length, λ is the wavelength of the beam and θ is the angle seen in figure 1.

2.4 Birefringence in the Kerr Effect

An optically isotropic substance when placed in a strong electric field becomes doubly refracting (i.e. birefringent). This effect was discovered in 1875 by Reverend John Kerr when he found that glass placed in a strong electric field becomes birefringent.[3,4] The glass when placed in an electric field behaved as if placed under mechanical tension in a direction parallel to the lines of force.The Kerr electro-optic effect is attributed to the alignment and distortion of molecules in the presence of an electric field. The Kerr constant K is determined by the following equation:[4]

$$n_{\|} - n_{\perp} = KE^2\lambda, \tag{2.3}$$

illustrating that the magnitude of the effect is found to be proportional to the strength of the electric field squared. $n_{\|}$ is the refractive index for light vibrating parallel to the direction of the applied electric field E, while $n_{\perp}$ is the refractive index for light vibrating perpendicular to the applied field.

2.5 Measuring the Birefringence Induced in a Medium

One must first define the initial polarization state of a probing light beam and be able to observe any changes in this polarization state after the light has propagated through the optically anisotropic (birefringent) medium.[5] The light source is usually a laser providing polarized, continuous, monochromatic radiation. A polarizer is used to improve the polarization quality of the beam. The orientation of the polarizer provides light linearly polarized at 45 degrees to the uniform applied field, E or H. The cell should be as long as possible so as to increase the induced phase difference and reduce the significance of end effects due to nonuniformities in the fields at the extremities. It would be advantageous for the beam to transverse the cell a number of times but the loss of polarization at each reflection needs to be considered.

To quantify the induced birefringence a useful technique is to use a nulling device or compensator. One type of compensator includes a quarter-wave plate and a Faraday cell. Such a compensator is used in this work. The compensator, in conjuction with the quarter-wave plate and Faraday cell, converts the induced phase difference ϕ into a rotation of the plane of polarization, $\phi/2$, which is then compensated by an equal but opposite rotation induced in the Faraday cell by the magnetic field. A photomultiplier tube or photodiode linked to a phase-sensitive detector is used as the detector.[5] Another typical type of compensator often used is an additional Kerr cell containing a standard reference fluid.

2.6 Field and Temperature Dependence

The field dependence of a given birefringence can be written in general terms as follows:[2]

$$\Delta n = w \times F_1^{n_1} F_2^{n_2} \times_m W(\lambda, T), \tag{2.4}$$

The second virial coefficient B_p for two spherical particles 1 and 2 is determined as follows:[2]

$$B_p = 4\pi N_A^2 \int_0^\infty [\frac{1}{2} p_{12}(R) - \frac{\overline{p}_1 + \overline{p}_2}{2}] exp(-\frac{V(R)}{kT}) R^2 dR, \qquad (2.8)$$

where R is the distance between particles 1 and 2, $V(R)$ is the interaction potential of the particles, and p_{12} is the property p of the couple formed by the two particles.

2.8 References

1. R. Guenther, *Modern Optics*, New York, John Wiley and Sons, 1990, 521-522.

2. A. Rizzo and S. Coriani, *Advances in Quantum Chemistry*, 2005, **50**, 144-147,149,157.

3. K. D. Moller, *Optics*, New Jersey, University Science Books, 1998.

4. G. R. Fowles, *Introduction to Modern Optics*, New York, Holt, Rinehart and Winston, 1968, 191-192.

5. M. Evans and S. Kielich, *Modern Nonlinear Optics* part 2, New York, John Wiley and Sons, 1993, 361-414.

6. A. Singh, MSc thesis, University of KwaZulu-Natal, 2005.

Chapter 3

Theory of the Cotton-Mouton Effect

3.1 Introduction

The Cotton-Mouton effect is the magnetic analogue of the Kerr electro-optic effect. A magnetic field applied to a material causes the molecules to tend to align, resulting in the material becoming anisotropic. Just as the Kerr electro-optic effect is attributed to the alignment and distortion of molecules in the presence of an electric field, so the Cotton-Mouton magneto-optic effect is attributed to the alignment and distortion of molecules in the presence of a magnetic field.[1] Here too, the Cotton-Mouton effect is proportional to the square of the applied field strength (in this case the magnetic field, H). The medium becomes birefringent meaning that it has two different refractive indices for light polarized parallel to and perpendicular to the applied magnetic field direction, respectively. Therefore light travelling through the medium has a different velocity when linearly polarized perpendicular to the magnetic field than when polarized in the parallel direction. Reverend John Kerr, who discovered the Kerr effect in 1875, first observed this optical effect due to a transverse magnetic field in 1901. This effect was further studied by Cotton and Mouton in 1905, and is traditionally termed the Cotton-Mouton effect, despite its earlier recovery.

When two orthogonally polarized waves propagate perpendicular to the applied magnetic field, the phase shift that is produced between the waves is

given by[2]

$$\delta = \frac{n_{\parallel} - n_{\perp}}{\lambda} l = ClH^2, \tag{3.1}$$

where l is the distance the two waves travel through the birefringent material.

3.2 Historical Background

In 1901, one of Kerr's experiments involved suspending finely divided powder of Fe_3O_4 in water and applying a magnetic field across the medium. He discovered that when linearly polarized light traversed the medium normal to the lines of force of the applied magnetic field the medium became birefringent.[3]

Although this effect was initially reported by Kerr, most of the early investigations were undertaken by A. Cotton and H. Mouton starting in 1905. They discovered that many pure liquids became birefringent when placed in a magnetic field.[3] Cotton and Mouton were able to show that their effect was analogous to the Kerr effect and possessed the same type of relations. The phase difference, which is a measure of the induced birefringence, is given by[3]

$$\phi = \frac{2\pi l(n_{\parallel} - n_{\perp})}{\lambda_0} = 2\pi ClH^2, \tag{3.2}$$

where $n_{\parallel}$ and $n_{\perp}$ are the refractive indices for the components of light vibrating parallel and perpendicular to the direction of the magnetic field. l is the distance the light has passed through the medium, λ_0 is the vacuum wavelength of the light beam and C is the Cotton-Mouton constant.

The Cotton-Mouton Effect has provided valuable information about the electromagnetic properties of molecules such as magnetic susceptibilities. Although the Cotton-Mouton effect is very small, various measurements in gases have been conducted over the past few decades, these results being summarized in an excellent review article.[4]

3.3 The Cotton-Mouton Experiment

The experimental procedure involves passing a monochromatic light beam, at right angles to the plane of the applied magnetic field, the plane of polar-

ization of which is at 45° to the applied magnetic field. The Cotton-Mouton effect induces a phase difference between the components of the field oscillating parallel and perpendicular to the magnetic field. As for the Kerr effect, a compensator (comprising a quarter-wave plate, an analyzer and a photodiode) allows this phase difference to be measured. Hence the Cotton-Mouton effect for a gas sample can be determined. Sensitive electronic equipment needs to be used in detecting the tiny phase difference in order to obtain consistent and accurate results. The Cotton-Mouton effect is a very small effect and the sensitivity of the apparatus needs to be within one millionth of a radian.[4,5]

3.4 Uses of the Cotton-Mouton Effect

Since the discovery of the Cotton-Mouton effect it has been studied by many researchers using many different substances in the gasous, liquid and solid states. From the measurements of the Cotton-Mouton effect of gases and liquids one is able to determine the electric and magnetic properties of these molecular species which provides insight into the structure and charge distribution of these molecules.[14]

Owing to recent advances in both theoretical methods and computational techniques, calculations of electric, magnetic and optical properties of molecules in the gas phase have proliferated. Among some of these properties which have been investigated using the Cotton-Mouton effect are the mixed electric and magnetic hyperpolarizabilities (e.g. hypermagnetizabilities) and corresponding anisotropies.[14]

3.5 Theory of the first and second Cotton-Mouton virial coefficiets

3.5.1 Introduction

In a dilute gas molecular interactions are usually negligible, and the observed Cotton-Mouton constant can be expressed in terms of the interactions of single molecules independently responding to the applied external fields. However, in dense gases, where molecular nteractions become significant, a virial

expansion is used to describe the molar Cotton-Mouton Constant,

$$ {}_mC = A_{CME} + \frac{B_{CME}}{V_m} + \frac{C_{CME}}{(V_m)^2} + ..., \tag{3.3} $$

where A_{CME} (the first CME virial coefficient) is the zero interaction term, B_{CME} (the second virial coefficient) is for pair interactions, C_{CME} (the third virial coefficient) is for triplet interactions. V_m is the molar volume of the gas.

In the pressure range 0 to 10 atmospheres, often used in experimental studies of molecular-optic effects, the triplet interaction term is usually negligible and density effects are adequately described by the first two terms in 3.3.

This chapter develops theories of the first and second Cotton-Mouton virial coefficients A_{CME} and B_{CME}, and allows us to estimate pair-interaction effects at intermediate pressures.

Chloromethane is the molecule we have chosen to study in the computational part of this chapter in view of the existence in the literature of a comprehensive set of molecular data necessary for the evaluation of B_{CME}. Chloromethane belongs to the $C_{3\nu}$ symmetry point-group, and consists of three hydrogen atoms symmetrically arranged about the line-of-centres of the carbon and the chlorine atoms. It is therefore a quasi-linear molecule.

3.5.2 The Polarization of a Molecule in a Strong Electromagnetic Field:

We consider a diamagnetic molecule in a closed-shell ground state. There is therefore no Zeeman splitting in the magnetic field. The translational and rotational degrees of freedom are treated classically. The energy $U(\sigma, E, H)$ corresponds to a molecule with position and orientation represented by σ, in an electric field E and magnetic field H. This may be expanded in a power series:[4,6,7]

$$ \begin{aligned} U(\sigma, E, H) = U^{(0)} - \mu_\alpha^{(0)} E_\alpha - \frac{1}{2}\alpha_{\alpha\beta} E_\alpha E_\beta - \frac{1}{2}\chi_{\alpha\beta} H_\alpha H_\beta \\ - \frac{1}{2}\xi_{\alpha\beta\gamma} E_\alpha H_\beta H_\gamma - \frac{1}{4}\eta_{\alpha\beta\gamma\delta} E_\alpha E_\beta H_\gamma H_\delta + ... \end{aligned} \tag{3.4} $$

where $\mu_\alpha^{(0)}$ is the permanent electric dipole moment, $\alpha_{\alpha\beta}$ and $\chi_{\alpha\beta}$ are the static electric polarizability and magnetic susceptibility tensors respectively,

and $\xi_{\alpha\beta\gamma}$ and $\eta_{\alpha\beta\gamma\delta}$ are higher-order tensors representing the effect of a magnetic field on electric properties.

The electric dipole moment μ_α is determined from the relation

$$dU = -\mu_\alpha dE_\alpha \tag{3.5}$$

resulting in

$$dU = -\mu_\alpha dE_\alpha \Rightarrow \mu_\alpha = -\frac{dU}{dE_\alpha} \tag{3.6}$$

so that the total dipole moment of a molecule becomes

$$\mu_\alpha(\sigma, E, H) = \mu_\alpha^{(0)} + \alpha_{\alpha\beta}E_\beta + \frac{1}{2}\xi_{\alpha\beta\gamma}H_\beta H_\gamma + \frac{1}{2}\eta_{\alpha\beta\gamma\delta}E_\beta H_\gamma H_\delta + ..., \tag{3.7}$$

where μ_α^0 is the permanent electric dipole moment of the molecule, and $\alpha_{\alpha\beta}$ is the familiar molecular electric polarizability. The tensor $\xi_{\alpha\beta\gamma}$ measures the change in electric dipole moment induced by the magnetic field (which is an effect that is proportional to H^2).

We are concerned with the electric polarizability in the magnetic field, which is obtained by further differentiation with respect to E, yielding

$$\pi_{\alpha\beta} = \frac{d\mu_\alpha}{dE_\beta} = \alpha_{\alpha\beta} + \frac{1}{2}\eta_{\alpha\beta\gamma\delta}H_\gamma H_\delta + ..., \tag{3.8}$$

where $\pi_{\alpha\beta}$ is the differential polarizability and $\eta_{\alpha\beta\gamma\delta}$ is a measure of the distortion of the molecular polarizability by the applied magnetic field.

The theory for the Cotton-Mouton effect in non-interacting molecules (i.e. dilute gases), and gases at densities where pair interactions are significant, is now discussed.

3.5.3 Theory of the Cotton-Mouton Effect in a dilute gas

In this section we derive the first Cotton-Mouton virial coefficient, A_{CME}, for axially-symmetric molecules.

In the limit of low densities the molecular Cotton-Mouton constant ${}_mC$ (in SI units) is[4,6,7]

$$ {}_mC = \lim_{V_m \to \infty} \left[\frac{2(n_{\|} - n_{\perp})V_m}{27(4\pi\epsilon_0)H^2} \right]_{H \to 0} = \frac{2\pi N_A}{27(4\pi\epsilon_0)} \left(\frac{\partial^2 \overline{\pi}}{\partial H^2} \right)_{H=0} \tag{3.9} $$

where the differential polarizability for a particular configuration σ is given by

$$ \pi(\sigma, H) = \pi_{\alpha\beta}(a_\alpha^{\|} a_\beta^{\|} - a_\alpha^{\perp} a_\beta^{\perp}), \tag{3.10} $$

and where $a_\alpha^{\|}$ and $a_\alpha^{\perp}$ are unit vectors in directions parallel and perpendicular to the applied magnetic field, respectively.

Here, $\pi_{\alpha\beta}$ is the differential polarizability tensor

$$ \pi_{\alpha\beta} = \frac{\partial \mu_\alpha}{\partial E_\beta} = \alpha_{\alpha\beta}^{\nu} + \frac{1}{2}\eta_{\alpha\beta\gamma\delta}^{\nu} H_\gamma H_\delta + ..., \tag{3.11} $$

where $\alpha_{\alpha\beta}^{\nu}$ and $\eta_{\alpha\beta\gamma\delta}^{\nu}$ are frequency dependent. $\overline{\pi}$ is the biased average over configurations using a Boltzmann-type weighting factor,

$$ \overline{\pi} = \frac{\int \pi(\sigma, H) e^{(-U^{(\sigma,H)}/kT)} d\sigma}{\int e^{(-U^{(\sigma,H)}/kT)} d\sigma}. \tag{3.12} $$

It is assumed that the period of oscillation of the light waves is much smaller than the time of rotation of the molecule, and that the rotational levels are sufficiently close for the orientation to be effectively continuous.

The energy corresponding to a molecule with configuration σ in an electric field and magnetic field is expanded in a power series as follows:

$$ \begin{aligned} U(\sigma, E, H) = U^{(0)} - \mu_\alpha^{(0)} E_\alpha - \frac{1}{2}\alpha_{\alpha\beta}^{S} E_\alpha E_\beta - \frac{1}{2}\chi_{\alpha\beta}^{S} H_\alpha H_\beta \\ - \frac{1}{2}\xi_{\alpha\beta\gamma}^{S} E_\alpha H_\beta H_\gamma - \frac{1}{4}\eta_{\alpha\beta\gamma\delta}^{S} E_\alpha E_\beta H_\gamma H_\delta + O(E^3, H^4), \end{aligned} \tag{3.13} $$

where the (hyper)polarizability and (hyper)magnetizability tensors are in the static limit.

Now, considering there to be no static electric field present (i.e. E=0), the above equation simplifies to

$$ U(\sigma, H) = U^{(0)} - \frac{1}{2}\chi_{\alpha\beta}^{S} H_\alpha H_\beta + O(H^4). \tag{3.14} $$

It is now necessary to expand $\overline{\pi}$ as a power series in H, bearing in mind that it depends on H both through $\pi(\sigma, H)$ and $U(\sigma, H)$. The isotropic average of a quantity $X(\sigma, H)$ with $X = 0$ is denoted as

$$\langle X \rangle = \frac{\int X(\sigma, 0) e^{(-U^{(0)}/kT)} d\sigma}{\int e^{(-U^{(0)}/kT)} d\sigma}. \tag{3.15}$$

If we expand $\overline{\pi}$ in powers of H, the leading term is in H^2, the coefficient being[6,7]

$$\frac{1}{2}\left(\frac{\partial^2 \overline{\pi}}{\partial H^2}\right)_{H=0} = \frac{1}{2}\left\langle \frac{\partial^2 \pi}{\partial H^2} \right\rangle - \frac{1}{2kT}\left\langle 2\frac{\partial \pi}{\partial H}\frac{\partial U}{\partial H} - \pi\frac{\partial^2 U}{\partial H^2} \right\rangle + \frac{1}{2k^2T^2}\left\langle \pi\left(\frac{\partial U}{\partial H}\right)^2 \right\rangle. \tag{3.16}$$

The second derivatives of equations 3.14 and 3.11 are[6,7]

$$\left(\frac{\partial^2 U}{\partial H^2}\right)_{H=0} = -\chi^S_{\alpha\beta}(a^{\parallel}_{\alpha} a^{\parallel}_{\beta}) \tag{3.17}$$

and

$$\left(\frac{\partial^2 \pi}{\partial H^2}\right)_{H=0} = \eta^{\nu}_{\alpha\beta\gamma\delta}(a^{\parallel}_{\alpha} a^{\parallel}_{\beta} a^{\parallel}_{\gamma} a^{\parallel}_{\delta} - a^{\perp}_{\alpha} a^{\perp}_{\beta} a^{\parallel}_{\gamma} a^{\parallel}_{\delta}), \tag{3.18}$$

where $H_\alpha = H a^{\parallel}_{\alpha}$, etc. Using equations 3.10, 3.11 and 3.13 we can show that

$$\left(\frac{\partial \pi}{\partial H}\right)_{H=0} = 0 \tag{3.19}$$

and

$$\left(\frac{\partial U}{\partial H}\right)_{H=0} = 0, \tag{3.20}$$

while

$$(\pi)_{H=0} = \alpha_{\alpha\beta}(a^{\parallel}_{\alpha} a^{\parallel}_{\beta} - a^{\perp}_{\alpha} a^{\perp}_{\beta}). \tag{3.21}$$

Considering each term in equation 3.16, and making use of the standard results for isotropic averages,[6,7] we obtain for the molar Cotton-Mouton constant in equation 3.9

$${}_mC = \frac{2\pi N_A}{27(4\pi\epsilon_0)}\frac{3}{15}\left[\left(\eta^{\nu}_{\alpha\beta\alpha\beta} - \frac{1}{3}\eta^{\nu}_{\alpha\alpha\beta\beta}\right) + \frac{1}{kT}\left(\alpha_{\alpha\beta}\chi_{\alpha\beta} - \frac{1}{3}\alpha_{\alpha\alpha}\chi_{\gamma\gamma}\right)\right]. \tag{3.22}$$

For axially-symmetric molecules

$$\alpha_{\alpha\beta} = \begin{pmatrix} \alpha_\perp & 0 & 0 \\ 0 & \alpha_\perp & 0 \\ 0 & 0 & \alpha_{||} \end{pmatrix} \tag{3.23}$$

and

$$\chi_{\alpha\beta} = \begin{pmatrix} \chi_\perp & 0 & 0 \\ 0 & \chi_\perp & 0 \\ 0 & 0 & \chi_{||} \end{pmatrix}, \tag{3.24}$$

while

$$\Delta\alpha = \alpha_\perp - \alpha_{||} \tag{3.25}$$

and

$$\Delta\chi = \chi_\perp - \chi_{||}. \tag{3.26}$$

It is a simple matter to show that

$$\alpha_{\alpha\beta}\chi_{\alpha\beta} - \frac{1}{3}\alpha_{\alpha\alpha}\chi_{\beta\beta} = \frac{2}{3}\Delta\alpha\Delta\chi. \tag{3.27}$$

If $\Delta\eta$ is defined as

$$\Delta\eta = \eta^\nu_{\alpha\beta\alpha\beta} - \frac{1}{3}\eta^\nu_{\alpha\alpha\gamma\gamma}, \tag{3.28}$$

then equation 3.22 becomes

$${}_mC = \frac{N_A}{270\epsilon_0}\left[\Delta\eta + \frac{2}{3kT}\Delta\alpha\Delta\chi\right] \tag{3.29}$$

where ${}_mC = A_{CME}$, the first Cotton-Mouton-effect virial coefficient for a dilute gas.

3.5.4 Theory of the Cotton-Mouton effect for interacting non-linear molecules

In developing this theory, we will consider a space-fixed system of axes $O(x, y, z)$ fixed in the Cotton-Mouton experiment such that z is in the direction of propagation of the light beam, x is in the direction of the applied magnetic field H_x, and y is perpendicular to the field. Then, in the limit of

infinite dilution, the refractive index difference $(n_x - n_y)$ of a gas in a strong static magnetic field H_x is

$$(n_x - n_y) = \frac{2\pi N_A}{(4\pi\epsilon_0)V_m}\bar{\pi}, \tag{3.30}$$

where

$$\bar{\pi} = \frac{1}{2}\left(\frac{\partial^2\bar{\pi}}{\partial H^2}\right)_{H=0} H^2. \tag{3.31}$$

For higher gas densities, a representative molecule 1 must at times be treated as half of an interacting pair. If molecule 1 has a neighbouring molecule 2, the relative configuration of which is given by the collective symbol τ, then the contribution of molecule 1 to $(n_x - n_y)$ at that instant is[6,8,9]

$$\frac{1}{2}\left\{\frac{2\pi N_A}{(4\pi\epsilon_0)V_m}\pi^{(12)}(\tau, H)\right\}, \tag{3.32}$$

where

$$\pi^{(12)}(\tau, H) = \pi_{ij}^{(12)}(a_i^x a_j^x - a_i^y a_j^y), \tag{3.33}$$

and where $\pi_{ij}^{(12)}$ is the differential polarizability of the interacting pair.

If the pair of molecules is held in a fixed relative configuration τ and rotates as a rigid whole in the presence of H_i, the resulting biased orientational average $\overline{\pi^{(12)}(\tau, H)}$ can be converted into isotropic averages by Taylor expanding in powers of H. Analogous to the isolated-molecule case, the leading term is

$$\overline{\pi^{(12)}(\tau, H)} = \frac{1}{2}\left(\frac{\partial^2\overline{\pi^{(12)}(\tau, H)}}{\partial H^2}\right)_{H=0} H^2, \tag{3.34}$$

where

$$\left(\frac{\partial^2\overline{\pi^{(12)}(\tau, H)}}{\partial H^2}\right)_{H=0} = \left\langle\frac{\partial^2\pi^{(12)}}{\partial H^2}\right\rangle - \frac{1}{kT}\left\langle 2\frac{\partial\pi^{(12)}}{\partial H}\frac{\partial U^{(12)}}{\partial H} + \pi^{(12)}\frac{\partial^2 U^{(12)}}{\partial H^2}\right\rangle + \frac{1}{k^2T^2}\left\langle\pi^{(12)}\left(\frac{\partial U^{(12)}}{\partial H}\right)^2\right\rangle. \tag{3.35}$$

Here, $U^{(12)}(\tau, H)$ is the potential energy of the interacting pair of molecules in the presence of H_i.

Recall that in the limit of low densities

$$A_{CME} =_m C = \lim_{V_m \to 0} \left[\frac{2(n_x - n_y)V_m}{27(4\pi\epsilon_0)H^2} \right]_{H \to 0} = \frac{2\pi N_A}{27(4\pi\epsilon_0)} \left(\frac{\partial^2 \overline{\pi}}{\partial H^2} \right)_{H=0}. \quad (3.36)$$

Extrapolating this expression to higher densities we obtain

$${}_mC = A_{CME} + \int_\tau \frac{2\pi N_A}{27(4\pi\epsilon_0)} \left\{ \frac{1}{2} \left(\frac{\partial^2 \overline{\pi^{(12)}(\tau, H)}}{\partial H^2} \right)_{H=0} - \left(\frac{\partial^2 \overline{\pi}}{\partial H^2} \right)_{H=0} \right\} P(\tau) d\tau, \quad (3.37)$$

where $P(\tau)d\tau$ is the probability of molecule 1 having a neighbouring molecule in the range $(\tau, \tau + d\tau)$. This is related to the intermolecular potential $U_{12}(\tau)$ by

$$P(\tau) = \frac{N_A}{\Omega V_m} e^{-U_{12}(\tau)/kT}, \quad (3.38)$$

where Ω is a normalization constant.

Now recalling the virial expansion of the Cotton-Mouton constant

$${}_mC = A_{CME} + \frac{B_{CME}}{V_m} + \frac{C_{CME}}{(V_m)^2} + ..., \quad (3.39)$$

and comparing this to equation 3.37, we obtain for the second Cotton-Mouton virial coefficient

$$B_{CME} = \frac{2\pi(N_A)^2}{27\Omega(4\pi\epsilon_0)} \int_\tau \left\{ \frac{1}{2} \left(\frac{\partial^2 \overline{\pi^{(12)}(\tau, H)}}{\partial H^2} \right)_{H=0} - \left(\frac{\partial^2 \overline{\pi}}{\partial H^2} \right)_{H=0} \right\} e^{(-U_{12}(\tau)/kT)} d\tau. \quad (3.40)$$

The relative configuration for two non-linear molecules can be described by seven parameters,[10] namely the distance R between the molecular centres, and the direction cosines describing the relative orientations of the molecule-fixed axes of molecules 1 and 2 relative to the space-fixed system $O(x, y, z)$. These direction cosines can be described by the three Euler angles α, β and γ, with subscripts 1 and 2 denoting molecules 1 and 2, respectively.[10] Therefore, for two non-linear molecules we have

$$B_{CME} = \frac{N_A^2}{216\pi^2(4\pi\epsilon_0)} \int_{R=0}^{\infty} \int_{\alpha_1=0}^{2\pi} \int_{\beta_1=0}^{\pi} \int_{\gamma_1=0}^{2\pi} \int_{\alpha_2=0}^{2\pi} \int_{\beta_2=0}^{\pi} \int_{\gamma_2=0}^{2\pi} \tag{3.41}$$
$$\times \left\{ \frac{1}{2} \left(\frac{\partial^2 \overline{\pi^{(12)}(\tau, H)}}{\partial H^2} \right)_{H=0} - \left(\frac{\partial^2 \bar{\pi}}{\partial H^2} \right)_{H=0} \right\} e^{(-U_{12}(\tau)/kT)}$$
$$\times R^2 sin\beta_1 sin\beta_2 dR d\alpha_1 d\beta_1 d\gamma_1 d\alpha_2 d\beta_2 d\gamma_2.$$

When dealing with molecules that have axial symmetry (i.e. linear and quasi-linear molecules) this seven-dimensional integral can be reduced to a more manageable four-dimensional integral.

$\left(\frac{\partial^2 \bar{\pi}}{\partial H^2}\right)_{H=0}$ has already been evaluated in section 3.5.3, yielding

$$\left(\frac{\partial^2 \bar{\pi}}{\partial H^2} \right)_{H=0} = \left\{ \frac{1}{5} \Delta\eta + \frac{1}{5kT} (\alpha_{ij}\chi_{ij} - 3\alpha\chi) \right\}. \tag{3.42}$$

where $\alpha = \frac{1}{3}\alpha_{ii}$ and $\chi = \frac{1}{3}\chi_{ii}$.

We now need to evaluate $\frac{1}{2}\left(\frac{\partial^2 \overline{\pi^{(12)}(\tau,H)}}{\partial H^2}\right)_{H=0}$.

The refractive index of a gas is determined by the total oscillating dipole moment induced in a molecule. In a dense gas, the dipole moment of a representative molecule 1 is induced not only by the oscillating electric field E_{0i} associated with the light wave, but also in part by the field $F_i^{(1)}$ arising at molecule 1 due to the oscillating moments of the neighbouring molecule 2. Neglecting the small field gradient effects, we have

$$\mu_i^{(1)}(E_0) = \left(\alpha_{ij}^{(1)} + \frac{1}{2}\eta_{ijkl}^{(1)} H_k H_l + \ldots \right) \left(E_{0j} + F_j^{(1)} \right) \tag{3.43}$$

where H_j is the applied static magnetic field. $F_i^{(1)}$ has the form

$$F_i^{(1)} = T_{ij}^{(1)} \mu_j^{(2)}, \tag{3.44}$$

where the T-tensor is given by[11]

$$T_{\alpha\beta}^{(1)} = \frac{1}{4\pi\epsilon_0} \nabla_\alpha \nabla_\beta R^{-1} = \frac{1}{4\pi\epsilon_0} \left(3R_\alpha R_\beta - R^2 \delta_{\alpha\beta} \right) R^{-5}. \tag{3.45}$$

R_α is the position of molecule 2 from the centre of molecule 1 while $\mu_k^{(2)}$ is the oscillating dipole induced in molecule 2 by the field arising there due to both the direct influence of E_0 and the oscillating dipole of molecule 1:

$$\mu_k^{(2)}(E_0) = \left(\alpha_{kl}^{(2)} + \frac{1}{2}\eta_{klmn}^{(2)} H_m H_n + \ldots\right)\left(E_{0l} + F_l^{(2)}\right), \tag{3.46}$$

where

$$F_l^{(2)} = T_{lm}^{(2)} \mu_m^{(1)}. \tag{3.47}$$

It can be shown that $T_{\alpha\beta}^{(1)} = T_{\alpha\beta}^{(2)}$.[11] Substitution of equations 3.46 and 3.47 into equation 3.44, followed by successive substitutions of $F_i^{(1)}$ and $F_i^{(2)}$, leads to a lengthy series of terms contributing to the net field $F_i^{(1)}$ in equation 3.44; substitution of which into equation 3.43 yields a complete expression for the total oscillating dipole induced on molecule 1 by the light-wave field in the presence of molecule 2:

$$\begin{aligned}\mu_i^{(1)}(E_0) = \alpha_{iw}^{(1)} E_{0w} + \alpha_{ij}^{(1)} T_{jk} \alpha_{kw}^{(2)} E_{0w} + \alpha_{ij}^{(1)} T_{jk} \alpha_{kl}^{(2)} T_{lm} \alpha_{mw}^{(1)} E_{0w} \\ + \alpha_{ij}^{(1)} T_{jk} \alpha_{kl}^{(2)} T_{lm} \alpha_{mn}^{(1)} T_{np} \alpha_{pw}^{(2)} E_{0w} \\ + \frac{1}{2}\eta_{iwkl}^{(1)} H_k H_l E_{0w} + \frac{1}{2}\eta_{ijkl}^{(1)} H_k H_l T_{jm} \alpha_{mw}^{(2)} E_{0w} \\ + \frac{1}{2}\eta_{ijkl}^{(1)} H_k H_l T_{jm} \alpha_{mn}^{(2)} T_{np} \alpha_{pw}^{(1)} E_{0w} \\ + \frac{1}{2}\alpha_{ij}^{(1)} T_{jk} \eta_{kwmn}^{(2)} H_m H_n E_{0w} + \cdots.\end{aligned} \tag{3.48}$$

The differential polarizability of molecule a general molecule 1 in the presence of the applied magnetic field H_i and a neighbouring molecule 2 in a specific relative configuration τ is

$$\begin{aligned}\pi_{iw}^{(p)} = \frac{\partial \mu_i^{(p)}(E_0)}{\partial E_{0w}} = \alpha_{iw}^{(1)} + \alpha_{ij}^{(1)} T_{jk} \alpha_{kw}^{(2)} + \alpha_{ij}^{(1)} T_{jk} \alpha_{kl}^{(2)} T_{lm} \alpha_{mw}^{(1)} \\ + \alpha_{ij}^{(1)} T_{jk} \alpha_{kl}^{(2)} T_{lm} \alpha_{mn}^{(1)} T_{np} \alpha_{pw}^{(2)} + \frac{1}{2}\eta_{iwkl}^{(1)} H_k H_l + \cdots.\end{aligned} \tag{3.50}$$

For an interacting pair the differential polarizability is

$$\pi_{iw}^{(12)} = \frac{\partial \mu_i^{(12)}}{\partial E_{0w}} \approx \frac{\partial(\mu_i^{(1)} + \mu_i^{(2)})}{\partial E_{0w}}, \tag{3.51}$$

where $\mu_i^{(12)}(E_{0w})$ is the total oscillating dipole induced on the interacting pair by the light-wave field, and where it has been assumed that the two interacting molecules each retain their separate identities. This assumption should be valid in the long-range limit.

The difference between the differential polarizabilities $\pi_{iw}^{(12)} a_i^x a_w^x$ and $\pi_{iw}^{(12)} a_i^y a_w^y$ of an interacting pair in a specific relative interaction configuration τ in the presence of the applied field may be written

$$\begin{aligned} \pi^{(12)}(\tau, H) &= \pi_{iw}^{(12)}(a_i^x a_w^x - a_i^y a_w^y) \\ &= (\pi_{iw}^{(1)} + \pi_{iw}^{(2)})(a_i^x a_w^x - a_i^y a_w^y) \\ &= \pi^{(1)}(\tau, H) + \pi^{(2)}(\tau, H), \end{aligned} \tag{3.52}$$

where $\pi_{iw}^{(p)}$ is given by equation 3.50.

The potential of the interacting pair in the presence of the static magnetic field H_i is[8–10]

$$U^{(12)}(\tau, H) = U^{(12)}(\tau, 0) + U^{(1)}(\tau, H) + U^{(2)}(\tau, H), \tag{3.53}$$

where

$$U^{(p)}(\tau, H) = -\frac{1}{2}\chi_{iw}^{(p)} H^2 a_i^x a_w^x. \tag{3.54}$$

It is now possible to evaluate the term $\frac{1}{2}\left(\frac{\partial^2 \overline{\pi^{(12)}(\tau,H)}}{\partial H^2}\right)_{H=0}$ in the expression for B_{CME} given in equation 3.41. The isotropic averages in equation 3.35 are now systematically evaluated. Equation 3.52 allows the average $\frac{1}{2}\left\langle \frac{\partial^2 \pi^{(12)}}{\partial H^2} \right\rangle$ to be written as $\frac{1}{2}\left\langle \frac{\partial^2 \pi^{(1)}}{\partial H^2} \right\rangle + \frac{1}{2}\left\langle \frac{\partial^2 \pi^{(2)}}{\partial H^2} \right\rangle$, and since molecules 1 and 2 are identical, the isotropic averages of their polarizabilities must be the same. Hence,

$$\frac{1}{2}\left\langle \frac{\partial^2 \pi^{(12)}}{\partial H^2} \right\rangle = \left\langle \frac{\partial^2 \pi^{(1)}}{\partial H^2} \right\rangle. \tag{3.55}$$

Using similar arguments, together with equation 3.53, we have

$$\frac{1}{2}\left(\frac{\partial^2 \overline{\pi^{(12)}(\tau, H)}}{\partial H^2}\right)_{H=0} = \left\langle \frac{\partial^2 \pi^{(1)}}{\partial H^2} \right\rangle - \frac{1}{kT}\left\{ \left\langle \pi^{(1)} \frac{\partial^2 U^{(1)}}{\partial H^2} \right\rangle + \left\langle \pi^{(1)} \frac{\partial^2 U^{(2)}}{\partial H^2} \right\rangle \right\} \tag{3.56}$$

$$-\frac{1}{kT}\left\{\left\langle 2\frac{\partial\pi^{(1)}}{\partial H}\frac{\partial U^{(1)}}{\partial H}\right\rangle+\left\langle 2\frac{\partial\pi^{(1)}}{\partial H}\frac{\partial U^{(2)}}{\partial H}\right\rangle\right\}$$
$$+\frac{1}{(kT)^2}\left\{\left\langle\pi^{(1)}\left(\frac{\partial U^{(1)}}{\partial H}\right)^2\right\rangle+2\left\langle\pi^{(1)}\frac{\partial U^{(1)}}{\partial H}\frac{\partial U^{(2)}}{\partial H}\right\rangle+\left\langle\pi^{(1)}\left(\frac{\partial U^{(2)}}{\partial H}\right)^2\right\rangle\right\}.$$

Now from equation 3.54,

$$\left(\frac{\partial U^{(1)}}{\partial H}\right)_{H=0}=0 \tag{3.57}$$

and

$$\left(\frac{\partial^2 U^{(1)}}{\partial H^2}\right)_{H=0}=-\chi^{(1)}_{iw}a^x_i a^x_w. \tag{3.58}$$

And so equation 3.56 simplifies to

$$\frac{1}{2}\left(\frac{\partial^2\overline{\pi^{(12)}(\tau,H)}}{\partial H^2}\right)_{H=0}=\left\langle\frac{\partial^2\pi^{(1)}}{\partial H^2}\right\rangle-\frac{1}{kT}\left\{\left\langle\pi^{(1)}\frac{\partial^2U^{(1)}}{\partial H^2}\right\rangle+\left\langle\pi^{(1)}\frac{\partial^2U^{(2)}}{\partial H^2}\right\rangle\right\}. \tag{3.59}$$

Now $\left\langle\frac{\partial^2\pi^{(1)}}{\partial H^2}\right\rangle$ are the terms with the hypermagnetizability tensor $\eta^{(1)}$. Typical values for this tensor are extremely tiny:[4] for chloromethane, $\Delta\eta\approx10^{-48}$ while $\Delta\chi\approx10^{-29}$. Therefore we are justified in neglecting these terms, and we focus instead on the $\left\langle\pi^{(1)}\frac{\partial^2U^{(1)}}{\partial H^2}\right\rangle$ and $\left\langle\pi^{(1)}\frac{\partial^2U^{(2)}}{\partial H^2}\right\rangle$ terms.

$$-\frac{1}{kT}\left\langle\pi^{(1)}\frac{\partial^2U^{(1)}}{\partial H^2}\right\rangle=\underbrace{+\frac{1}{kT}\alpha^{(1)}_{iw}\chi^{(1)}_{pq}\left\langle a^x_i a^x_w a^x_p a^x_q-a^y_i a^y_w a^x_p a^x_q\right\rangle}_{\alpha\chi} \tag{3.60}$$
$$\underbrace{+\frac{1}{kT}\alpha^{(1)}_{ij}T_{jk}\alpha^{(2)}_{kw}\chi^{(1)}_{pq}\left\langle a^x_i a^x_w a^x_p a^x_q-a^y_i a^y_w a^x_p a^x_q\right\rangle}_{\alpha^2\chi}$$
$$\underbrace{+\frac{1}{kT}\alpha^{(1)}_{ij}T_{jk}\alpha^{(2)}_{kw}T_{lm}\alpha^{(1)}_{mw}\chi^{(1)}_{pq}\left\langle a^x_i a^x_w a^x_p a^x_q-a^y_i a^y_w a^x_p a^x_q\right\rangle}_{\alpha^3\chi}$$
$$\underbrace{+\frac{1}{kT}\alpha^{(1)}_{ij}T_{jk}\alpha^{(2)}_{kl}T_{lm}\alpha^{(1)}_{mn}T_{no}\alpha^{(2)}_{ow}\chi^{(1)}_{pq}\left\langle a^x_i a^x_w a^x_p a^x_q-a^y_i a^y_w a^x_p a^x_q\right\rangle}_{\alpha^4\chi}+\cdots$$

while

$$-\frac{1}{kT}\left\langle\pi^{(1)}\frac{\partial^2U^{(2)}}{\partial H_x^2}\right\rangle=\underbrace{+\frac{1}{kT}\alpha^{(1)}_{iw}\chi^{(2)}_{pq}\left\langle a^x_i a^x_w a^x_p a^x_q-a^y_i a^y_w a^x_p a^x_q\right\rangle}_{\alpha\chi} \tag{3.61}$$

$$+\underbrace{\frac{1}{kT}\alpha^{(1)}_{ij}T_{jk}\alpha^{(2)}_{kw}\chi^{(2)}_{pq}\left\langle a^x_i a^x_w a^x_p a^x_q - a^y_i a^y_w a^x_p a^x_q\right\rangle}_{\alpha^2\chi}$$

$$+\underbrace{\frac{1}{kT}\alpha^{(1)}_{ij}T_{jk}\alpha^{(2)}_{kw}T_{lm}\alpha^{(1)}_{mw}\chi^{(2)}_{pq}\left\langle a^x_i a^x_w a^x_p a^x_q - a^y_i a^y_w a^x_p a^x_q\right\rangle}_{\alpha^3\chi}$$

$$+\underbrace{\frac{1}{kT}\alpha^{(1)}_{ij}T_{jk}\alpha^{(2)}_{kl}T_{lm}\alpha^{(1)}_{mn}T_{no}\alpha^{(2)}_{ow}\chi^{(2)}_{pq}\left\langle a^x_i a^x_w a^x_p a^x_q - a^y_i a^y_w a^x_p a^x_q\right\rangle}_{\alpha^4\chi}+\cdots.$$

The term $\frac{1}{kT}\alpha^{(1)}_{iw}\chi^{(1)}_{pq}\left\langle a^x_i a^x_w a^x_p a^x_q - a^y_i a^y_w a^x_p a^x_q\right\rangle$ is the low-pressure $\left(\frac{\partial^2\pi}{\partial\pi^2}\right)_{H=0}$ term, and is subtracted out since it has already been accounted for in A_{CME}. We have

$$\left\{\frac{1}{2}\left(\frac{\partial^2\overline{\pi^{(12)}(\tau,H)}}{\partial H^2}\right)_{H=0}-\left(\frac{\partial^2\overline{\pi}}{\partial H^2}\right)_{H=0}\right\}e^{(-U_{12}(\tau)/kT)}=\alpha\chi+\alpha^2\chi+\alpha^3\chi+\alpha^4\chi+\cdots, \tag{3.62}$$

the terms in which each need to be evaluated. Hence we can calculate B_{CME} via equation 3.40. The isotropic averages of the series of terms are carried out using the results given by Buckingham *et al.*[8,12]

$$\alpha\chi=\frac{1}{kT}\alpha^{(1)}_{iw}\chi^{(2)}_{pq}\left\langle a^x_i a^x_w a^x_p a^x_q - a^y_i a^y_w a^x_p a^x_q\right\rangle \tag{3.63}$$

$$=\frac{1}{30kT}\alpha^{(1)}_{iw}\chi^{(2)}_{pq}(-2\delta_{iw}\delta_{pq}+3\delta_{ip}\delta_{wq}+3\delta_{iq}\delta_{wp})$$

$$=\frac{1}{30kT}\left\{-2\alpha^{(1)}_{ii}\chi^{(2)}_{pp}+3\alpha^{(1)}_{iw}\chi^{(2)}_{iw}+3\alpha^{(1)}_{qw}\chi^{(2)}_{wq})\right\}$$

$$=\frac{1}{30kT}\left\{6\alpha^{(1)}_{qw}\chi^{(2)}_{wq}-2\times 9\alpha\chi\right\}$$

$$=\frac{1}{5kT}\left\{\alpha^{(1)}_{qw}\chi^{(2)}_{wq}-3\alpha\chi\right\} \tag{3.64}$$

Therefore the $\alpha\chi$ term for the pair interaction virial coefficient is determined as

$$B_{CME}(\alpha\chi)=\frac{N_A^2}{216\pi^2(4\pi\epsilon_0)}\times\frac{1}{5kT}\int_{R=0}^{\infty}\int_{\tau}\left\{\alpha^{(1)}_{qw}\chi^{(1)}_{wq}-3\alpha\chi\right\}e^{(-U_{12}(\tau)/kT)}R^2dRd\tau. \tag{3.65}$$

The terms in $\alpha^2\chi$ become

$$\frac{1}{kT}\alpha^{(1)}_{ij}T_{jk}\alpha^{(2)}_{kw}\chi^{(1)}_{pq}(-2\delta_{iw}\delta_{pq}+3\delta_{ip}\delta_{wq}+3\delta_{iq}\delta_{wp}) \tag{3.66}$$

$$= \frac{1}{30kT}\left\{-2\alpha_{ij}^{(2)}T_{jk}\alpha_{kl}^{(2)}\chi_{qq}^{(1)} + 3\alpha_{ij}^{(1)}T_{jk}\alpha_{kq}^{(2)}\chi_{iq}^{(1)} + 3\alpha_{ij}^{(1)}T_{jk}\alpha_{kp}^{(2)}\chi_{pi}^{(1)})\right\}$$

$$= \frac{1}{30kT}\left\{6\alpha_{ij}^{(1)}T_{jk}\alpha_{kp}^{(2)}\chi_{pi}^{(1)} - 6\alpha_{ij}^{(1)}T_{jk}\alpha_{ki}^{(2)}\chi\right\}$$

$$= \frac{1}{5kT}\left\{\alpha_{ij}^{(1)}T_{ij}\alpha_{kp}^{(2)}\chi_{pi}^{(1)} - \chi\alpha_{ij}^{(1)}T_{ij}\alpha_{ki}^{(2)}\right\},$$

while the terms in $\alpha^3\chi$ are

$$\frac{1}{kT}\alpha_{ij}^{(1)}T_{jk}\alpha_{kl}^{(2)}T_{lm}\alpha_{mw}^{(1)}\chi_{pq}^{(1)}(-2\delta_{iw}\delta_{pq} + 3\delta_{ip}\delta_{wq} + 3\delta_{iq}\delta_{wp}) \tag{3.67}$$

$$= \frac{1}{30kT}\left\{6\alpha_{ij}^{(1)}T_{jk}\alpha_{kl}^{(2)}T_{lm}\alpha_{mq}^{(1)}\chi_{qi}^{(1)} - 6\chi\alpha_{ij}^{(1)}T_{jk}\alpha_{kl}^{(2)}T_{lm}\alpha_{mi}^{(1)}\right\}$$

$$= \frac{1}{5kT}\left\{\alpha_{ij}^{(1)}T_{jk}\alpha_{kl}^{(2)}T_{lm}\alpha_{mq}^{(1)}\chi_{qi}^{(1)} - \chi\alpha_{ij}^{(1)}T_{jk}\alpha_{kl}^{(2)}T_{lm}\alpha_{mi}^{(1)}\right\}.$$

To evaluate the $\alpha\chi$ term's contribution to the pair-interaction virial coefficient for molecules with axial symmetry, we have

$$B_{CME}(\alpha\chi) = \frac{(N_A)^2(\mu_0)^2}{216\pi^2(4\pi\epsilon_0)} \times \frac{1}{5kT}\int_R\int_{\theta_1}\int_{\theta_2}\int_{\phi}\left(\alpha_{ij}^{(1)}\chi_{ji}^{(2)} - 3\alpha\chi\right) \times e^{(-U_{12}(R,\theta_1,\theta_2,\phi)/kT)}R^2 sin\theta_1 sin\theta_2 dR d\theta_1 d\theta_2 d\phi \tag{3.68}$$

where

$$\alpha = \frac{1}{3}\alpha_{ii} = \frac{1}{3}(\alpha_{11} + \alpha_{22} + \alpha_{33}), \tag{3.69}$$

and

$$\chi = \frac{1}{3}\chi_{ii} = \frac{1}{3}(\chi_{11} + \chi_{22} + \chi_{33}). \tag{3.70}$$

For two interacting axially-symmetric molecules, the relative configuration τ may be specified by the four parameters θ_1, θ_2, ϕ and R,[11] where R is the distance between molecular centres; θ_1 and θ_2 are the angles between the line of centres and the dipole axes of molecules 1 and 2; and ϕ is the angle between the planes formed by the molecular axes and the line of centres.

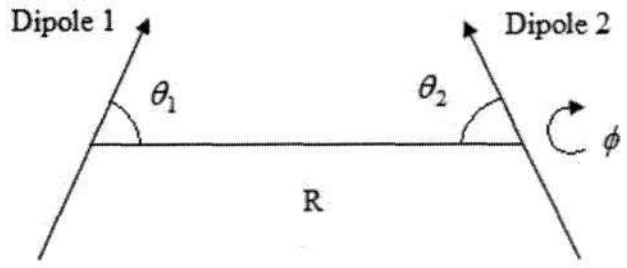

The unit vectors $\boldsymbol{l}^{(1)}$ and $\boldsymbol{l}^{(2)}$ along the dipole axes, and λ along $\boldsymbol{R}$, will be required in the ensuing analysis. For a molecule with a threefold or higher rotation axis coinciding with the 3-axis of a molecule-fixed system $O(1,2,3)$, α_{ij} and χ_{ij} are diagonal, with $\alpha_{11} = \alpha_{22} = \alpha_\perp$, $\alpha_{33} = \alpha_\parallel$, $\chi_{11} = \chi_{22} = \chi_\perp$, and $\chi_{33} = \chi_\parallel$. Buckingham has also shown that for axially-symmetric molecules, the molecular-property tensors themselves can be expressed in terms of $\boldsymbol{l}_i^{(2)}$.[11] We have

$$\chi_{ij}^{(2)} = \chi_\perp \delta_{ij} + (\chi_\parallel - \chi_\perp) l_i^{(2)} l_j^{(2)}, \tag{3.71}$$

where $(\chi_\parallel - \chi_\perp) = \Delta\chi$, so that

$$\alpha_{ij}^{(1)} \chi_{ji}^{(2)} = \alpha_\perp [\chi_\perp + \Delta\chi \left(l_1^{(2)}\right)^2] + \alpha_\perp [\chi_\perp + \Delta\chi \left(l_2^{(2)}\right)^2] + \alpha_\parallel [\chi_\perp + \Delta\chi \left(l_3^{(2)}\right)^2]. \tag{3.72}$$

Simplification of this result is achieved by making use of the following well-established relationships:[11]

$$l_3^{(2)} = cos\theta_{12} = -cos\theta_1 cos\theta_2 + sin\theta_1 sin\theta_2 cos\phi \tag{3.73}$$

and

$$(l_1^{(2)})^2 + (l_2^{(2)})^2 = 1 - cos^2\theta_{12}. \tag{3.74}$$

This yields

$$\alpha_{ij}^{(1)} \chi_{ji}^{(2)} = 3\alpha\chi_\perp + \Delta\chi(\alpha_\perp(1 - cos^2\theta_{12}) + \alpha_\parallel cos^2\theta_{12}), \tag{3.75}$$

which can be used directly in equation 3.68 for computation of $B_{CME}(\alpha\chi)$. Numerical integration is achieved using Gaussian quadratures, as discussed in the next section. A similar procedure is used for terms in $\alpha^2\chi$ and $\alpha^3\chi$.

3.5.5 Computation of B_{CME} for chloromethane

By modifying computer code developed during an Honours course, the Gaussian quadrature numerical-integration method was implemented using a Fortran program, allowing for evaluation of the $\alpha^n\chi$ series of terms contributing to the pair-interaction virial coefficient B_{CME} for the molecule chloromethane. We chose this molecule because its molecular parameters are precisely known, and it provides a useful test of our new theory. To compute the virial coefficients, an expression is required for the intermolecular potential appearing in equation 3.68. We use[10,11]

$$U_{12}(R,\theta_1,\theta_2,\phi) = U_{LJ} + U_{\mu,\mu} + U_{\mu,\theta} + U_{\theta,\theta} + U_{\mu,in\mu} + U_{\theta,in\mu} + U_{Shape} \quad (3.76)$$

where the contributions are given by: Lennard-Jones:

$$U_{LJ} = 4\epsilon\left(\left(\frac{R_0}{R}\right)^{12} - \left(\frac{R_0}{R}\right)^{6}\right) \quad (3.77)$$

Dipole-dipole:

$$U_{\mu,\mu} = \frac{1}{4\pi\epsilon_0}\left(\mu^2 R^{-3}\left(2\cos\theta_1\cos\theta_2 + \sin\theta_1\sin\theta_2\cos\phi\right)\right) \quad (3.78)$$

Dipole-quadrupole:

$$U_{\mu,\theta} = \frac{1}{4\pi\epsilon_0}\left(\frac{3}{2}\mu\theta R^{-4}\left[\cos\theta_1(3\cos^2\theta_2 - 1) + \cos\theta_2(3\cos^2\theta_1 - 1)\right.\right. \quad (3.79)$$
$$\left.\left. +2\sin\theta_1\sin\theta_2\cos\theta_2\cos\phi + 2\sin\theta_1\cos\theta_1\sin\theta_2\cos\phi\right]\right)$$

Quadrupole-quadrupole:

$$U_{\theta,\theta} = \frac{1}{4\pi\epsilon_0}\left(\frac{3}{4}\theta^2 R^{-5}\left[1 - 5\cos^2\theta_1 - 5\cos^2\theta_2 + 17\cos^2\theta_1\cos^2\theta_2\right.\right. \quad (3.80)$$
$$\left.\left. +2\sin^2\theta_1\sin^2\theta_2\cos^2\phi + 16\sin\theta_1\cos\theta_1\sin\theta_2\cos\theta_2\cos\phi\right]\right)$$

Dipole-induced dipole:

$$U_{\mu,in\mu} = \frac{1}{(4\pi\epsilon_0)^2}\left(-\frac{1}{2}\alpha_S\mu^2 R^{-6}\left((3\cos^2\theta_1 - 1) + (3\cos^2\theta_2 - 1)\right)\right) \quad (3.81)$$

Quadrupole-induced dipole:

$$U_{\theta,in\mu} = \frac{1}{(4\pi\epsilon_0)^2}\left(-\frac{9}{8}\alpha_S\theta^2 R^{-8}(4\cos^4\theta_1 + 4\cos^4\theta_2 + \sin^4\theta_1 + \sin^4\theta_2)\right) \quad (3.82)$$

Shape:

$$U_{Shape} = 4D\epsilon \left(\frac{R_0}{R}\right)^{12} \left(3\cos^2\theta_1 + 3\cos^2\theta_2 - 2\right) \tag{3.83}$$

The first three terms for the pair-interaction Cotton-Mouton virial coefficient for chloromethane were found to be:

Argument being integrated	10^{30} Integral (m^8 A^{-2} mol^{-2})
$\alpha\chi$	-0.049652
$\alpha^2\chi$	0.106217
$\alpha^3\chi$	-0.003649

B_{CME} is determined by summing the terms $\alpha\chi + \alpha^2\chi + \alpha^3\chi$, yielding $B_{CME} = 0.052916 \times 10^{-30}$ m^8 A^{-2} mol^{-2}.

The percentage contributions of the terms with respect to the pair-interaction virial coefficient B_{CME} are shown below, and since the third term contributes only -6.5%, we can safely assume that the series of terms is rapidly converging, so that higher-order terms make a negligible contribution, and can be safely ignored.

Term	10^{30} Integral (m^8 A^{-2} mol^{-2})	Percentage contribution (%)
$\alpha\chi$	-0.049652	-94.0
$\alpha^2\chi$	0.106217	$+200.5$
$\alpha^3\chi$	-0.003649	-6.5
B_{CME}	0.052916	100

The experimental analysis for the Cotton-Mouton effect of chloromethane (taken from Lukins, pg 111)[13] is given below:

Property	Value
$\Delta\eta$	$(0.47 \pm 0.033) \times 10^{-48}$ J m^2 V^{-2} T^{-2}
$\Delta\alpha$	$(1.705 \pm 0.054) \times 10^{-40}$ J m^2 V^{-2}
$\Delta\chi$	$(-15.0 \pm 1.3) \times 10^{-29}$ J T^{-2}
$\bar{\chi}$	$(-53.1 \pm 1.0) \times 10^{-29}$ J T^{-2}
χ_{zz}	$(-63.1 \pm 1.3) \times 10^{-29}$ J T^{-2}
χ_{xx}	$(-48.1 \pm 1.1) \times 10^{-29}$ J T^{-2}

Here, the magnetic susceptibility and the magnetic hyperpolarizability have been defined in terms of the magnetic induction, B, rather than the

magnetic field strength, H. The conversion factors are[15]:

$$\chi^B_{\alpha\beta} = \frac{1}{\mu_0}\chi^H_{\alpha\beta} \tag{3.84}$$

and

$$\eta^B_{\alpha\beta\gamma\delta} = \frac{1}{\mu_0^2}\eta^H_{\alpha\beta\gamma\delta}. \tag{3.85}$$

The first Cotton-Mouton virial coefficient measured for chloromethane at a wavelength of 632.8 nm and a temperature of 294.6K is (Lukins, pg 105)[13] $A_{CME} = (-1.51 \pm 0.02) \times 10^{-27}$ m^5 A^{-2} mol^{-1}.

To see the effect of intermolecular pair-interactions, we take one of the typical maximum working pressures of 573 kPa, which corresponds to a molar volume of V_m^{-1} =257.1 mol m^{-3}. The Cotton-Mouton constant for chloromethane including molecular interaction effects is obtainable from the virial expansion

$$_mC = A_{CME} + \frac{B_{CME}}{V_m}, \tag{3.86}$$

which yields $_mC = -1.49_6 \times 10^{-27}$ m^5 A^{-2} mol^{-1} .

The pair-interaction virial coefficient B_{CME} is seen to contribute only 0.9% to the Cotton-Mouton constant for chloromethane at this gas density. This is a very small contribution considering that the percentage error for Lukins' measured A_{CME} value is 1.3%. This small pair-interaction contribution illustrates how difficult it would be to measure the pair-interaction virial coefficient for chloromethane. We have not attempted calculations for any other molecules in this work, since the Kerr effect was a major thrust of the project, and proved very time-consuming. The theory presented here could certainly be used to good effect in searching for a molecule where the pair-interaction contribution would be large enough to measure, and to check if the dilute gas approximation is adequate in any experimental programme.

3.6 References

1. G. R. Fowles, *Introduction to Modern Optics*, New York, Holt, Rinehart and Winston, 1968, 192.

2. R. Guenther, *Modern Optics*, New York, John Wiley and Sons, 1990, 571,596

3. M. Evans and S. Kielich, *Modern Nonlinear Optics* part 2, New York, John Wiley and Sons, 1993, 361-414.

4. C. Rizzo, A. Rizzo and D. M. Bishop, *International Reviews in Physical Chemistry*, 1997, **16**, 81-111

5. A. Janse van Rensburg, Honours Project, University of KwaZulu-Natal, 2005.

6. A. D. Buckingham and J. A. Pople, *Proceedings of the Physical Society B*, 1956, **69**, 1133-1138.

7. J. H. Williams, *Advances in Chemical Physics*, 1993, **85**, 316-414.

8. A. D. Buckingham and J. A. Pople, *Proceedings of the Physical Society A*, 1955, **68**, 905-909.

9. A. D. Buckingham and J. A. Pople, *Faraday Society Discussions*, 1956, **22**, 17-21.

10. V. W. Couling, PhD thesis, University of KwaZulu-Natal, 1995.

11. A. D. Buckingham, *Advances in Chemical Physics*, 1967, **12**, 107-142.

12. A. L. Andrews and A. D. Buckingham, *Molecular Physics*, 1960, **3**, 183-189.

13. P. B. Lukins, PhD thesis, University of Sydney, 1984.

14. J. W. Beams, *Reviews of Modern Physis*, 1932, **4**, 133-172.

15. P. B. Lukins, D. R. Laver, A. D. Buckingham and G. L. D. Ritchie, *J. Phys. Chem.*, 1985, **89**, 1309-1312.

Chapter 4

Theory - The Kerr Effect

4.1 Introduction

The Kerr Effect is an electro-optical effect attributed to the alignment and/or distortion of molecules in the presence of an electric field. An optically isotropic substance when placed in an electric field (or magnetic field) becomes birefringent. A birefringent medium has different refractive indices $n_{\|}$ and $n_{\perp}$ for light polarized parallel and perpendicular with respect to the applied field. The Kerr constant K is determined by the following equation:

$$n_{\|} - n_{\perp} =_m K E^2 \lambda, \tag{4.1}$$

which illustrates that the magnitude of the effect is proportional to the strength of the electric field squared. $n_{\|}$ is the refractive index parallel to the direction of the applied field and $n_{\perp}$ is the refractive index perpendicular to the field. λ is the wavelength of the light.

A virial expansion is used to describe the molar Kerr constant.

$$_mK = A_K + \frac{B_K}{V_m} + \frac{C_K}{(V_m)^2} + ... \tag{4.2}$$

where the first virial coefficient A_K is the zero-interaction term, while the second virial coefficient B_K accounts for pair interactions and the third virial coefficient C_K for triplet interactions. C_K is only significant at very high pressures, which have been avoided in the experimental work described here. V_m is the molar volume of the gas.

The importance of studying the Kerr and Cotton-Mouton effects is that they are an important means of determining the electric and magnetic properties of molecules, thereby providing insight into the structure and charge distribution of molecules.

The birefringent medium is optically anisotropic, having different refractive indices $n_{\parallel}$ and $n_{\perp}$ for light polarized parallel and perpendicular with respect to the applied electric field. Reverend John Kerr observed that an optically anisotropic material exhibits birefringent behaviour when placed in an electric field.[1] This effect has a quadratic dependence on the applied electric field and hence is also referred to as the quadratic electro-optic effect.[3] The Kerr effect is distinct from the Pockels effect in that the induced index change is proportional to the square of the electric field as opposed to just the magnitude of the field.

There are two cases of the Kerr effect that are normally considered: the *Kerr electro-optic effect* (DC Kerr effect), and the *optical Kerr effect* (AC Kerr effect).[5] The Kerr electro-optic effect occurs when the electric field is a slowly varying external field, for example a voltage on electrodes across the medium. We will concern ourselves with this case. The optical Kerr effect occurs when the applied electric field is due to the light-wave itself, or a second very intense light wave which causes the allignment.

4.2 Historical Background

The Kerr effect was discovered in 1875 by Reverend John Kerr, a Scottish physicist. Kerr's initial experiments used soft glass and he discovered that birefringence developed in the glass when placed in an intense electric field. This effect was most noticeable when the wave front of the incident light was orientated perpendicular to the applied electric field with its plane of polarization inclined to the field direction by an angle of 45°.[4] After his observations on glass Kerr measured a variety of liquids and he showed that the induced effect was proportional to the square of the applied electric field, as seen in equation 2.3.

Analagous to the phase difference (defined by equation 3.2) for the Cotton-

Mouton effect, the phase difference for the Kerr effect is given by[4]

$$\delta = \frac{2\pi l(n_{\parallel} - n_{\perp})}{\lambda_0} = 2\pi B l E^2, \tag{4.3}$$

where the applied magnetic field **H** is exchanged for the electric field **E**, and the Cotton-Mouton constant C with the Kerr constant B.

The Kerr Effect has provided valuable information about molecular moments and polarizabilities.[4,5]

4.3 Theory

The theory in this chapter is a review of work achieved by previous researchers, and involves two separate cases, namely gases at low pressures where molecular interactions are negligible, and the more complex case of gases at higher pressures where the effects of intermolecular interactions need to be taken into account.

4.3.1 Low Pressures: Non-Interacting Molecules

Linearly-polarized light passing through a birefringent medium emerges elliptically polarized. This change in polarization state is due to the phase difference induced between the resolved components of the incident beam linearly polarized parallel and perpendicular to the direction of the applied field. A maximum phase difference, δ, occurs when the azimuth angle of the linearly-polarized incident beam is at 45° relative to the applied field. This maximum phase difference is given by

$$\delta = \frac{2\pi l(n_{\parallel} - n_{\perp})}{\lambda_0} \tag{4.4}$$

where l is the path length of the beam through the birefringent medium, $n_{\parallel}$ and $n_{\perp}$ are the refractive indices parallel and perpendicular to the applied field respectively, and λ_0 is the vacuum wavelength of the beam. The phase difference, δ, is related to the Kerr effect through

$$\delta = 2\pi B l E^2 \tag{4.5}$$

where B is the Kerr constant which is a function of the substance under investigation, its temperature, and the vacuum wavelength, λ_0, of the incident beam. E is the applied electric field.

In the experimental part of this work the molar Kerr constant which is reported is defined as[7,8]

$$ {}_mK = \frac{18nV_m}{3(n^2+2)(\epsilon_r+2)^2} \lim_{E\to 0}\left[\frac{n_{\|}-n_{\perp}}{E^2}\right] \tag{4.6} $$

where n and ϵ_r are the refractive index and relative permittivity of the medium (in the absence of the field) respectively. E is the electric field and V_m is the molar volume of the gas under study. The molar volume V_m can be determined using the following equation, provided the pressure P and temperature T are known:

$$ \frac{PV_m}{RT} = 1 + \frac{B_p}{V_m} + \frac{C_p}{V_m^2}. \tag{4.7} $$

Here, B_p and C_p are the second and third pressure virial coefficients respectively. Use was made of a program which iteratively solves the above equation to determine the molar volume of a gas for a predefined pressure and temperature. The second and third pressure virial coefficients B_p and C_p were obtained from recent Landolt-Börnstein tabulations.[19]

The molar Kerr constant ${}_mK$ defined in equation 4.6 can be expressed by the virial expansion

$$ {}_mK = A_K + \frac{B_K}{V_m} + \frac{C_K}{V_m^2} + ..., \tag{4.8} $$

where A_K, B_K and C_K are the first, second and third Kerr-effect virial coefficients. B_K and C_K describe deviations from the zero-density (first) Kerr virial coefficient A_K due to pair and triplet molecular interactions respectively.

For dilute fluids, Otterbein[9] proposed that the molar Kerr constant ${}_mK$ reduces to

$$ {}_mK = \lim_{V_m\to\infty}\left[\frac{2(n_{\|}-n_{\perp})V_m}{27(4\pi\epsilon_0)E^2}\right]_{E\to 0}. \tag{4.9} $$

In order to relate this birefringent behaviour to the molecular property tensors of the sample's individual molecules a system of space-fixed axes $O(x,y,z)$ needs to be established. This system of axes is chosen such that x and y are parallel and perpendicular to the direction of the applied electric flied respectively, while z is in the direction of the propagating beam.

For the case of a dilute fluid having negligible molecular interactions the induced dipole moment $\mu_i^{(p)}$ in molecule p arises purely due to the oscillating electric field ξ_{0j} of the propagating beam. Upon application of a strong static electric field E_i the total dipole moment of a molecule is written as[4]

$$\mu_i = \mu_i^{(0)} + \alpha_{ij}\xi_{0j} + \frac{1}{2}\beta_{ijk}\xi_{0j}E_k + \frac{1}{6}\gamma_{ijkl}\xi_{0j}E_kE_l + ... \tag{4.10}$$

where $\mu_i^{(0)}$ is the permanent electric dipole moment of the molecule, α_{ij} is the molecular polarizability, and β_{ijk} and γ_{ijkl} are the first and second hyperpolarizabilities which describe the distorting effect of the applied field on the polarizability.

And so, when a strong static electric field E_i is applied to the fluid the optical-frequency polarizability α_{ij} is seen to change to a new effective polarizability π_{ij}, written as

$$\pi_{ij} = \frac{\partial \mu_i}{\partial \xi_{0j}} = \alpha_{ij} + \beta_{ijk}E_k + \frac{1}{2}\gamma_{ijkl}E_kE_l + ... \tag{4.11}$$

This new effective polarizability π_{ij} is physically interpreted as the increase in moment per unit increase in field, and has components parallel and perpendicular to the biasing field given by

$$\pi_{xx} = a_i^x a_j^x \pi_{ij} \tag{4.12}$$

and

$$\pi_{yy} = a_i^y a_j^y \pi_{ij} \tag{4.13}$$

respectively. Here, a_i^x is the direction cosine between the x space-fixed and the i molecule-fixed axis and a_j^y is the direction cosine between the y space-fixed and the j molecule-fixed axis.

The differential polarizability for a molecule held in a fixed configuration τ in the presence of a biasing field is written as

$$\pi(\tau, E) = \pi_{ij}(a_i^x a_j^x - a_i^y a_j^y) = (\alpha_{ij} + \beta_{ijk} E a_k^x + \frac{1}{2}\gamma_{ijkl} E^2 a_k^x a_l^x + ...)(a_i^x a_j^x - a_i^y a_j^y) \tag{4.14}$$

in which E_i has been written $E a_i^x$.

Since the molecule is in fact tumbling in space, this quantity has to be averaged over all configurations in the presence of the biasing influence of E_i, and a Boltzmann-type weighting factor may be used to average over molecular configurations τ in the presence of the external field:[4]

$$\overline{\pi} = \frac{\int \pi(\tau, E) e^{-U(\tau,E)/kT} d\tau}{\int e^{-U(\tau,E)/kT} d\tau} \tag{4.15}$$

where $U(\tau, E)$ is the potential energy of the molecule in the presence of the biasing field and in the orientation τ, written as

$$U(\tau, E) = U^{(0)} - \mu_i^{(0)} E_i - \frac{1}{2} a_{ij} E_i E_j - \frac{1}{6} b_{ijk} E_i E_j E_k + ... \tag{4.16}$$

$$= U^{(0)} - \mu_i^{(0)} E a_i^x - \frac{1}{2} a_{ij} E^2 a_i^x a_j^x - \frac{1}{6} b_{ijk} E^3 a_i^x a_j^x a_k^x + ... \tag{4.17}$$

Here, $U^{(0)}$ is the potential energy of the molecule in the absence of the biasing field, $\mu_i^{(0)}$ is the permanent dipole of the molecule and a_{ij} and b_{ijk} are the static polarizability and static first-order hyperpolarizability respectively.

The biased average in equation 4.15 can be converted into an isotropic average by Taylor expanding the differential polarizability $\overline{\pi}$ in terms of E, and writting

$$\overline{\pi} = A + BE + CE^2 + ... \tag{4.18}$$

with

$$A = (\overline{\pi})_{E=0}, B = \left(\frac{\partial \overline{\pi}}{\partial E}\right)_{E=0}, C = \frac{1}{2}\left(\frac{\partial^2 \overline{\pi}}{\partial E^2}\right)_{E=0}. \tag{4.19}$$

In order to be able to determine A, B and C the isotropic averages of the direction cosines need to be evaluated. For this some general results summarized in Barron[10]

$$\left\{ \begin{array}{c} \langle a_i^x \rangle = \langle a_i^y \rangle = \langle a_i^z \rangle = 0 \\ \left\langle a_i^x a_j^x \right\rangle = \left\langle a_i^y a_j^y \right\rangle = \left\langle a_i^z a_j^z \right\rangle = \frac{1}{3}\delta_{ij} \\ \left\langle a_i^x a_j^x a_k^x \right\rangle = \left\langle a_i^y a_j^y a_k^y \right\rangle = \left\langle a_i^z a_j^z a_k^z \right\rangle = \frac{1}{6}\epsilon_{ijk} \end{array} \right\} \tag{4.20}$$

and Buckingham and Pople[7]

$$\left\{ \begin{array}{c} \left\langle a_i^x a_j^x a_k^x a_l^x \right\rangle = \frac{1}{15}(\delta_{ij}\delta_{kl} + \delta_{ik}\delta_{jl} + \delta_{il}\delta_{kj}) \\ \left\langle a_i^z a_j^z a_k^x a_l^x \right\rangle = \frac{1}{30}(4\delta_{ik}\delta_{jl} - \delta_{ij}\delta_{kl} - \delta_{il}\delta_{kj}) \end{array} \right\} \tag{4.21}$$

are required. Now when E=0, A becomes zero (because the isotropic average of the polarizability, $\langle\pi\rangle$, is zero), meaning that no birefringence is being induced in the medium. For determining B when E=0, equation 4.15 is differentiated with respect to E resulting in

$$B = \left(\frac{\partial\overline{\pi}}{\partial E}\right)_{E=0} = \left\langle \frac{\partial\pi}{\partial E} \right\rangle - \frac{1}{k_B T}\left\langle \pi \frac{\partial U}{\partial E} \right\rangle \tag{4.22}$$

where

$$\left\{ \begin{array}{c} \left(\frac{\partial\pi}{\partial E}\right)_{E=0} = \beta_{ijk} a_k^x (a_i^x a_j^x - a_i^y a_j^y) \\ \left(\frac{\partial U}{\partial E}\right)_{E=0} = -\mu_i^{(0)} a_i^x \end{array} \right\}. \tag{4.23}$$

When the isotropic averages of the direction cosines (given in equation 4.20) are implemented in the above equation both terms average to zero over all directions of a_i^x. Now since it has been shown that both A and B evaluate to zero the leading non-vanishing term for the differential polarizability, $\overline{\pi}$, is C. This coefficient is given by[7]

$$C = \frac{1}{2}\left(\frac{\partial^2\overline{\pi}}{\partial E^2}\right) = \frac{1}{2}\left\langle \frac{\partial^2\pi}{\partial E^2} \right\rangle - \frac{1}{2kT}\left\langle 2\frac{\partial\pi}{\partial E}\frac{\partial U}{\partial E} + \pi\frac{\partial^2 U}{\partial E^2} \right\rangle + \frac{1}{2(kT)^2}\left\langle \pi\left(\frac{\partial U}{\partial E}\right)^2 \right\rangle \tag{4.24}$$

where

$$\left\{ \begin{array}{c} \left(\frac{\partial^2\pi}{\partial E^2}\right)_{E=0} = \gamma_{ijkl} a_k^x a_l^x (a_i^x a_j^x - a_i^y a_j^y) \\ \left(\frac{\partial^2 U}{\partial E^2}\right) = -\alpha_{ij} a_i^x a_j^x \end{array} \right\}. \tag{4.25}$$

Buckingham and Pople used the isotropic averages in 4.21 to evaluate the above expressions, and obtained the following relationship between the differential polarizability $\overline{\pi}$ and the biasing field:

$$\overline{\pi} = \left\{ \begin{array}{c} \frac{2}{30}\gamma_{iijj} + \frac{2}{15k_B T}\beta_{iij}\mu_j^{(0)} + \frac{1}{15k_B T}(\alpha_{ij}a_{ij} - 3\alpha a) \\ + \frac{3}{15k_B^2 T^2}(\alpha_{ij}\mu_i^{(0)}\mu_j^{(0)} - \alpha(\mu^{(0)})^2) \end{array} \right\} E^2 \tag{4.26}$$

where α is the mean dynamic polarizability and a is the mean static polarizability given by

$$\left\{ \begin{array}{l} \alpha = \frac{1}{3}(\alpha_{11} + \alpha_{22} + \alpha_{33}) \\ a = \frac{1}{3}(a_{11} + a_{22} + a_{33}) \end{array} \right\}. \tag{4.27}$$

Making use of equations 4.26 and 4.6 as well as the relationship between the difference between refractive indices and the differential polarizability (i.e. $n_x - n_y = \frac{2\pi N_A}{(4\pi\epsilon_0)}\overline{\pi}$) results in the molar Kerr constant for dilute gases becoming

$$ {}_mK = A_K = \frac{2\pi N_A}{405(4\pi\epsilon_0)} \left\{ \begin{array}{c} 2\gamma_{iijj} + \frac{1}{k_BT}\left[4\beta_{iij}\mu_j^{(0)} + 3(\alpha_{ij}a_{ij} - 3\alpha a)\right] \\ + \frac{3}{k_B^2T^2}(\alpha_{ij}\mu_i^{(0)}\mu_j^{(0)} - \alpha(\mu^{(0)})^2) \end{array} \right\}. \tag{4.28} $$

This is the general form of the Langevin-Born equation and takes into account the effect of high field strengths on the polarizability. Simplification of this equation results when considering molecular symmetry. One of the molecules studied in this work is dimethyl ether, which has C_{2v} symmetry. This molecule is taken to lie in the 1-3 plane of the molecule-fixed axes $O(1,2,3)$, where 3 is taken to be the principal molecular axis, so that A_K becomes[2,6]

$$ A_K = \frac{N_A}{81\epsilon_0}\left\{\gamma^K + \frac{1}{k_BT}\left[\frac{2}{3}\mu\beta^K + \frac{1}{5}\Delta\alpha\Delta a\right] + \frac{3}{10}\frac{1}{k_B^2T^2}\mu^2(\alpha_{33} - \alpha)\right\} \tag{4.29} $$

where the first and second Kerr hyperpolarizabilities, β^K and γ^K, are defined by[7]

$$ \left\{ \begin{array}{l} \beta^K = \frac{3}{10}(3\beta_{i3i} - \beta_{ii3}) \\ \gamma^K = \frac{1}{10}(3\gamma_{ijij} - \gamma_{iijj}) \end{array} \right\}. \tag{4.30} $$

The dipole moment μ is along the 3-axis of the molecule giving $\mu = \mu_3^{(0)}$, and the dynamic and static polarizability anistropies, $\Delta\alpha$ and Δa respectively, are defined as:

$$ \left\{ \begin{array}{l} \Delta\alpha = \frac{1}{\sqrt{2}}\left[(\alpha_{11} - \alpha_{22})^2 + (\alpha_{22} - \alpha_{33})^2 + (\alpha_{33} - \alpha_{11})^2\right]^{\frac{1}{2}} \\ \Delta a = \frac{1}{\sqrt{2}}\left[(a_{11} - a_{22})^2 + (a_{22} - a_{33})^2 + (a_{33} - a_{11})^2\right]^{\frac{1}{2}} \end{array} \right\} \tag{4.31} $$

The molar Kerr constant for atomic gases such as argon, and isotropically polarizable molecules such as methane, is

$$ {}_mK = \frac{4\pi N_A}{81(4\pi\epsilon_0)}\gamma^K. \tag{4.32} $$

In such systems, the measurement of the molar Kerr constant results directly from the second Kerr hyperpolarizability γ_K which is proportional to

the temperature-independent term.

When dealing with molecules of lower symmetry there exist two alternative methods for analyzing experimental data. The first requires an estimate of γ from some other experiment (e.g. electric-field-induced second-harmonic generation, ESHG) and to then convert equation 4.29 into a straight-line of the form

$$\left[A_K - \frac{N_A}{81\epsilon_0}\gamma^K\right] T = \frac{N_A}{81\epsilon_0}\frac{1}{k_B}\left[\frac{2}{3}\mu\beta^K + \frac{1}{5}\Delta\alpha\Delta a\right] + \frac{N_A}{270\epsilon_0}\frac{1}{k_B^2 T}\mu^2(\alpha_{33} - \alpha). \tag{4.33}$$

Plotting the left-hand side of the above expression as a function of T^{-1} allows for β_K to be determined from the intercept provided the parameters μ, $\Delta\alpha$ and Δa are known. $(\alpha_{33} - \alpha)$ can be extracted from the slope.

The alternative method for analyzing experimental data for molecules of lower symmetry requires expressing the molar Kerr constant in the form of a polynomial expression[11,12]

$${}_mK = A_K = P + \frac{Q}{T} + \frac{R}{T^2} + ..., \tag{4.34}$$

where P represents the temperature-independent term in equation 4.29. Q and R are the coefficients of the terms in the inverse and inverse square of the absolute temperature, respectively. By fitting a quadratic polynomial in T^{-1} to measured $A_K(T)$ data, the coefficients P, Q and R can be determined and used to calculate Kerr hyperpolarizabilities as well as the polarizability anisotropy $(\alpha_{33} - \alpha)$.

4.3.2 Higher Pressures: Interacting Molecules

At higher pressures molecular interactions become significant and so the previously discussed theory needs to be modified. In this case the molar Kerr constant is expressed as a virial expansion:

$${}_mK = A_K + \frac{B_K}{V_m} + \frac{C_K}{V_m^2} + ... \tag{4.35}$$

where A_K, B_K and C_K are the first, second and third Kerr-effect virial coefficients describing the contributions to the molar Kerr constant due to isolated

molecules, interacting pairs and interacting triplets of molecules, respectively. A_K, the low-density molar Kerr constant, is given in the previous section in equation 4.28. The second Kerr virial coefficient B_K describes deviations of ${}_mK$ arising from the pair-interaction contributions, and is written as

$$B_K = \lim_{V_m \to \infty} ({}_mK - A_K)V_m. \tag{4.36}$$

Buckingham[8] was the first to establish the theory of the second Kerr-effect virial coefficient, B_K. Couling and Graham have since extended the molecular-tensor theory for B_K to molecules of general symmetry.[13] This theory is outlined here and will be used to calculate B_K values for dimethyl ether and trifluoromethane against which the experimental results of this work will be compared. The theory follows the approach first used by Buckingham and Pople.[14]

In the previous section it was noted that birefringence induced in a fluid by the presence of a strong static electric field E_x is

$$n_x - n_y = \frac{2\pi N_A}{(4\pi\epsilon_0)V_m}\overline{\pi} \tag{4.37}$$

where $\overline{\pi}$ is the average over all configurations of $\pi_{ij}(a_i^x a_j^x - a_i^y a_j^y)$ of a representative molecule in the presence of the biasing influence E_x. At higher gas densities the contribution of a representative molecule 1 to the difference between refractive indices, $(n_x - n_y)$, is modified by the presence of a neighbouring molecule 2. Couling and Graham[13] have argued that for two interacting molecules in the specified relative configuration τ, molecule 1's contribution to the induced birefringence is a half of the total contribution of the pair at a particular instant in time, hence written as

$$\frac{1}{2}\left\{\frac{2\pi N_A}{(4\pi\epsilon_0)V_m}\pi^{(12)}(\tau, E)\right\} \tag{4.38}$$

where $\pi^{(12)}$ is defined to be the differential polarizability of the interacting pair in molecule-fixed axes. We can write

$$\pi^{(12)}(\tau, E) = \pi_{ij}^{(12)}(a_i^x a_j^x - a_i^y a_j^y). \tag{4.39}$$

The pair of interacting molecules is considered to be held in a fixed relative configuration τ and is allowed to rotate as a rigid whole in the presence of

the biasing electric field E_i. The biased orientational average $\overline{\pi^{(12)}(\tau, E)}$ is converted into an isotropic average by Taylor expanding in powers of E. The leading non-vanishing term in the series expansion is proportional to E^2 and is given by

$$\overline{\pi^{(12)}(\tau, E)} = \frac{1}{2}\left(\frac{\partial^2 \overline{\pi^{(12)}(\tau, E)}}{\partial E^2}\right)_{E=0} E^2 \tag{4.40}$$

where

$$\begin{aligned}\tfrac{1}{2}\left(\frac{\partial^2 \overline{\pi^{(12)}(\tau,E)}}{\partial E^2}\right)_{E=0} &= \tfrac{1}{2}\left\langle \frac{\partial^2 \pi^{(12)}}{\partial E^2}\right\rangle - \frac{1}{2kT}\left\langle 2\frac{\partial \pi^{(12)}}{\partial E}\frac{\partial U^{(12)}}{\partial E} + \pi^{(12)}\frac{\partial^2 U^{(12)}}{\partial E^2}\right\rangle \\ &+ \frac{1}{2k^2T^2}\left\langle \pi^{(12)}\left(\frac{\partial U^{(12)}}{\partial E}\right)^2\right\rangle\end{aligned} \tag{4.41}$$

and $U^{(12)}(\tau, E)$ is the potential energy of the interacting pair of molecules in the presence of the applied field E_i. Including the pair interactions the molar Kerr constant is now written as

$${}_mK = A_K + \int_\tau \frac{2\pi N_A}{27(4\pi\epsilon_0)}\left\{\frac{1}{2}\left(\frac{\partial^2 \overline{\pi^{(12)}(\tau, E)}}{\partial E^2}\right)_{E=0} - \left(\frac{\partial^2 \overline{\pi}}{\partial E^2}\right)_{E=0}\right\} P(\tau)d\tau. \tag{4.42}$$

$P(\tau)d\tau$ is the probability of molecule 1 having a neighbouring molecule in the range τ to $\tau + d\tau$, and is related to the intermolecular potential $U_{12}(\tau)$ by

$$P(\tau) = \frac{N_A}{\Omega V_m} e^{-U_{12}(\tau)/k_B T} \tag{4.43}$$

where Ω denotes the integral over the orientational coordinates of the neighbouring molecule 2 and is given by $\Omega = V_m^{-1}\int d\tau$. After implementing equations 4.35 and 4.42 the second Kerr virial coefficient B_K now takes the form[13,15]

$$B_K = \frac{2\pi N_A^2}{27\Omega(4\pi\epsilon_0)}\int_\tau \left\{\frac{1}{2}\left(\frac{\partial^2 \overline{\pi^{(12)}(\tau, E)}}{\partial E^2}\right)_{E=0} - \left(\frac{\partial^2 \overline{\pi}}{\partial E^2}\right)_{E=0}\right\} e^{-U_{12}(\tau)/k_B T} d\tau. \tag{4.44}$$

For interacting pairs of molecules with symmetry that is lower than linear, B_K can be expressed as:[13,15]

$$B_K = \frac{N_A^2}{216\pi^2(4\pi\epsilon_0)} \int_{R=0}^{\infty} \int_{\alpha_1=0}^{2\pi} \int_{\beta_1=0}^{\pi} \int_{\gamma_1=0}^{2\pi} \int_{\alpha_2=0}^{2\pi} \int_{\beta_2=0}^{\pi} \int_{\gamma_2=0}^{2\pi} \tag{4.45}$$
$$\times \left\{ \frac{1}{2} \left(\frac{\partial^2 \overline{\pi^{(12)}(\tau, E)}}{\partial E^2} \right)_{E=0} - \left(\frac{\partial^2 \overline{\pi}}{\partial E^2} \right)_{E=0} \right\} \times e^{-U_{12}(\tau)/k_B T}$$
$$\times R^2 sin\beta_1 sin\beta_2 dR d\alpha_1 d\beta_1 d\gamma_1 d\alpha_2 d\beta_2 d\gamma_2.$$

Here, as in Chapter 3, the interaction coordinates are expressed by Euler angles and the intermolecular displacement by R.

Due to the fact that the molecules in the interacting pair are within close proximity to each other, the dipole moment is not induced solely by the oscillating field of the incident light beam ξ_{0i}, but also by the field $F_i^{(1)}$ at molecule 1 due to the oscillating moment of the neighbouring molecule 2. For this interacting pair the dipole moment of molecule 1 is then given as

$$\mu_i^{(1)}(\xi_0) = (\alpha_{ij}^{(1)} + \beta_{ijk}^{(1)} E_k + \frac{1}{2} \gamma_{ijkl}^{(1)} E_k E_l + ...)(\xi_{0j} + F_j^{(1)}) \tag{4.46}$$

where the relationship between the dipole moment of molecule 2 and the field due to this oscillating moment at the origin of molecule 1 is described via a T-tensor:

$$F_i^{(1)} = T_{ij}^{(1)} \mu_j^{(2)}. \tag{4.47}$$

Using the same reasoning as above, the dipole moment of molecule 2 is given as

$$\mu_i^{(2)}(\xi_0) = (\alpha_{ij}^{(2)} + \beta_{ijk}^{(2)} E_k + \frac{1}{2} \gamma_{ijkl}^{(2)} E_k E_l + ...)(\xi_{0j} + F_j^{(2)}). \tag{4.48}$$

In turn, the electric field due to the oscillating dipole moment of molecule 1 arising at the origin of molecule 2 is given as

$$F_i^{(2)} = T_{ij}^{(2)} \mu_j^{(1)}. \tag{4.49}$$

In order to obtain the expression for the total dipole moment of molecule 1, equations 4.48 and 4.49 are substituted into equation 4.47. This expression is then substituted into equation 4.46 producing the total oscillating dipole moment induced on molecule 1 by the light-wave field in the presence of molecule 2. Differentiating this expression with respect to ξ_{0i} yields the differential polarizability of a general molecule p in the presence of the applied

static field and the neighbouring molecule q. These last two expressions, the total oscillating dipole moment induced on molecule 1 by the light-wave field and the differential polarizability of a general molecule, are too lengthy to reproduce here, and have been omitted, but may be found in references 13 and 16.

In the molecule-fixed frame (for a specific interaction configuration τ of molecules p and q) the difference between differential polarizabilities is written as

$$\pi^{(p)}(\tau, E) = \pi_{ij}^{(p)}(a_i^x a_j^x - a_i^y a_j^y). \tag{4.50}$$

We now assume that each of the molecules in the interaction pair retain their separate identities. In the long-range limit, this assumption is valid. However, when molecules come so close to each other that their charge distributions overlap, *ab initio* quantum calculations need to be used. Such an analysis is beyond the scope of this work, and so we treat the interacting molecules as if they maintain their separate identities even in the overlap region of their charge distributions. Hence the total dipole moment of these interacting molecules can be written as[14,17]

$$\mu_i^{(12)} = \mu_i^{(1)} + \mu_i^{(2)}, \tag{4.51}$$

and the differential polarizability of the interacting pair becomes

$$\pi_{ij}^{(12)} = \frac{\partial \mu_i^{(12)}}{\partial \xi_{0j}} = \frac{\partial(\mu_i^{(1)} + \mu_i^{(2)})}{\partial \xi_{0j}}. \tag{4.52}$$

And so the difference between the differential polarizabilities, $\pi_{ij}^{(12)} a_i^x a_j^x$ and $\pi_{ij}^{(12)} a_i^y a_j^y$ of the interacting pair in the presence of an applied field becomes

$$\begin{aligned} \pi^{(12)}(\tau, E) &= \pi_{ij}^{(12)}(a_i^x a_j^x - a_i^y a_j^y) \\ &= (\pi_{ij}^{(1)} + \pi_{ij}^{(2)})(a_i^x a_j^x - a_i^y a_j^y) \\ &= \pi^{(1)}(\tau, E) + \pi^{(2)}(\tau, E). \end{aligned} \tag{4.53}$$

The potential energy of the interacting pair in the presence of the biasing electric field is written as

$$U^{(12)}(\tau, E) = U^{(12)}(\tau, 0) - \int_0^E \mu_i^{(12)}(\tau, E) a_i^x dE. \tag{4.54}$$

The dipole moment of molecule p in the presence of another molecule q and in the presence of an applied field can be generally written as:

$$\mu_i^{(p)} = \mu_{0i}^{(p)} + a_{ij}^{(p)}(E_j + F_j^{(p)}) \tag{4.55}$$

where $F_j^{(p)}$ is the static field arising at molecule p when E_i and molecule q are present and $\mu_{0i}^{(p)}$ is the permanent dipole moment of molecule p. As previously seen, such a field can be related to the inducing dipole moment via a T-tensor:

$$F_i^{(p)} = T_{ij}\mu_j^{(q)}. \tag{4.56}$$

Similarly the dipole moment of molecule q is expressed as

$$\mu_i^{(q)} = \mu_{0i}^{(q)} + a_{ij}^{(q)}(E_j + F_j^{(q)}) \tag{4.57}$$

where the field $F_i^{(q)}$ is once again related to the inducing dipole moment via a T-tensor:

$$F_i^{(q)} = T_{ij}\mu_j^{(p)}. \tag{4.58}$$

A series of substitutions (similar to those carried out in equations 4.46 to 4.49) for determining the total oscillating dipole moment of molecule 1 are carried out for the above equations (4.55 to 4.58). And so the potential energy for the interacting pair is obtained:

$$U^{(12)}(\tau, E) = U^{(12)}(\tau, 0) + U^{(1)}(\tau, E) + U^{(2)}(\tau, E) \tag{4.59}$$

We are now in a position to determine the expression for B_K. Assuming that the molecules retain their separate identities, equation 4.41 becomes:

$$\begin{aligned}\tfrac{1}{2}\left(\frac{\partial^2\overline{\pi^{(12)}(\tau,E)}}{\partial E^2}\right)_{E=0} &= \left\langle\tfrac{\partial^2\pi^{(1)}}{\partial E^2}\right\rangle - \tfrac{1}{k_BT}\left\{\left\langle 2\tfrac{\partial\pi^{(1)}}{\partial E}\tfrac{\partial U^{(1)}}{\partial E}\right\rangle + \left\langle 2\tfrac{\partial\pi^{(1)}}{\partial E}\tfrac{\partial U^{(2)}}{\partial E}\right\rangle\right\} \\ &\quad - \tfrac{1}{k_BT}\left\{\left\langle\pi^{(1)}\tfrac{\partial^2U^{(1)}}{\partial E^2}\right\rangle + \left\langle\pi^{(1)}\tfrac{\partial^2U^{(2)}}{\partial E^2}\right\rangle\right\} \\ &\quad + \tfrac{1}{k_B^2T^2}\left\{\left\langle\pi^{(1)}\left(\tfrac{\partial U^{(1)}}{\partial E}\right)^2\right\rangle + 2\left\langle\pi^{(1)}\tfrac{\partial U^{(1)}}{\partial E}\tfrac{\partial U^{(2)}}{\partial E}\right\rangle + \left\langle\pi^{(1)}\left(\tfrac{\partial U^{(2)}}{\partial E}\right)^2\right\rangle\right\}.\end{aligned} \tag{4.60}$$

The above equation is simplified using isotropic averages:[15]

$$\begin{aligned}\left\{\frac{1}{2}\left(\frac{\partial^2\overline{\pi^{(12)}(\tau,E)}}{\partial E^2}\right)_{E=0} - \left(\frac{\partial^2\overline{\pi}}{\partial E^2}\right)_{E=0}\right\} &= \alpha_2 + \alpha_3 + \alpha_4 + \alpha_5 + \ldots \\ &\quad + \gamma_1\alpha_1 + \gamma_1\alpha_2 + \ldots \\ &\quad + \mu_2\alpha_1 + \mu_2\alpha_2 + \mu_2\alpha_3 + \ldots \\ &\quad + \mu_1\beta_1 + \mu_1\beta_1\alpha_1 + \ldots.\end{aligned}$$

The sometimes very lengthy explicit equations for each of these terms has been omitted but can be found in[13].

In the computation of B_K the intermolecular energy is required. In their work Couling and Graham[13] used the classical potential

$$U_{12}(\tau) = U_{LJ} + U_{\mu,\mu} + U_{\mu,\theta} + U_{\theta,\theta} + U_{\mu,ind\ \mu} + U_{\theta,ind\ \mu} + U_{shape} \qquad (4.61)$$

where U_{LJ} is the Lennard-Jones potential, and $U_{\mu,\mu}$, $U_{\mu,\theta}$ and $U_{\theta,\theta}$ are the dipole-dipole, dipole-quadrupole and quadrupole-quadrupole interaction energies of the interacting pair. $U_{\mu,ind\ \mu}$ and $U_{\theta,ind\ \mu}$ are the dipole-induced-dipole and quadrupole-induced-dipole interaction energies. The shape potential U_{shape} accounts for the angular dependence of short-range repulsive forces for molecules having a non-spherical shape.

The interaction energies are symmetry dependent and are expressed in terms of direction cosines through the use of Euler angles. These expressions have been determined[16,18] and the shape potential is given as[16]:

$$U_{shape} = 4\epsilon \left(\frac{R_0}{R}\right)^{12} \left\{D_1[3cos^2\beta_1 + 3cos^2\beta_2 - 2] + D_2[3sin^2\beta_1 cos^2\gamma_1 + 3sin^2\beta_2 cos^2\gamma_1 - 2]\right\} \qquad (4.62)$$

By using the above expressions numerical values for B_K can be calculated and then compared against the experimental data.

4.4 References

1. G. R. Fowles, *Introduction to Modern Optics*, New York, Holt, Rinehart and Winston, 1968, 191-192.

2. A. Singh, MSc thesis, University of KwaZulu-Natal, 2005.

3. R. Guenther, *Modern Optics*, New York, John Wiley and Sons, 1990, 571.

4. M. Evans and S. Kielich, *Modern Nonlinear Optics* part 2, New York, John Wiley and Sons, 1993,361-414.

5. www.wikipedia.org/wiki/Kerr Effect.

6. T. J. Sono, MSc thesis, University of Natal, 2003.

7. A. D. Buckingham and J. A. Pople, *Proc. Phys. Soc. A,* 1955, **68**, 905

8. A. D. Buckingham, *Proc. Phys. Soc. A,* 1955, **68**, 910

9. G. Otterbein, *Phys. Z,* 1934, **35**, 249

10. L. D. Barron, *Molecular Light Scattering and Optical Activity,* Cambridge University Press, Cambridge, 1982

11. I. R. Gentle, D. R. Laver and G. L. D. Ritchie, *J. Phys. Chem.*, 1990, **94**, 3434

12. V. W. Couling, B. W. Halliburton, R. I. Keir and G. L. D. Ritchie, *J. Phys. Chem. A*, 2001, **105**, 4365

13. V. W. Couling and C. Graham, *Mol. Phys.*, 1998, **93**, 31

14. A. D. Buckingham and J. A. Pople, *Faraday Soc. Disc.*, 1956, **22**, 17

15. V. W. Couling PhD thesis, University of Natal, 1995

16. V. W. Couling and C. Graham, *Mol. Phys.*, 1996, **87**, 779

17. A. D. Buckingham, P. A. Galwas and Liu Fan-Chen, *J. Mol. Struct.*, 1983, **100**, 3

18. A. D. Buckingham, *Adv. Chem. Phys.*, 1967, **12**, 107

19. Landolt-Börnstein, Inorganic Compounds

20. A. D. Buckingham and B. J. Orr, *Trans. Farad. Soc.*, 1969, **65**, 673.

Chapter 5

Experiment - The Kerr Effect

5.1 Introduction

We have chosen to measure the Kerr effect for dimethyl ether and fluoromethane. The reasons for this are that polar molecules produce a birefringence which is orders of magnitude larger than that for nonpolar molecules, hence making measurement of the effect more readily accessible. In addition, these molecules have already been investigated[8,9], and so we have a benchmark against which to test our results. The earlier measurements were performed at relatively low pressures, so that the extracted second Kerr-effect virial coefficients B_K appear with very large error bars. One of the aims of this work was to obtain more precise B_K data against which to compare values computed using our molecular-tensor theories over a large temperature range. This approach should deepen our understanding of molecular interaction phenomena

Accurate temperature control of the cell is important, and the experiment should be able to be run over a wide range of temperature, typically from around 0 to 200^0C. Low-temperature measuremnts are particularly useful, since one is attempting to orient molecules, whereas the thermal energy of the system tends to randomise the induced molecular orientation.[1]

The setup of the experiment has been developed over the last few years and was inherited from a previous masters student, Mr Sono.[3] Modifications made to the arangement will be discussed in the relevant sections. This

chapter begins with a brief overview of the experiment and the apparatus used.

5.2 Brief Overview of the Experiment

In this experiment we wish to obtain measured values for the phase difference, δ, induced between the coherent components of an incident linearly-polarized light beam resolved parallel and perpendicular to the applied electric field as the beam traverses a gas. This phase difference allows for calculation of the molar Kerr constant. The experiment requires a cell containing a gas sample situated in the presence of an accurately-known electric field.

In our experiment, a helium-neon laser provides the monochromatic linearly-polarized light. The laser beam is passed through a polarizer having its transmission axis set at 45° to the applied electric field. Before the light passes through the applied electric field the components of the light vibrating parallel and perpendicular to the field are in phase with each other. The beam then passes through the Kerr cell which is situated in a well-insulated oven.

Once the light emerges from the birefringent medium a phase difference as described above has been induced, and the beam is elliptically polarized. To find the magnitude of the induced phase difference, use is made of a compensator which comprises a quarter-wave plate in conjunction with a Faraday cell, an analyzer and photodiode detector. Since the light emerging from the cell is elliptically polarized, it is passed through a quarter-wave plate, which converts the beam back into linearly polarized light, but with its axis of polarization rotated from the initial 45° position by an angle $\theta = \frac{\delta}{2}$.

After emerging from the quarter-wave plate the now linearly-polarized light passes through a Faraday cell, which is used to rotate the plane of polarization of the beam back to its initial plane of 45° to the applied electric field. By precisely measuring this rotation, the value of the phase difference δ induced by the Kerr cell can be determined. Since the phase difference is tiny, at around a millionth of a radian, the technique of phase-sensitive detection proves useful in extracting the signal from the background noise. This method of detection requires modulation of the signal, which can be

detected using a photodiode, the signal from which is fed to the lock-in amplifier. To achieve modulation, a high ac voltage of frequency ω is applied to the Kerr electrodes, and since the effect is quadratic in the field, the phase difference varies with frequency 2ω. A quarter-wave plate and ac Faraday cell is used as the compensator, nulling the Kerr signal. The PSD output is monitored by a Hewlett Packard data-acquisition unit (DAC) controlled by a personal computer (PC). The data are record and analyzed on the PC via an HP BASIC program which was written by Dr Couling and Mr Sono,[3] and later modified during the course of this project.

The intensity reaching the photodiode can be defined as follows[2]:

$$I_f = \frac{-I_0}{2}(4\epsilon\theta + 2\epsilon\delta) \tag{5.1}$$

where ϵ is the offset of the quarter-wave plate, θ is the nuling rotation from the Faraday cell and δ is the retradance in the Kerr cell. Illustrating that the imperfection in the quarter-wave plate, κ, is negligible.

This experiment also requires electronic devices such as a high-voltage power supply (which is used to generate the electric field across the medium of interest), a waveform synthesizer (which provides the sinusoidal signal), a phase shifter and frequency doubler (which ensure that the signal to the Faraday cell is of the same frequency as that from the Kerr cell, and exactly in anti-phase to it).

Although the process of taking measurements and determining the induced phase difference from the collected data (which in turn allows for calculation of the molar Kerr constant) is achieved by the computer program there are tasks that need to be performed manually. Some of these tasks include calibrations of the high voltage power supply, the pressure transducer and the Faraday cell, all of which feature later in this chapter. Another parameter which needs to be manually adjusted is the phase of the Faraday cell which needs to be in anti-phase to the signal emerging from the Kerr cell. This is done before each experimental run to minimize drifts, and is achieved by switching off the signal to the Faraday cell and feeding the signal from the Kerr cell to the PSD, while the high voltage is applied. The phase on the PSD is then set to be -180°. The high voltage is switched off and the Faraday cell powered up, the phase of the voltage supplying the Faraday cell being

shifted to 0° on the PSD. When the high voltage is reapplied to the Kerr cell it is in anti-phase to that of the Faraday cell, which ensures that it is a nulling signal. Measurements can then be recorded by the computer.

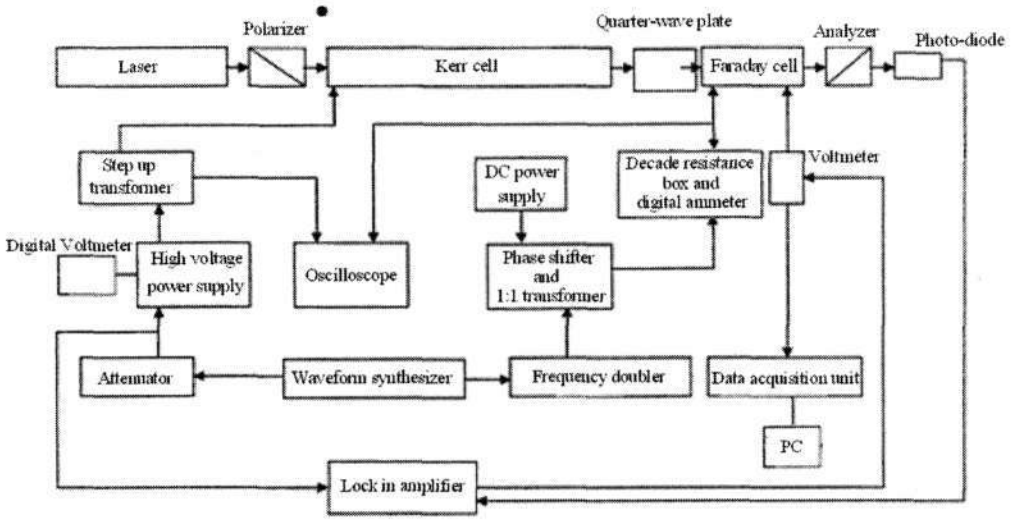

Figure 5.1: Block diagram of the experimental set-up

The components used in the experimental set-up for determining the Molar Kerr Constant are now discussed.

5.3 Apparatus

The apparatus for this work can be broadly categorized into either optical components or electronic components. Other components of the apparatus which do not fall into these two categories, but which are essential to the experiment, are listed separately (e.g. the optical bench, the Kerr Cell and the gas line).The optical train includes the laser, the polarizing and analysing prisms (which manipulate the state of polarizaton of the beam), the quarter-wave plate, the Faraday cell and the photodiode detector. The electronic components include apparatus to monitor the temperature of the oven as well as to acquire the experimental data.

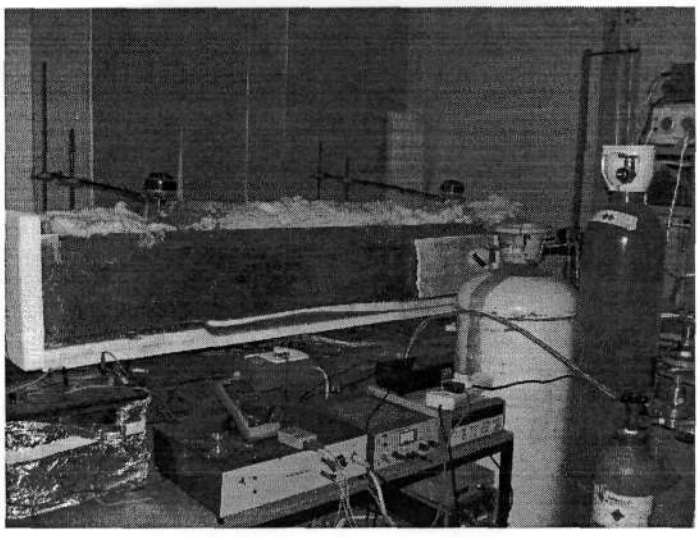

Figure 5.2: Photo of the Kerr-effect laboratory

5.3.1 The Optical Bench

The optical bench consists of a 4.25 m by 25 cm vibration-damped concrete slab 60 cm in height, which provides support for a metallic optical bench. The concrete slab is damped by resting on top of a 10 cm cork foundation. Any mechanical vibrations while the experiment is running will introduce excess contributions to the signal noise, and the cork is responsible for minimizing these vibrations. The metallic optical bench is made from mild-steel C-bar 4 m long, 23 cm wide and 9 cm high, resting on anti-vibration pads. A side arm concrete slab, also resting on a 10 cm cork foundation, is joined perpendicular to the initial wall and supports a metallic optical bench joined perpendicularly to the main bench, the purpose of which is to increase the stability of the optical bench. The optical components are attached to the optical bench by means of magnetic bases, while an adjustable brass screw-bolt system is used to support the Kerr cell.

5.3.2 The Optical Components

The Laser

In this work a Melles-Griot 25-LHP-928 linearly-polarized He-Ne laser is used. It produces a continuous-wave monochromatic beam having a wave-

length of 632.8 nm. The magnetic bases supporting the laser have fine-control adjustors allowing for fine directional adjustment, providing for precise alignment of the beam. The beam is collimated by means of a 2 m focal-length converging lens placed in front of the laser.

The laser was aligned by first removing the cell and making sure that the beam travelled parallel to the optical rail, while falling on the centre of the analyzing prism. Once the cell was placed back in the oven, the position of the oven was adjusted to accommodate the beam. Aligning the laser by this method eliminated the possibility of having multiple reflections off the electrodes. It was established that during Sono and Singh's work the beam emerging from the Kerr cell had in fact undergone multiple reflections which would have compromized the polarization state of the emergent beam. This probably accounts for the discrepancies in the results between this work and theirs.

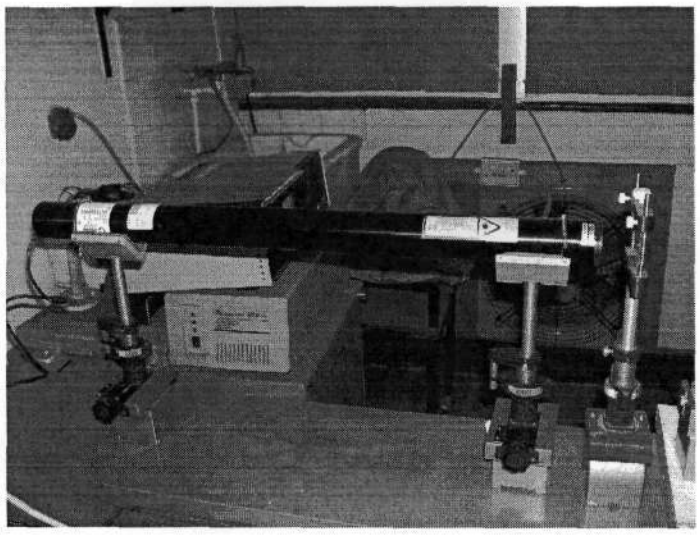

Figure 5.3: Photo of the laser

The Polarizer

In this experiment a Glan-Thompson prism with an extinction ratio of 10^6 was used as the polarizer. The polarizing prism is housed in a divided circle having a resolution of 2 minutes of arc. The prism housing was attached to

an aluminum rod and inserted into a magnetic holder.

A linear polarizer transmits light polarized in a single plane. The transmission axis of a linear polarizer corresponds to the direction of the emerging light's oscillating electric field. In our experiment we have almost linearly-polarized light, vibrating in a plane at 45° to the vertical, emerging from the laser, and which is passed through the linear polarizer with its transmission axis set at 45° to the vertical. This ensures that the components of the light wave parallel and perpendicular to the applied E-field are initially equal in magnitude. The method used to obtaining true vertical for the polarizer is discussed later in the chapter.

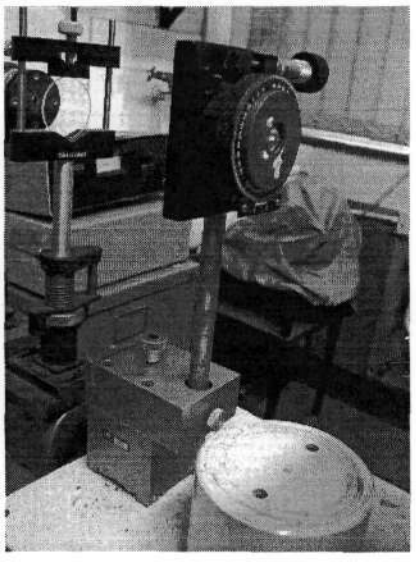

Figure 5.4: Photo of the polarizer

The Quarter-wave Plate

In this work we have made use of a zero-order quarter-wave plate with a retardance of $\frac{\pi}{2}$ for a wavelength of 632.8 nm. The quarter-wave plate is used to convert the elliptically-polarized light emerging from the Kerr cell back into linearly-polarized light. It is housed in a divided circle (similar to the polarizer), and a stepper motor is connected to the divided circle to automatically offset the quarter-wave plate from its null position of 45° for

the fast axis.

The signal arriving at the detector needs to be brought to a minimum value by a compensating device placed between the Kerr cell and analyzer. The compensating device used in this work is a Faraday cell in conjunction with the quarter-wave plate.

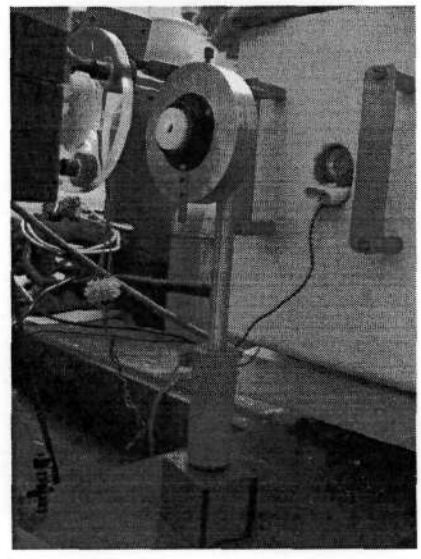

Figure 5.5: Photo of the quarter-wave plate

The Faraday Cell

The Faraday cell consists of a copper-wire coil with 100 turns which surrounds a thinner copper-wire coil of 10 000 turns. A glass tube 400 mm long with a 12 mm internal diameter, and filled with toluene, is situated in the cavity of both coils. Pockels-glass windows are sandwiched between teflon washers and attached to either end of the tube.

The Faraday cell in conjunction with the quarter-wave plate is used to compensate the phase difference induced in the beam while it propagates through the cell. The Faraday cell rotates the linearly-polarized light emerging from the quarter-wave plate back to a null position. The light emerging from the quarter-wave plate is offset by an angle $\theta = \frac{\delta}{2}$ where δ is the induced phase

difference. Therefore the induced phase difference can be determined from the amount of current required by the Faraday cell coil to rotate the linearly-polarized light back to its null position, provided the Faraday cell has been accurately calibrated.

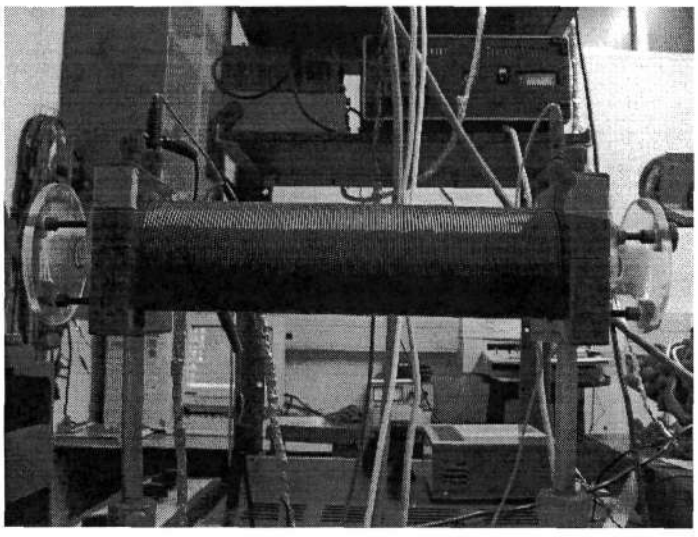

Figure 5.6: Photo of the Faraday cell

The Analyzing Prism

The analyzer prism is a Glan-Taylor prism embedded in a cork support and housed in a rotating device. The analyzing system was built and designed by Imrie[5]. A micrometer placed 1.0415 m from the axis of rotation of the analyzer is used to make fine rotations of the prism. If coarse rotations need to be made the micrometer can be disengaged. Due to the distance between the prism and the micrometer the calibration of the micrometer is found to be

$$\theta = s \times 0.0243879, \tag{5.2}$$

where θ is the rotation of the prism in radians and s the distance the micrometer moves in inches. This equation is required in the calibration of the Faraday cell.

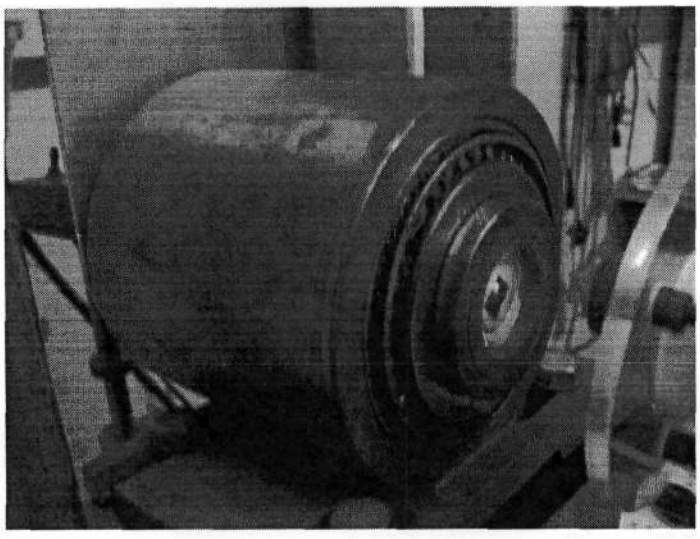

Figure 5.7: Photo of the analyzing prism

The Detector

The element at the end of the optical bench is the photodiode detector, which is used to measure the intensity of the light emerging from the analyzer. It is connected to the phase-sensitive detector by means of a screened coaxial cable.

The Kerr Cell

The Kerr cell consists of a cylinder to hold the electrodes and the gas under investigation, a bulkhead which permits feedthrough for the high voltage to the electrodes, a gas inlet, a pair of flanges onto which end-plates with windows can be bolted, and an adjustable cell stand. The cell containing the fluid of interest should be chemically inert so that a range of potentially corrosive fluids can be studied. The cell is a 316-stainless steel cylinder of length 1.450 m having internal diameter 54.4 mm and wall thickness 3.8 mm.

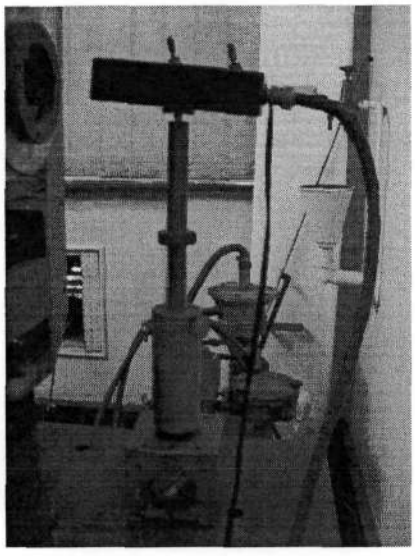

Figure 5.8: Photo of the photodiode detector

A flange of diameter 10.5 cm is welded onto each end of the cell so as to allow end caps to be bolted in place. The end caps, two flat stainless steel disks, also having diameter 10.5 cm, are 1.0 cm in thickness each with a central hole of 0.5 cm. Pockels glass is sandwiched between teflon seals and held in place by a smaller disk which is attached using Alan screws. Pockels glass is used as it has low residual strain even when under mechanical stress, and hence introduces minimal stray birefringence into the experiment. To prevent the windows from being damaged by the corrosive gases the windows are coated with a 0.5 μm layer of quartz. An AC voltage is applied to one of the stainless-steel electrodes while the other electrode is grounded. The electrodes are aligned by magnifying the diffraction pattern of the beam emerging from the cell onto a wall by means of a lens. In order for the electrodes to be aligned correctly the diffraction lines in the beam need to be perfectly horizontal as determined by a laser level.

Two stainless-steel electrodes were used to generate the required electric field. The two electrodes are close to parallel over their entire length of 1.468 m and width of 3.2 cm, with a spacing of $\overline{d} = (3.107 \pm 0.004)$ mm. Small blocks of Macor ceramic serve as electrode spacers, this material being an excellent insulator. The electrodes are held together by spring-loaded ring supports

made from teflon. The electric field needs to be uniform over the entire length of the electrodes and therefore it is important that the electrodes be flat and smooth. This was achieved by hand-polishing in the Mechanical Instrument Workshop. The edges of the electrodes were rounded so as to avoid corona points at sharp edges, since this would lead to unwanted breakdowns in the cell. The procedure employed in the polishing process is described fully in Sono's[3] thesis.

The experiment requires that the components be absolutely clean, and this was achieved by washing with soap solution followed by several rinses with distilled water, acetone and then ethanol. The cell was then placed back in the oven and the oven was left on at 120^0C overnight with the cell under vacuum to remove any remaining moisture.

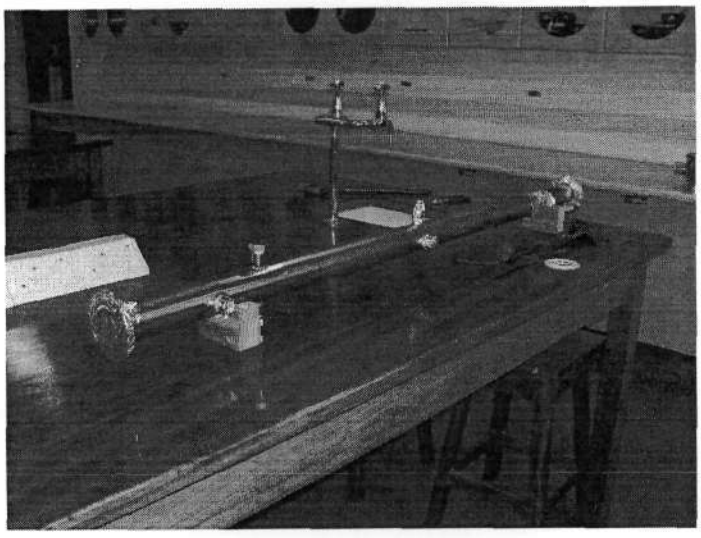

Figure 5.9: Photo of the Kerr cell

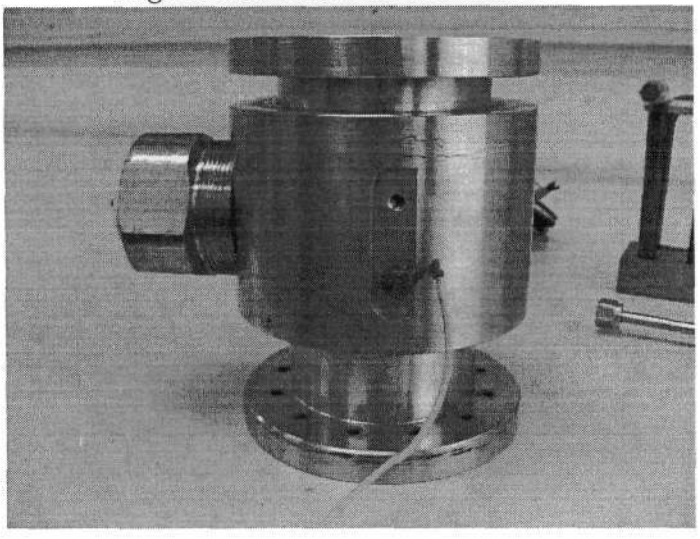

Figure 5.10: Photo of the bulk head

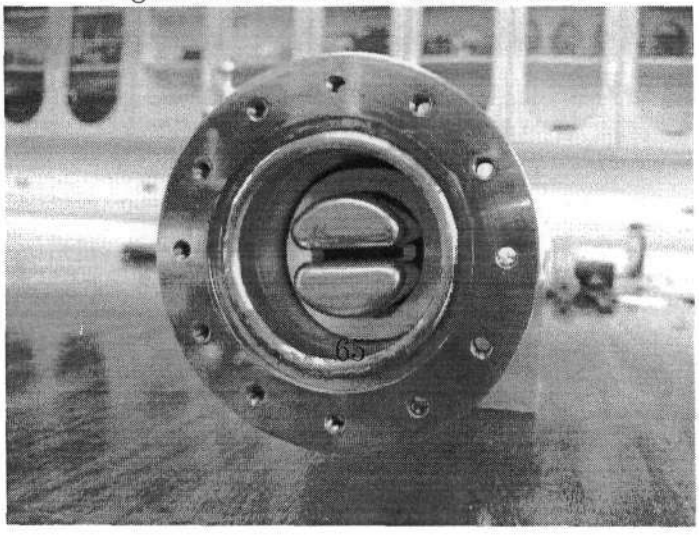

Figure 5.11: End-on view of the electrodes

5.3.3 The Gas Line

$\frac{1}{4}$-inch Hoke 316-stainless-steel tubing is used to construct the gas line. The gas is initially filtered by means of a sintered glass filter with porosity 15 to 40 μm, and a 0.22 μm Millipore filter is used to further filter the gas ensuring that it reaches the cell free of dust particles. A flexible stainless-steel hose connects the cell and the gas line allowing for independent movement of the cell during alignment of the electrodes with respect to the beam.

The admittance and removal of gas samples is facilitated by inlet and outlet taps to and from the Kerr cell, and the rate of gas flow is controlled by a fine-metering valve. The system is designed such that gas can be admitted or evacuated without opening the oven, thereby maintaining the oven equilibrium temperature.

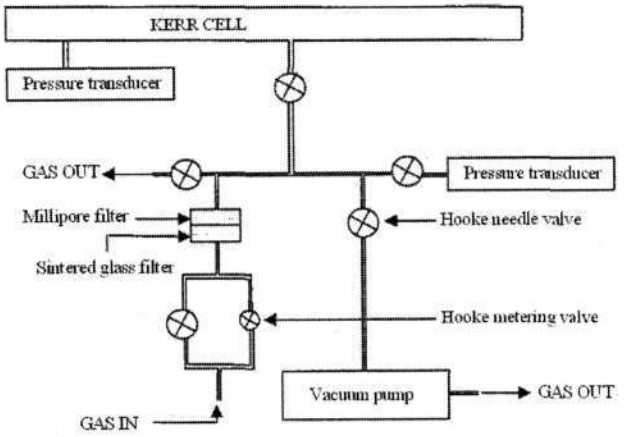

Figure 5.12: Block diagram of the gas line

5.3.4 The Electronic Components

The Waveform Synthesizer

A Phillips PM5190-LF synthesizer was used to produce a sinusoidal signal of frequency 363 Hz and peak-to-peak voltage 1.41 V. Part of this signal

was attenuated to 50 mV rms and fed to the high-voltage power supply. The other part was fed to the Faraday cell through a frequency doubler and phase shifter. The signal from the synthesizer was also used as a reference signal for the phase-sensitive detector. To avoid the mains frequency of 50 Hz or its harmonics from interfering with the signal being detected, a frequency of 363 Hz was chosen as the reference frequency.

Figure 5.13: Photo of the waveform synthesizer

The Phase-Sensitive Detector (PSD)

In order to obtain measurements of the induced phase difference δ, the signal from the photodiode is fed to a phase-sensitive detector. An EG&G Princeton Applied Research model-5210 lock-in amplifier was used throughout. The phase-sensitive detector is used by feeding in a reference signal (in this case the signal from the waveform synthesizer) and the signal to be analyzed (in this case the signal from the photo-detector). The phase-sensitive detector extracts from the photo-detector only the signal with the same frequency as that of the reference signal, or its harmonics, as required. All other frequencies are rejected as noise.

Figure 5.14: Photo of the phase-sensitive Detector

The High-Voltage Power Supply

The power supply is connected to a step-up transformer which converts 1 V ac to 1 kV ac. Two transformers are used in this process: a primary transformer which steps up the signal by a factor of 1000, an insulated high-tension connector allowing it to be applied to the electrode via the bulkhead connector; and a secondary transformer which steps the signal back down by a factor of 1000. This stepped-down signal is fed back to the high-voltage power suppply, allowing it to monitor the driving signal accurately to within 0.1%. Part of this feedback signal is then converted into a dc signal by a precision rectifier, so that 1 V dc corresponds to 1000 V rms ac signal on the high-voltage output, thereby allowing us to precisely measure the ac voltage applied to the cell. The calibration of the high-voltage power supply is discussed in section 5.5.3. Mr Woodley from the Electronics Centre built the transformer as well as the amplifier. Aluminium foil is wrapped around the transformer to minimise the radiation of stray fields which could interfere with the detection electronics. The bottom electrode in the Kerr cell is connected to the output of the high-voltage tranformer while the other electrode is grounded. An electric field is thereby generated in the cell.

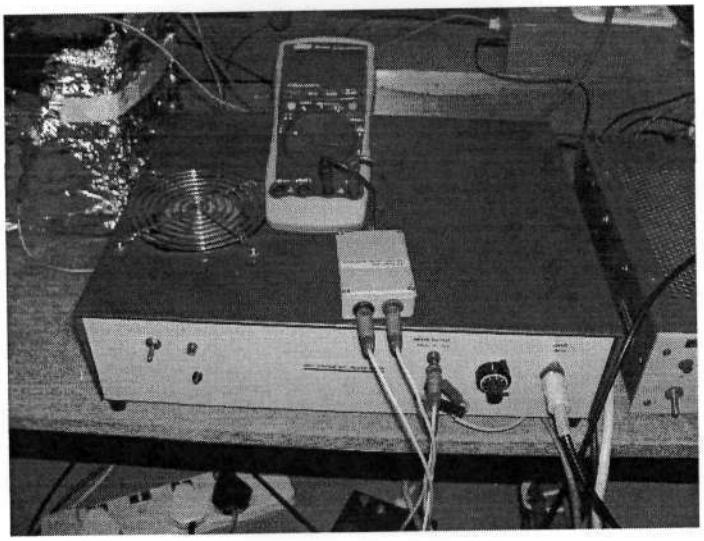

Figure 5.15: Photo of the high-voltage power supply

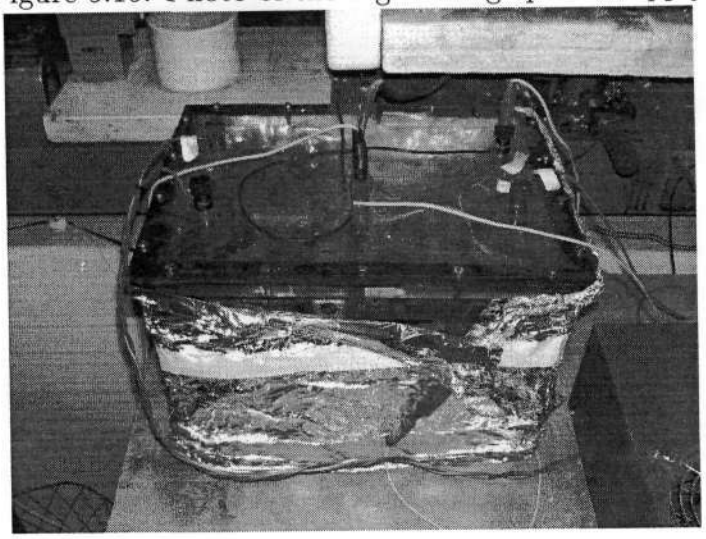

Figure 5.16: Photo of the high-voltage transformer

The Automated System: Data Acquisition and Computer Control

The program used to control and analyze the data is written in HP BASIC and an IEEE interface is used to enable communication and interaction between the various pieces of equipment, including the data-acquisition unit, the multimeter and the high-voltage power supply. Communication between the computer and the apparatus is made possible through the data-acquisition unit, which receives measurements from the thermistors in the cell and oven, the phase-sensitive detector, the Faraday cell and the pressure-transducer.

The HP BASIC program collects and processes the data as well as monitoring any changes in the temperature and pressure in the the oven, the interior of the cell and the laboratory. The details of this program appear in Sono's thesis.[3] Mr Dewar, in February 2006 at the start of this project, built a new stepper-motor controller which was used to rotate the quarter-wave plate. A stepper motor is an electric motor that can divide a full rotation into a large number of precisely reproducible steps. The motor's position can be controlled precisely. Changes made to the HP BASIC program in this work included the insertion of the commands necessary to control the new stepper motor, as well as changes in the time taken to cool or heat the system.

Figure 5.17: Photo of the data-aquisition unit

Figure 5.18: Photo of the PC

Pressure and Temperature Control

The Kerr effect is temperature and pressure dependent. In this work the molar Kerr constant was measured over a range of pressure for each temperature. A 200 PSIA pressure gauge is used to monitor the pressure in the cell. In addition the temperatures in the cell, oven and room need to be measured. PT100 resistance temperature devices (RTDs) are placed at different points along the length of the cell and oven to accurately measure the temperature. Sono's thesis[3] gives a comprehensive account of the way in which the RTDs are connected as well as information on the oven design and how it incorporates temperature control.

The PT100 RTDs have platinum thermistors with resistence of 100 ohms at 0°C, a temperature coefficient of $0.00385°C^{-1}$ and a temperature precision of $\pm 0.44°C$ within $\pm 200°C$. Three RTDs were placed in the oven and two in the cell. All five RTDs were connected to the data-acquisition unit so that the proportional-integral-derivative (PID) algorithm in the control program could maintain the temperature in the cell as registered by the RTDs. Later in this work Mr Dewar installed a commercial temperature controller to maintain the temperature of the oven.

A proportional-integral-derivative (PID) controller or algorithm attempts to correct the error between a measured variable and a desired set point. This is achieved by calculating and then outputting a corrective action (in our case heating or cooling) that can adjust the process appropriately.

Two circulating fans (one at each end of the oven) are used to help circulate the air in the oven and hence maintain a uniform temperature throughout. In order to obtain high temperatures in the oven and cell a 1.5 kW heating element is used. The coil of the element had been cut into two segments, and these were connected in series along opposite walls of the oven. As a precautionary measure against overheating, a thermal fuse having a melting point of 250°C is connected in series with the coil.

Reaching temperatures below room temperature is more painstaking and time consuming than above room temperature. In order to achieve low temperatures cold nitrogen, boiled off from a pressurised dewar of liquid nitrogen, is pumped into the oven. The flow-rate of the coolant is controlled by a

solenoid valve. Pressurizing the dewar required application of between 6 to 12V across a heating coil which is situated inside the dewar.

A novel switch is used as a safety device when the oven is being heated or cooled. Since the experiment is automated to run unsupervisored (e.g. overnight), it is crucial to ensure that in the event of a power failure, the elements shut down, since once mains power returns, the elements could then continue to heat in an uncontrolled fashion. Upon occurrence of a power failure, the novel switch effectively shuts the experiment down. This safety feature prevents the the cell from overheating or overcooling in the case of a dip in the mains supply.

The PID algorithm written into the HP BASIC controller program monitors the temperature of the experimental environment. The temperature in the laboratory needs to be controlled as the Verdet constant of the toluene in the Faraday cell is temperature dependent, and this is achieved by means of an air conditioner. The windows in the laboratory were also insulated with polystyrene sheets to help maintain the temperature in the room. The temperature in the room is monitored using RTDs placed near the laser and Faraday cell so as to track the temperature across the experimental assembly.

When heating the cell from 30°C to 200°C, spurious leaks could arise as the cell and teflon seals expanded during the temperature increase. Before an experimental run a Spectron 300E helium leak detector is used to locate any leaks in the cell. The cell is pressurized with helium and then the sniffer of the leak detector is placed at possible leak sources and the concentration of helium (indicated on the Spectron) is measured. Once detected, leaks were sealed up appropriately. Once all leaks had been eliminated, the pressure was monitored over a period of a few hours to be certain that the system was stable, after which measurements commenced.

For work below room temperature, when the temperature in the oven enclosure rises above the set point, the action sent to the controller is to inject coolant into the oven. The duration for which the coolant is injected is proportional to the magnitude of the control output. If the temperature in the oven drops below the set point, the action sent to the controller is to apply a potential difference across the heating element for a time proportional to the control output.

Our own PID algorithm (written for the HP BASIC program to control the data-acquistion unit) was initially used to set and control the temperature in the oven. During 2007 Mr Dewar installed a commercial temperature controller and our own PID program was no longer needed. The HP BASIC program was modified to acquire the temperatures of the oven, cell and room as well as the pressure of the gas in the cell once the new controller had established a temperature equilibrium in the cell. The PID algorithm became redundant as the new temperature controller fulfills that purpose.

We now move onto the proceure followed in determining the molar Kerr constant.

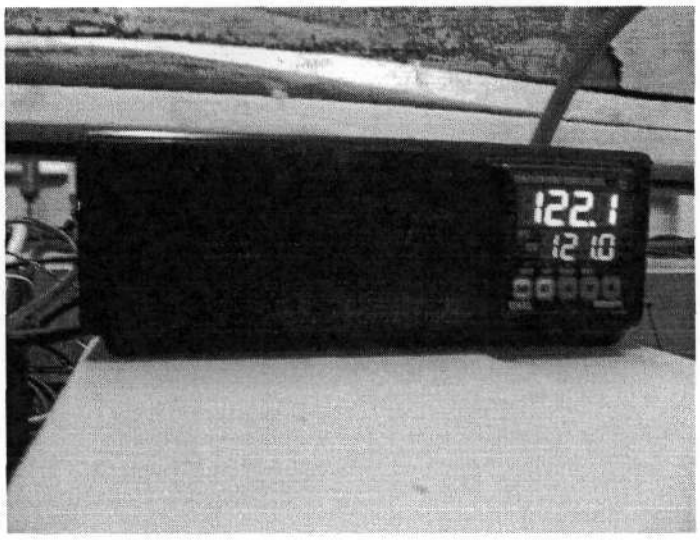

Figure 5.19: Photo of the new temperature controller

5.4 Method of Measurement

In this experiment we wish to obtain an experimental value for the phase difference δ, which will lead to the calculation of the molar Kerr constant. The experiment requires a gas sample of known temperature and pressure situated in an accurately-known electric field.

A helium-neon laser was used as the source of monochromatic linearly-polarized light. The laser beam is passed through a polarizer having its transmission axis set at 45° to the electric field. Before the light passes through the electric field in the Kerr cell, the components of the field oscillating parallel and perpendicular to the electric field are in phase with each other.

Once the light emerges from the birefringent medium a phase difference between the two component fields has been introduced. To find the magnitude of the induced phase difference, a compensator comprising a quarter-wave plate in conjugation with a Faraday cell and an analyzer and photodiode, is used. The light emerging from the birefringent medium is elliptically polarized. Once the beam emerges from the birefringent medium, it is passed through a quarter-wave plate to convert the elliptically-polarized light into linearly-polarized light, but with its axis of polarization rotated from the initial 45° position by an angle $\theta = \frac{\delta}{2}$. This is then compensated by an equal-in-magnitude but opposite-in-direction rotation of the plane of polarization induced by the applied magnetic field in the Faraday cell.

The amount by which the plane of polarization is rotated by the Faraday cell in order to bring it back to its initial plane of polarization is given by

$$\theta = VH_z l, \tag{5.3}$$

where V is the Verdet constant of the substance used in the Faraday cell, H_z is the strength of the magnetic field induced by the coils in the direction of propagation of the light, and l is the path length of the Faraday cell.

The strength of the magnetic field which is induced by the current in the coils is related to the current as follows:

$$H_z = \frac{\mu_0 N i}{L}, \tag{5.4}$$

where N is the number of turns, L is the length of the solenoid and i is the current through the coil.

Before measurements are taken the Faraday cell is calibrated. The Faraday cell calibration constant which is determined during the calibration process is given by

$$k_F = \mu_0 NV. \tag{5.5}$$

Using equations 5.3, 5.4 and 5.5 the induced rotation can be simplified to

$$\theta = k_F i. \tag{5.6}$$

So by varying the current i we are able to return the plane of polarization of the light back to 45° to the applied magnetic field. To ensure that this is achieved, use is made of a detector. The detector consists of an analyzer (analyzing prism) at -45° to the applied electric field in conjunction with a photodiode. The output signal from the photodiode is fed to a phase-sensitive detector, which displays a reading which is proportional to the intensity of light (at a specific reference frequency) reaching the photodiode.

When no voltage is applied across the electrodes, but with an ac current passing through the Faraday cell coil, the laser beam can be extinguished by the analyzer by crossing it with the polarizer, resulting in a minimum intensity reaching the photodiode. Once an oscillating electric field has been applied across the gas sample, the current in the Faraday cell needs to be varied until a minimum is recorded by the PSD, hence re-achieving null. This procedure is now discussed in detail.

If the fast axis of the quarter-wave plate is offset from 45° by a small ($\approx 1°$) rotation $-\epsilon_1$ and the Faraday cell current is varied, a straight line plot of the PSD output as a function of the current can be obtained. Then by off-setting the quarter-wave plate by $+\epsilon_2$, a second line having a slope with an opposite sign to the first is obtained. The intersection of these two lines occurs at $\theta_{null} = \frac{-\delta}{2}$, resulting in an accurate reading for the phase difference. This method for obtaining the true null was devised by Graham, Pierrus and Raab,[6] and is much more sensitive than obtaining a single null value with the Faraday cell. The phase difference is obtained by using equation 5.6, where k_F is the Faraday cell calibration constant and i is the current at which the two lines intersect, this produces the angle of rotation which in turn is used to determine the phase difference. It is crucial that the signals which drive the Kerr and Faraday cells be exactly in anti-phase so that the rotation of the plane of polarization of the light by the Faraday cell will be to the null position. A full Mueller analysis of the optical train has been performed elsewhere.[3]

The field which results from a voltage V being applied to the electrodes

is

$$E = \frac{V}{d}. \tag{5.7}$$

In our work, an alternating voltage

$$V = V_0 cos\omega t \tag{5.8}$$

is applied to the electrodes, where V_0 is the amplitude of the alternating voltage, ω is the corresponding frequency and t is the time. The square of applied electric field has the following form

$$E^2 = \frac{V_0^2 cos^2\omega t}{d^2} = \frac{V_0^2}{d^2}\left(\frac{1 + cos2\omega t}{2}\right). \tag{5.9}$$

δ will oscillate at twice the frequency of the driving voltage applied to the Kerr electrodes, and so the Faraday cell must be supplied with an AC signal of 2ω, the PSD locking in to the signal oscillating at this frequency. Once the phase difference is experimentally measured and the molar Kerr constant is calculated a graph of the molar Kerr constant ${}_mK_0$, versus the inverse molar volume V_m^{-1} can be plotted for each experimental temperature. Using the relation[7]

$${}_mK_0 = A_K + [B_K + A_K(2A_\epsilon + \frac{1}{2}A_R)]V_m^{-1} + \vartheta(V_m^{-1}) \tag{5.10}$$

the first and second Kerr virial coefficients, A_K and B_K, can be determined from the intercept and slope of the graph respectively. A_ϵ and A_R are the low-density molar dielectric polarization and molar refraction respectively, and are given by

$$A_\epsilon = \frac{N_A}{3\epsilon_0}\left\{a_0 + \frac{\mu_0^2}{3kT}\right\} \tag{5.11}$$

and

$$A_R = \frac{N_A\alpha_0}{3\epsilon_0}, \tag{5.12}$$

where N_A is Avogadro's number, ϵ_0 is the permittivity of free space, a_0 is the mean static polarizability, μ_0 is the permanent dipole moment and α_0 is the mean dynamic polarizability of the molecule.

5.5 Calibrations

5.5.1 Faraday Cell Calibration

The Faraday cell is calibrated by applying a dc voltage to the 100 turn coil, providing a current in the range 0 to 100 mA. A small ac voltage is applied to the 10 000 turn coil to modulate the signal and so easily measure the induced rotations using the PSD. The ac signal is produced by the waveform synthesizer and enables the PSD to lock on to the modulated signal reaching the photodiode. The micrometer of the analyzing prism is rotated until the PSD records an output of zero. The micrometer reading is recorded for each dc current. The data is then fitted to a straight line graph, the slope of which gives the Faraday cell constant, K_F.

A toroidal inductor is connected in series with the dc part of the circuit to prevent coupling between the two coils. The Fluke meter is used to measure the dc current.

The Toluene level in the Faraday cell needs to be monitored and topped up from time to time, as the toluene slowly evaporates off.

The micrometer reading (in inches) and the corresponding nulling currents (in mA) are listed in the table below. A graph showing the plot of micrometer reading as a function of current follows.

dc Current (mA)	Micrometer Reading (inches)
0.000	0.2779
0.102	0.2637
0.200	0.2490
0.306	0.2375
0.400	0.2261
0.500	0.2102
0.600	0.1966
0.700	0.1867
0.800	0.1706
0.900	0.1592
0.999	0.1475

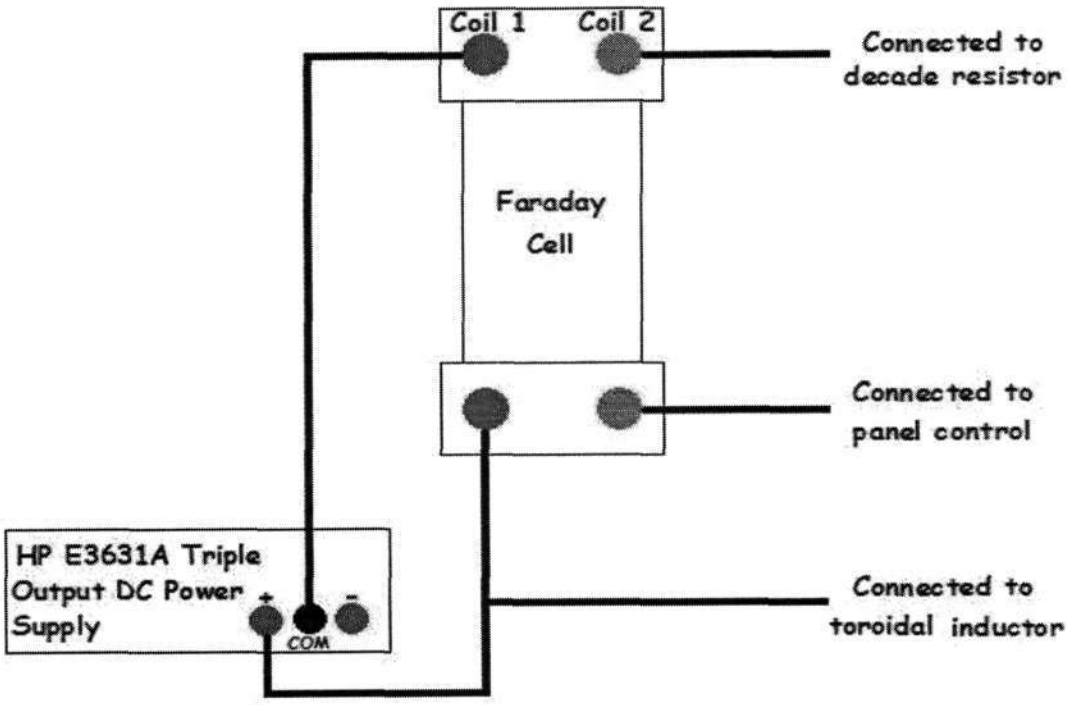

Figure 5.20: Faraday cell calibration circuit

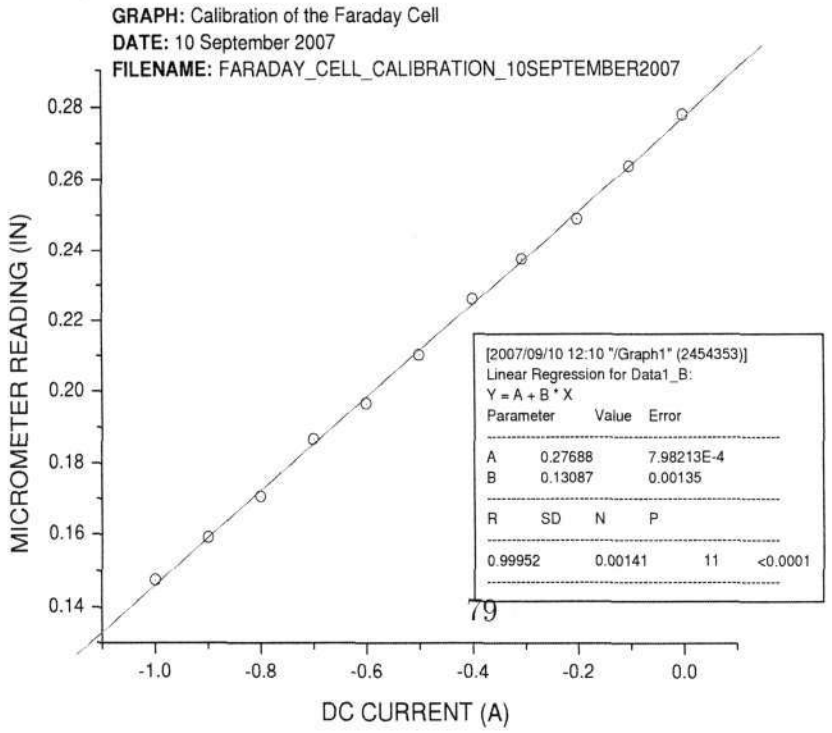

The slope of the graph produces a value of $K_F = (0.130_9 \pm 0.001_4) \times 10^{-4}$ inch mA^{-1}. Conversion into rad mA^{-1} is achieved by using equation 5.2. From knowing the Faraday nulling current for a particular measurement, the HP BASIC program uses the Faraday cell calibration constant along with equation 5.6 and the relationship $\delta = 2\theta$ to determine the induced phase difference. This parameter allows for calculation of the molar Kerr constant via equations 4.4 and 4.9.

It is essential that the laboratory be maintained at a constant temperature since the Verdet constant of toluene is temperature dependent and it is undesirable that K_F varies during this work.

5.5.2 High-Voltage Calibration

The calibration of the high-voltage power supply is performed by varying the high-voltage power supply (up to 1000 V rms) and reading off the corresponding voltage using a ` Major Tech MT1889 True RMS Multimeter ´. As stated on page 68, the ac high voltage is transformed down and passed through a precision rectifier, do that 1V dc corresponds as closely as possible to 1000 V ac. The ratio of ac to dc voltages is measured accurately up to 1000 V, and linear proportionality is assumed to hold at the higher voltages used in the experiment. The dc voltage is measured using a ` Fluke 45 Dual Display Multimeter ´.

The table below lists the dc and corresponding ac voltages for a typical calibration run and the calibration graph follows.

dc Voltage Reading (V):	True rms ac Voltage Reading (V)
1.0550	1005
0.9944	948
0.9448	900
0.8953	854
0.8458	807
0.7908	756
0.73575	702
0.6751	644
0.6366	609
0.5705	545
0.5216	502
0.4722	454
0.4164	398
0.3668	348.5
0.3116	296.4
0.26208	249.6
0.20757	197.9
0.15943	152.4
0.14595	139.6

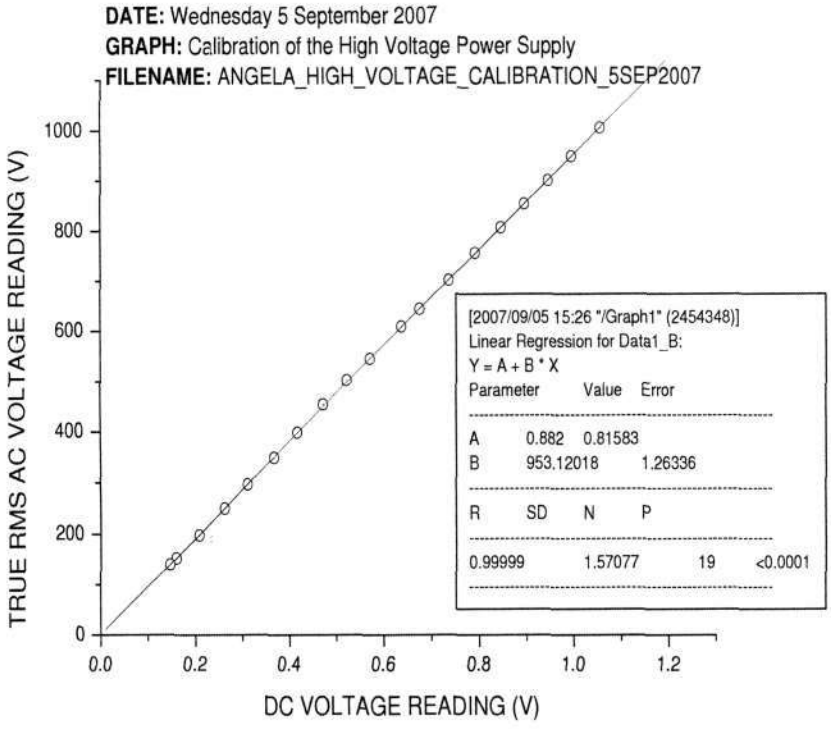

In order to determine the ac voltage that is applied to the electrode of the Kerr cell the experiment records the dc voltage from the precision rectifier and uses the straight-line equation from the calibration graph. Due to the excellent regression coefficient we are assured of the linear relationship of the voltages when extrapolating to voltages higher than 1kV (for most of the experimental runs the cell runs at ≈ 3 kV). Each time the Electronics Centre worked on the high-voltage power supply it was recalibrated, and drifts were found to be negligible.

5.5.3 Pressure Calibration

A Honeywell 200 PSIA model-SA pressure transducer is used to measure the cell gas pressure, and is powered by a 10 V dc supply. A Budenberg dead-weight tester is used to calibrate the transducer. Once measurements are completed a graph of dead-weight pressure vs transducer voltage is plotted.

Pressure Transducer Voltage (V)	Pressure (kPa) (Dead-Weight Tester)
0.3852	0.0
0.7226	94.05
1.154	214.05
1.517	314.05
1.876	414.05
2.057	464.05
2.603	614.05
2.962	714.05
3.321	814.05
3.682	914.05
4.047	1014.05

Graph of dead-weight pressure vs pressure-transducer voltage used to obtain pressure calibration constants.

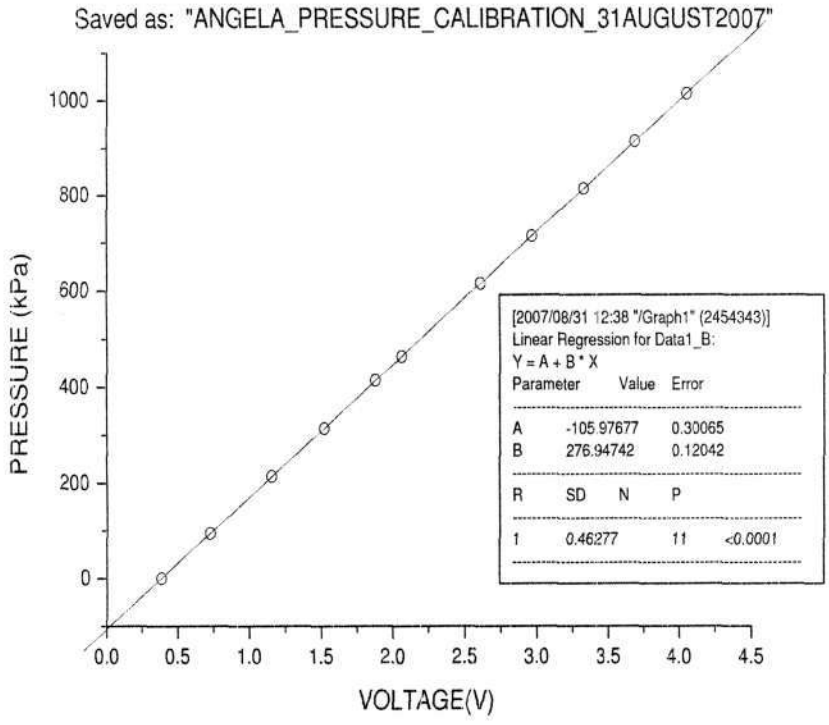

The pressure-transducer output voltage and the straight-line equation are used in the HP BASIC program to calculate the true pressure inside the Kerr cell.

5.6 Temperature Control

All of the platinum resistance thermometer elements both in the cell and the oven were replaced during this work. The platinum resistance thermometer elements were obtained from Mr Dewar who spot-welded them onto the connecting wires.

5.7 References

1. M. Evans and S. Kielich, *Modern Nonlinear Optics* part 2, New York, John Wiley and Sons, 1993,361-414.

2. A. Singh, MSc thesis, University of KwaZulu-Natal, 2005.

3. T. J. Sono, MSc thesis, University of Natal, 2003.

4. A. Janse van Rensburg, Honours Project, University of KwaZulu-Natal, 2005.

5. D. A. Imrie, PhD, University of Natal, 1995.

6. C. Graham, J. Pierrus and R. E. Raab, *Mol. Phys.*, 1989,67, 939.

7. M. P. Bogaard, A. D. Buckingham and G. L. D. Ritchie, *J. Chem. Soc. Faraday. Trans. II*, 1981, 77, 1547.

8. A. D. Buckingham and B. J. Orr, *Trans. Farad. Soc.*, 1969, **65**, 673.

9. M. P. Bogaard, A. D. Buckingham and G. L. D. Ritchie, *J. Chem. Soc., Faraday Trans. 2*, 1981, **77**, 1550.

Chapter 6

Results and Discussion

The goal at the outset of this project was to measure the Kerr effect of both dimethyl ether and trifluoromethane. The Kerr effect of trifluoromethane has been measured for the (approximate) temperatures 30, 60, 90, 120, 160 and 200°C and the graphs and analyses of these results appear later in this chapter. For dimethyl ether, measurements of the Kerr effect were taken at similar temperatures, the results of which are also presented later in this chapter. Attempts were made to measure the Kerr effect for dimethyl ether at 12°C, but ultimately proved fruitless, though the best results obtained have been included in this chapter for completeness.

The results reported in this chapter were achieved after a considerable amount of time since our initial measurements of dimethyl ether were discrepant with those of Sono and Singh.[1,2] In trying to account for the discrepancies, fresh calibrations of the high-voltage supply, the pressure transducer and the Faraday cell were systematically performed to check for consistency. Since this did not improve agreement, our next thought as to the source of these discrepancies was that quarter-wave plate used in the experiment might have a retardance significantly different to $\frac{\pi}{2}$ for 632.8 nm. After purchasing a new precision quarter-wave plate from Newport we simply reproduced our existing data. It was ultimately suspected that during Sono and Singh's work the laser beam was suffering multiple internal reflections as it transversed the electrodes, which would cumulatively degrade the polarization state of the beam, leading to the discrepancies in results.

We have also computed second Kerr-effect virial coefficients for ammonia,

for comparison with the experimantal data of Ritchie *et al.*[3] We now look at these computational details.

6.1 Computational Results

Part of this work comprised computation of the second Kerr-effect virial coefficients for ammonia, and the approach for calculating these coefficients is now discussed.

To compute the virial coefficients one requires knowledge of various molecular parameters, including the dipole and quadrupole moments, the shape parameter (D), the collision radius and $\frac{\epsilon}{k}$ (where ϵ is the minimum interaction energy between molecules and k is the Boltzmann constant). We obtained the dipole and quadrupole moments for ammonia from the literature[1], and proceeded to evaluate a self-consistent set of intermolecular potential parameters, namely the shape potential D, the collision radius R_0 and $\frac{\epsilon}{k}$ for ammonia by using Fortran code to calculate the second pressure virial coefficient B_p, and by varying the potential parameters to obtain the best possible agreement between computed and published[1] values of B_p over a wide range of temperatures. Once all these parameters had thus been determined, we were able to run the Fortran program which determines the second Kerr-effect virial coefficients for ammonia.

Table of Second Pressure Virial Coefficients for Ammonia B_p as a function of temperature. Taken from Inorganic Compounds pg 54 of Landolt-Börnstein, best fit to experimental data.[1]

T/K	$(B_p \pm 2\sigma_{est})$/cm^3 mol^{-1}
240	-526±10
250	-459±5
265	-380±5
280	-319±5
300	-257±5
320	-212±5
345	-171±5
370	-141±5
400	-115±5
430	-96±5
480	-73±5
530	-56±2
595	-41±2

The values for the three potential parameters were initially set to arbitrary values (as these values were unknown). These are shown in the table below, together with values for the other required molecular parameters.[5,6] The dynamic polarization is that for light with a wavelength of 632.8 nm.

Molecular data	Value in SI units
mean static polarizability	2.60×10^{-40} [2]
mean dynamic polarizability	2.47 [4]
dipole moment	4.90984×10^{-30} [2]
quadrupole moment	-11.0×10^{-40} [3]
κ	0.04246 [2]
collision diameter R_0 (nm)	0.2902
Shape Parameter, D	0.00
ϵ/k (K)	692.00

Values for the optimised potential parameters parameters now follow.

Parameter	Value in SI units
R_0 (nm)	0.330
D	-0.0341
$\frac{\epsilon}{k}$ (K)	208.9

The molecular data and optimized interaction parameters were then used, together with the molecular polarizability components $\alpha_{||} = 2.60 \times 10^{-40}$ C^2 m^2 J^{-1} and $\alpha_{\perp} = 2.30 \times 10^{-40}$ C^2 m^2 J^{-1}, to evaluate, by numerical computation, values for B_K over a range of temperature.

To illustrate the sensitivity of the computed B_p values, comparison is made with published experimental data over a range of temperature using a range of optimised values for the molecular paramters. The comparison is tabulated below.

		Parameters: D = -0.040 R_0 = 0.350nm $\frac{\epsilon}{k}$ = 300.0K	Parameters: D = -0.00098 R_0 = 0.321nm $\frac{\epsilon}{k}$ = 209.9K	Parameters: D = -0.00098 R_0 = 0.349nm $\frac{\epsilon}{k}$ = 309.9K
T(K):	Published[1] $B_p \times 10^6$ ($m^8V^{-2}mol^{-2}$)	Computed $B_p \times 10^6$ ($m^8V^{-2}mol^{-2}$)	Computed $B_p \times 10^6$ ($m^8V^{-2}mol^{-2}$)	Computed $B_p \times 10^6$ ($m^8V^{-2}mol^{-2}$)
240	-526	-481.8901	-666.1096	-492.9661
250	-459	-431.1786	-566.1689	-441.1904
265	-380	-370.2674	-455.0294	-379.0052
280	-319	-322.5573	-374.9152	-330.3014
300	-257	-273.2000	-298.5687	-279.9211
320	-212	-235.1859	-244.3491	-241.1232
345	-171	-198.5284	-195.8603	-203.7140
370	-141	-170.2060	-160.9476	-174.8139
400	-115	-143.7595	-130.3451	-147.8305
430	-96	-123.0618	-107.7309	-126.7143
480	-73	-97.08759	-80.99566	-100.2162
530	-56	-78.10707	-62.60605	-80.85318
595	-41	-59.98112	-45.94351	-62.36068

The graphs illustrating the comparison between our computed data and the measured results summarised in Landolt-Börnstein[1] for ammonia are given below. Three graphs are given, one for each of the computed results obtained using the three different sets of potential parameters. The values for the parameters are given above each graph. The label on the y axis 'BT' corresponds to the second pressure virial coeficient, B_p, as a function of temperature.

Parameters used in Fortran code

D:	-0.040
R_0 (nm):	0.350
$\frac{\epsilon}{k}$ (K):	300.0

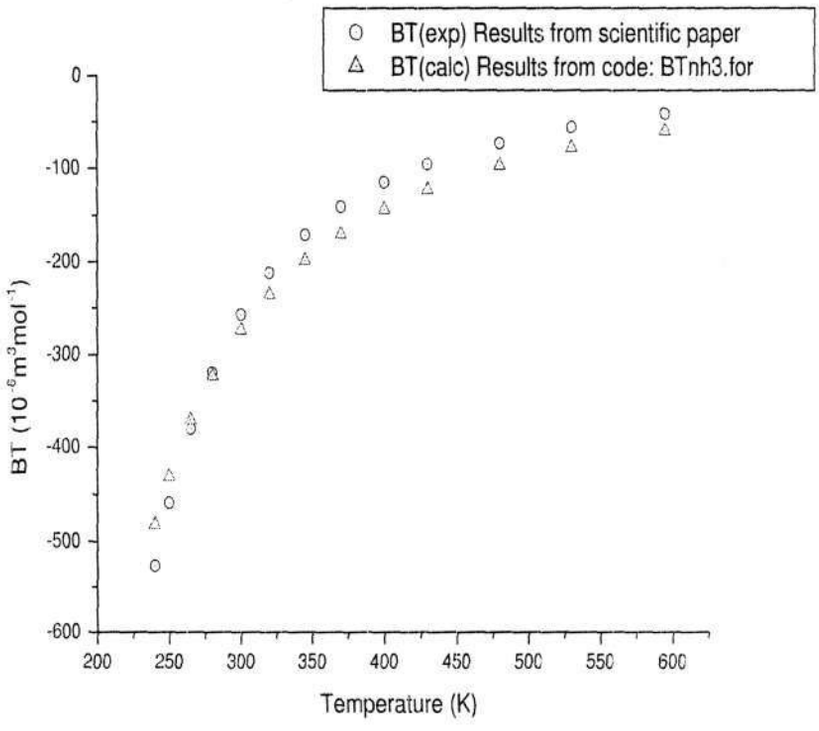

Figure 6.1: Plot of the second pressure virial coefficient B_p for ammonia

as a function of temperature for the above parameters.

Parameters used in Fortran code

D:	-0.00098
R_0 (nm):	0.321
$\frac{\epsilon}{k}$ (K):	209.9

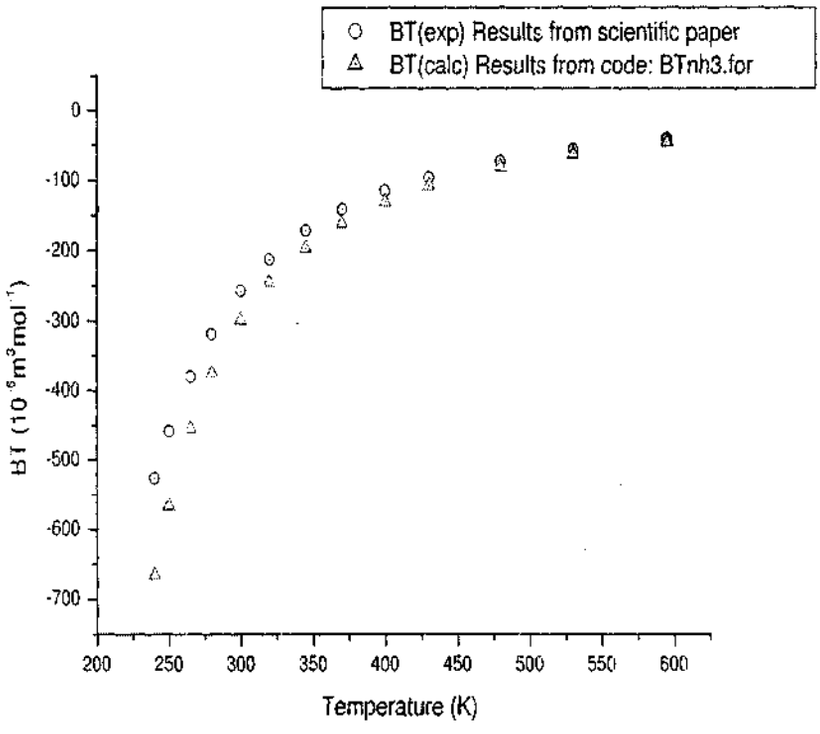

Figure 6.2: Plot of the second pressure virial coefficient B_p for ammonia as a function of temperature for the above parameters.

Parameters used in Fortran code

D:	-0.00098
R_0 (nm):	0.349
$\frac{\epsilon}{k}$ (K):	309.9

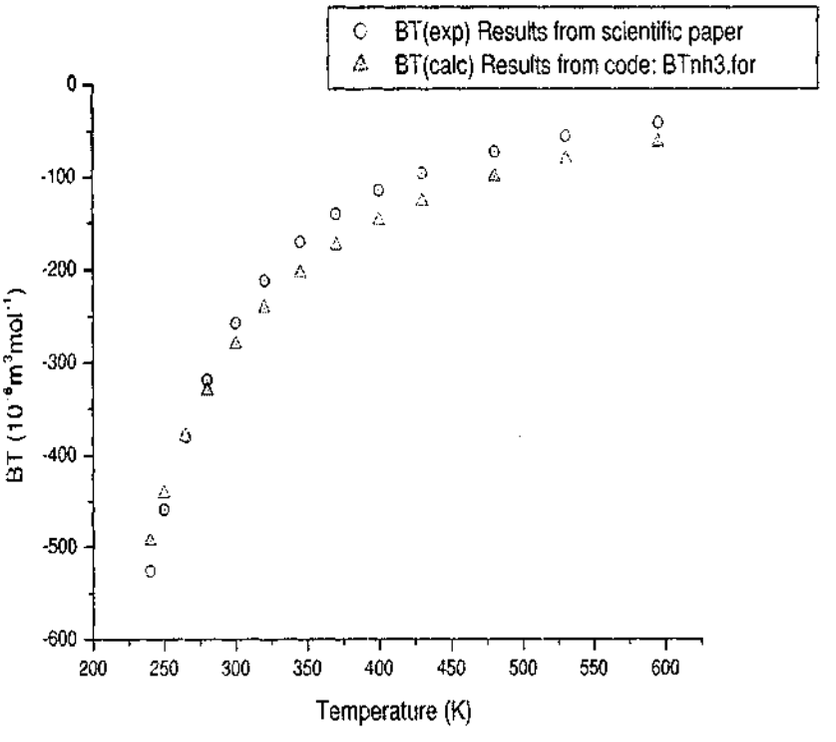

Figure 6.3: Plot of the second pressure virial coefficient B_p for ammonia as a function of temperature for the above parameters.

The second Kerr-effect virial coefficient B_K for ammonia was computed and compared with the measured data of Ritchie*etal.*[2] A tabulation of the measured and computed B_K for ammonia over the experimental temperature range appears below.

		Parameters: D = -0.040 R_0 = 0.350nm $\frac{\epsilon}{k}$ = 300.0K	Parameters: D = -0.00098 R_0 = 0.321nm $\frac{\epsilon}{k}$ = 209.9K	Parameters: D = -0.00098 R_0 = 0.349nm $\frac{\epsilon}{k}$ = 309.9K
T(K):	Published[2] B_K $\times 10^{30}$ ($m^8V^{-2}mol^{-2}$)	Computed B_K $\times 10^{30}$ ($m^8V^{-2}mol^{-2}$)	Computed B_K $\times 10^{30}$ ($m^8V^{-2}mol^{-2}$)	Computed B_K $\times 10^{30}$ ($m^8V^{-2}mol^{-2}$)
492.1	0.66 ± 0.21	0.61450	0.88024	0.57167
483.5	-	0.65019	0.93465	0.60445
476.6	1.32 ± 0.15	0.68101	0.98190	0.63274
449.9	1.19 ± 0.07	0.82220	1.20139	0.76212
422.1	1.80 ± 0.35	1.01813	1.51379	0.94106
395.8	1.86 ± 0.23	1.27081	1.92927	1.17099
375.7	1.89 ± 0.13	1.52829	2.36623	1.40444
356.6	1.87 ± 0.09	1.84710	2.92502	1.69245
342.9	1.99 ± 0.05	2.23663	3.44852	1.95316
330.2	2.17 ± 0.07	2.46556	4.06066	2.24846
319.3	2.67 ± 0.09	2.80755	4.71575	2.55459
306.8	2.73 ± 0.04	3.28755	5.66546	2.98288
297.5	2.68 ± 0.09	3.72243	6.5548	3.36967

A graphical illustration of the comparison between the computed and published results is now given.

Parameters used in B_K code

D:	-0.040
R_0 (nm):	0.350
$\frac{\epsilon}{k}$ (K):	300.0

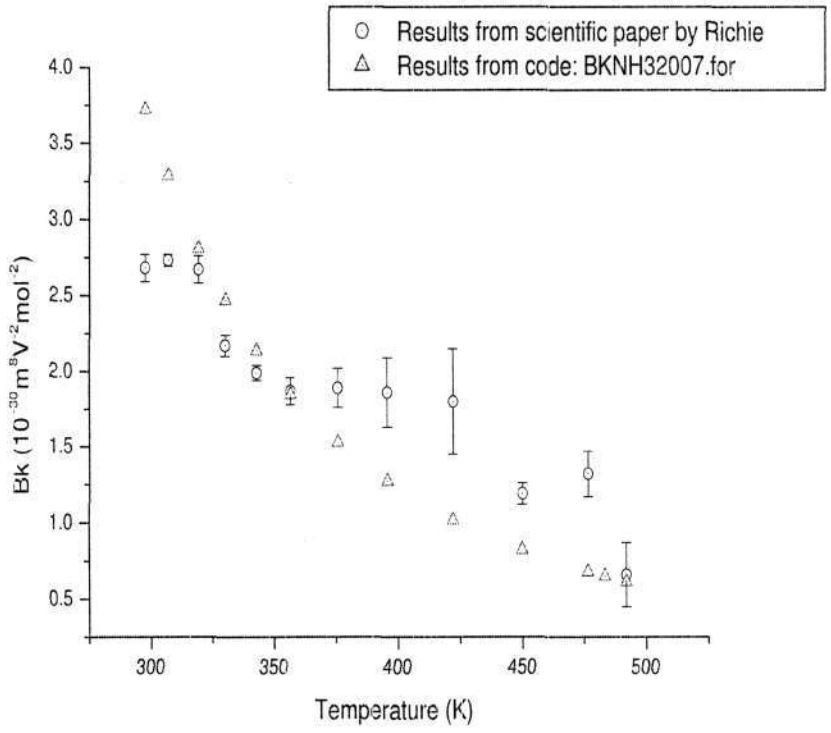

Figure 6.4: Plot of the second Kerr virial coefficient B_K for ammonia as a function of temperature for the above parameters.

This plot indicates that best agreement between the measured and computed B_K values occurs in the temperature range 310 to 350 K. The experimental scatter and error bars are often very large, indicating that it might

be worthwhile to re-measure the Kerr effect of ammonia in a future research project. Two more graphs comparing computed and measured results are given below. These graphs illustrate the sensitivity of computed B_K data to changes in the intermolecular potential parameters D, R_0 and $\frac{\epsilon}{k}$.

Parameters used in B_K code

D:	-0.00098
R_0 (nm):	0.321
$\frac{\epsilon}{k}$ (K):	209.9

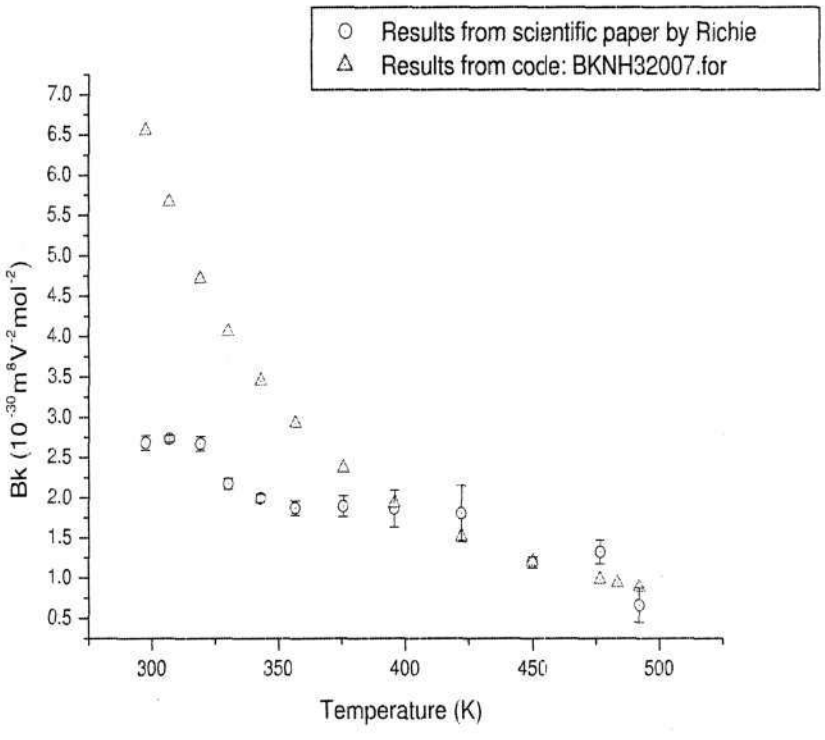

Figure 6.5: Plot of the second Kerr virial coefficient B_K for ammonia as a function of temperature for the above parameters.

Parameters used in B_K code

D:	-0.00098
R_0 (nm):	0.349
$\frac{\varepsilon}{k}$ (K):	309.9

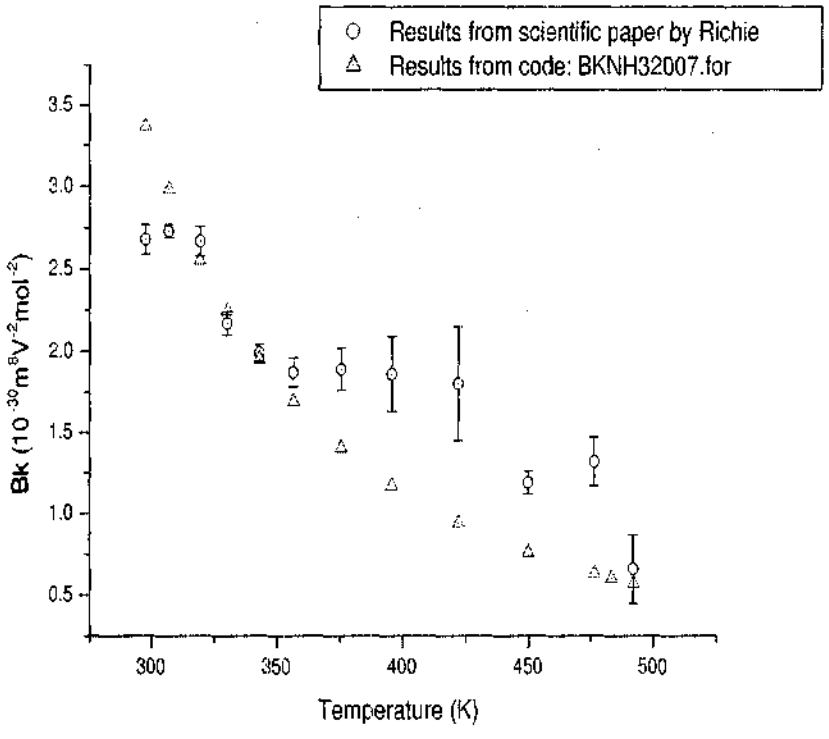

Figure 6.6: Plot of the second Kerr virial coefficient B_K for ammonia as a function of temperature for the above parameters.

6.2 Introduction to Experimental Results

The three main outcomes of experimental measurements of the Kerr electro-optical effect are data for the molar Kerr constant, polarizabilities and hy-

perpolarizabilities, and the first and second Kerr-effect virial coefficients of the molecule being studied.

The phase difference δ induced between the field oscillating parallel and perpendicular to the applied electric field in the sample is given by

$$\delta = \frac{2\pi l}{\lambda}(n_{\parallel} - n_{\perp}) \tag{6.1}$$

where λ is the wavelength of the beam, l is the path length of the beam through the medium in the presence of the electric field E, and $n_{\parallel}$ and $n_{\perp}$ are the refractive indices of the medium parallel and perpendicular to the applied field.

The phase difference δ can be expressed in terms of the Kerr constant B by

$$\delta = 2\lambda B l E^2. \tag{6.2}$$

The Kerr constant B varies with different substances, wavelengths and temperatures. In the limit of low densities the molar Kerr constant ${}_mK_0$ is defined as[5]

$${}_mK_0 = \frac{2(n_{\parallel} - n_{\perp})V_m}{27E_0^2} \tag{6.3}$$

where E_0 is the amplitude of the applied electric field and V_m is the molar volume of the gas. Combining equations 6.1 and 6.3 yields

$${}_mK_0 = \frac{\delta\lambda V_m}{27\pi l E_0^2}. \tag{6.4}$$

The molar volume V_m can be determined from the virial expansion

$$\frac{PV_m}{RT} = 1 + \frac{B_p}{V_m} + \frac{C_p}{V_m^2} \tag{6.5}$$

where B_p and C_p are the second and third pressure virial coefficients respectively. P is the pressure of the gas and T is its temperature.

In order to determine the molar Kerr constant ${}_mK_0$, the phase difference δ needs to be measured. The first and second Kerr-effect virial coefficients A_K and B_K can be determined from the molar Kerr constant ${}_mK_0$ using the equation[5]

$${}_mK_0 = A_K + \left(B_K + A_K(2A_\epsilon + \frac{1}{2}A_R)\right)V_m^{-1} \tag{6.6}$$

where A_ϵ is the molar dielectric polarization and A_R is the molar refraction.

From the above equation it is evident that if a graph of the molar Kerr constant ${}_mK_0$ is plotted versus the inverse molar volume, the first and second virial coefficients can be extracted. The first virial coefficient A_K is determined from the intercept and the second virial coefficient B_K is determined from the slope of the graph. The first Kerr virial coefficient A_K corresponds to the limit of infinite dilution where each molecule is unaffected by interactions with other molecules, while the second Kerr virial coefficient describes the effects of molecular pair interactions on the molar Kerr constant.

6.3 Experimental Results

6.3.1 Preparing the Apparatus for Measurements

The first step in preparing the apparatus for measurements is to check that the analyzer and polarizer are crossed. This involves removing the quarter-wave plate from the optical train and supplying the Faraday cell with a small ripple current for the PSD to lock onto. The micrometer on the analyzing system is rotated until null is reached on the PSD. The plane of polarization is then set at 45° to the applied electric field.

The quarter-wave plate is then reintroduced into the optical train such that the reflection from the quarter-wave plate lies directly on the incident beam as even small deviations will introduce alignment errors into the measured Kerr constants. A small offset from 45° is introduced to the quarter-wave plate setting. The high voltage is applied to the electrodes, bringing the phase of the Kerr cell to 180° on the PSD. The frequency doubler and phase shifter are switched on so as to apply an ac current to the Faraday cell. This current is varied until the signal is nulled.

Then the high voltage is switched off and the phase of the Faraday cell signal is set to 0°. The Faraday cell's nulling signal is now in anti-phase relative to the signal from the Kerr cell. The high voltage is switched on again and the Kerr program is initialized so as to commence the experimental run.

6.3.2 Results for H_2

Tammer *et al.*[5,6] have measured the Kerr effect of molecular hydrogen over a wide range of temperature, and on the basis of the close agreement in the extracted hyperpolarizability γ as determined by a variety of independent methods, experimental and computational[6,7], employed by a range of different researchers, they recommend hydrogen as a reference standard for Kerr-effect gas phase measurements.

Since our measurements for dimethyl ether were discrepant with those of Sono[7] and Singh,[8] we decided to perform a calibration of our cell using molecular hydrogen at room temperature. For purposes of comparison, we reproduce the experimental results of Tammer *et al.*[5,6] in the table below.

T (K)	T^{-1} (K^{-1})	$10^{29}A_K$ ($C^2m^5J^{-2}mol^{-1}$)
196.1	0.005099	8.765±0.033
207.1	0.004829	8.592±0.022
219.5	0.004556	8.408±0.017
232.3	0.004305	8.199±0.036
247.0	0.004049	8.095±0.025
259.5	0.003854	7.859±0.024
273.6	0.003655	7.722±0.034
288.9	0.003461	7.566±0.020
303.7	0.003293	7.472±0.023
328.0	0.003049	7.285±0.016
350.4	0.002854	7.004±0.017
376.5	0.002656	6.925±0.022
411.7	0.002429	6.634±0.020
303.7	0.003293	7.455±0.019

A plot of their A_K values versus inverse absolute temperature yields the following graph.

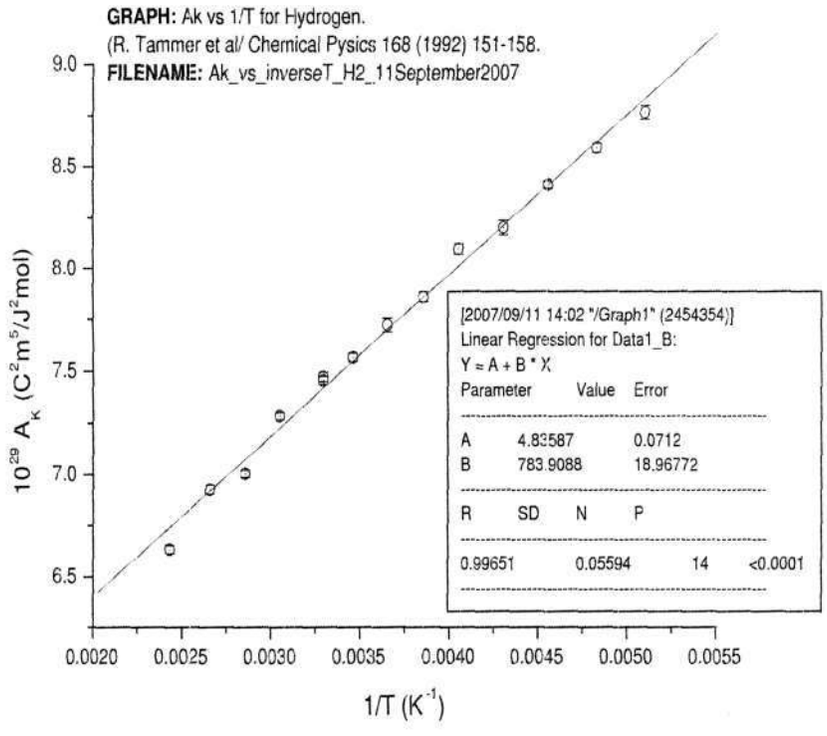

Figure 6.7: Plot of A_K versus inverse absolute temperature.

The graph yields the following relationship between A_K and T^{-1}: $A_K = m \times T^{-1} + c$ where m =slope= 783.9088 and c =y-intercept= 4.83587. And so we are able to interpolate their A_K value for our experimental temperature of 34°C or 307 K. This turns out to be $A_K = 7.3891 \times 10^{-29}$ $C^2m^5J^{-2}mol^{-1}$. A tabulation of our experimental results for hydrogen at 307 K appears below.

V_m^{-1} (mol m^{-3})	$10^{29}\ {}_mK_0$ (C^{2}m^{5}J^{-2}mol^{-1})
391.04	-8.829
391.24	-8.575
391.57	-8.730
391.56	-8.638
397.30	-8.438
397.16	-8.257
397.15	-8.194
397.04	-8.338
396.98	-8.270
396.77	-8.402
396.84	-8.269
396.90	-8.265
396.81	-8.474
396.79	-8.415
396.83	-8.276
396.82	-8.613
396.54	-8.369
396.75	-8.443

Our mean value of $A_K = (8.433 \pm 0.042) \times 10^{-29}$ C^{2}m^{5}J^{-2}mol^{-1}, when compared to the value interpolated from Tammer *et al.*, is seen to be 14.2% high. The reason for this discrepancy appears to lie in the field integral of the Kerr cell electrodes, $\int_0^L E^2 dL$. In their initial analysis of their Kerr-effect measurements for H_2, Tammer *et al.*[5] used the conventional method of determining E from voltage and plate distance. In a subsequent analysis,[6] they employed a more sophisticated technique using the Stark-effect splittings of a rotational transition of the OCS molecule in the millimetre wave region, and obtained a much more accurate field integral which differed from their earlier estimate by 6.37%. Their electrodes are 0.63 m long, while ours are 1.5 m long, and it is not surprising that small inconsistencies in the parallelity of our electrode plates over this distance leads to an accumulated error in the field integral. We rely on the hydrogen calibration to give our correction factor to the field integral, and so all our experimental data for both dimethyl ether and trifluromethane were adjusted accordingly. As a cross-check, we performed a room-temperature measurement of the Kerr-effect of carbon dioxide, comparing this measurement with experimental data due to

Ritchie et al[10].

6.3.3 Results for CO_2

Ritchie *et al.*[10] have measured the Kerr effect of carbon dioxide over a wide range of temperature. Their measurements will serve as a cross-check of our revised electrode field integral as obtained via a H_2 calibration. Their experimental results are tabulated below.

T (K)	T^{-1} (K^{-1})	$10^{27}A_K$ ($C^2m^5J^{-2}mol^{-1}$)
489.5	0.002043	1.508±0.004
455.8	0.002194	1.613±0.006
422.8	0.002366	1.740±0.003
394.5	0.002535	1.846±0.004
370.9	0.002697	1.979±0.005
348.8	0.002867	2.063±0.004
330.9	0.003023	2.219±0.005
314.9	0.003176	2.292±0.003
299.2	0.003343	2.404±0.003

A graphical treatment of their A_K values versus inverse absolute temperature follows.

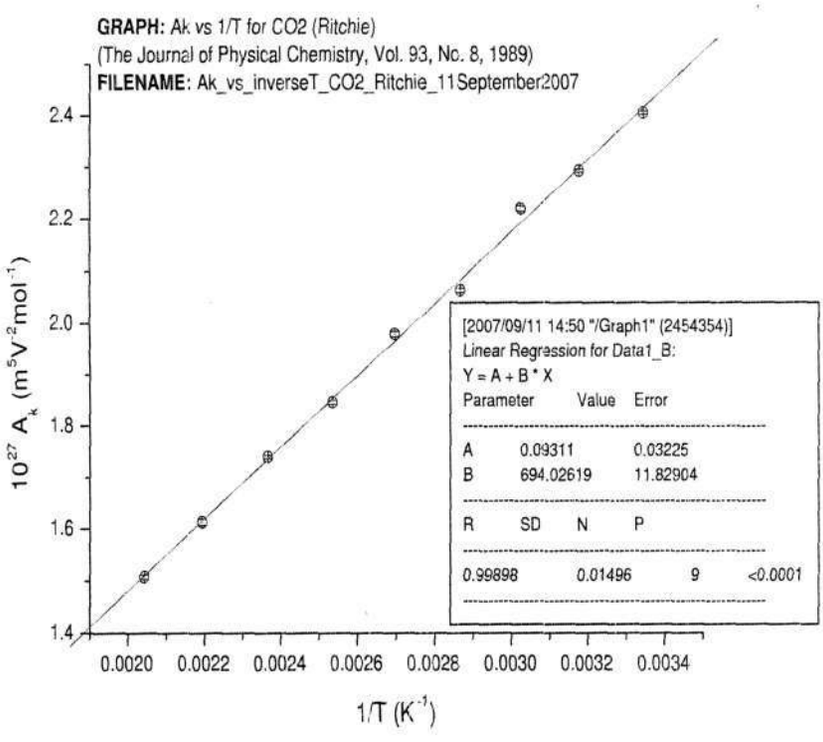

Figure 6.8: Plot of A_K versus inverse absolute temperature.

This graph shows the relationship between A_K and T^{-1} to be: $A_K = m \times T^{-1} + c$ where m =slope= 694.0262 and c =y-intercept= 0.09311. Interpolating their A_K value for our CO_2 experimental temperature of 34°C or 307 K yields $A_K = 2.354 \times 10^{-29}$ $C^2m^5J^{-2}mol^{-1}$.

Our experimental results (uncorrected for the H_2 calibration factor) for carbon dioxide at 307.3 K appear in the table below.

T (K)	P (Pa)	V_m^{-1} (mol m^{-3})	$10^{27}\ {}_mK_0$ (C^{2}m^{5}J^{-2}mol^{-1})
307.36	990317.7	406.50	-2.8148
307.47	990294.5	406.32	-2.8328
307.18	804722.2	327.41	-2.8090
307.22	804843.7	327.41	-2.7977
307.22	607235.3	244.60	-2.7657
307.28	607309.8	244.59	-2.7694
307.37	409448.9	163.27	-2.7494
307.24	409527.0	163.38	-2.7553

A graph of the Molar Kerr Constant ${}_mK_0$ vs the Inverse Molar Volume V_m^{-1} is now plotted. The intercept of the graph gives our A_K for carbon dioxide at 307.3 K.

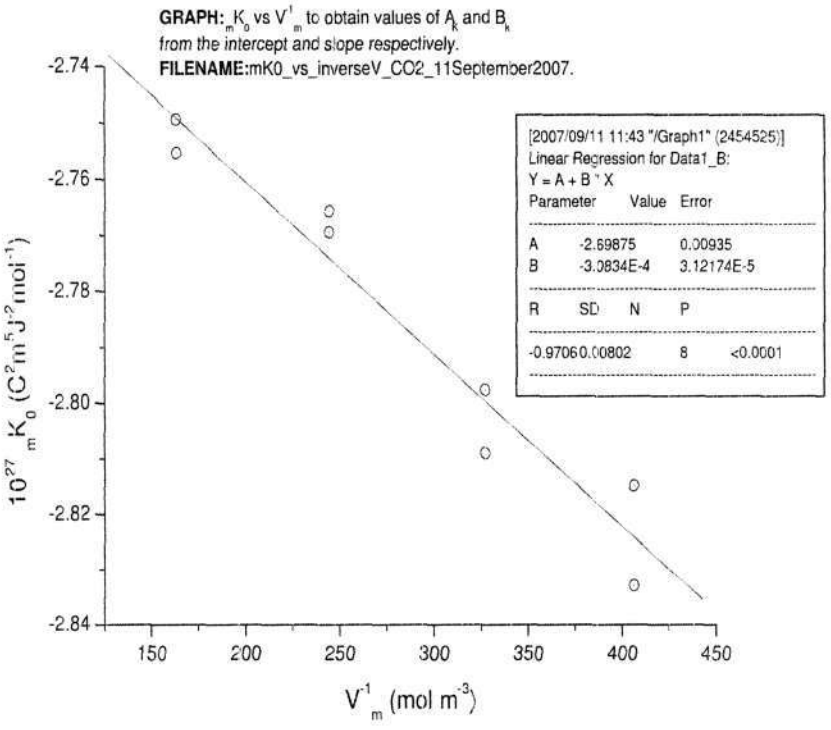

Figure 6.9: Plot of Molar Kerr constant versus inverse molar volume.

We note that our value of A_K = -(2.699 $\pm$ 0.009)$\times 10^{-29}$ $C^2m^5J^{-2}mol^{-1}$ is 11.4% larger (in magnitude) than the value of Tammer *et al.*, and 14.7% larger than the value of Ritchie *et al.* This is in accord with our hydrogen calibration, which indicated that the field integral was too high by a factor of 14.2%.

6.3.4 Results for $(CH_3)_2O$

The experimental Kerr-effect data measured for dimethyl ether over a range of temperature are now presented. For each experimental temperature a tabulation of V_m^{-1} and ${}_mK_0$ is presented, followed by a plot of ${}_mK_0$ versus V_m^{-1} from which A_K and B_K are extracted. The tabulated molar Kerr constants ${}_mK_0$ have already been adjusted for the field integral correction factor established by the H_2 calibration.

Results for $(CH_3)_2O$ at 307.18 K

T (K)	V_m^{-1} (mol m^{-3})	$10^{27}\ {}_mK_0$ (C^{2}m^{5}J^{-2}mol^{-1})
307.22	247.85	-8.912
307.22	234.45	-9.054
307.08	192.60	-9.345
307.14	169.78	-9.634
307.17	148.25	-9.811
307.27	126.14	-10.000

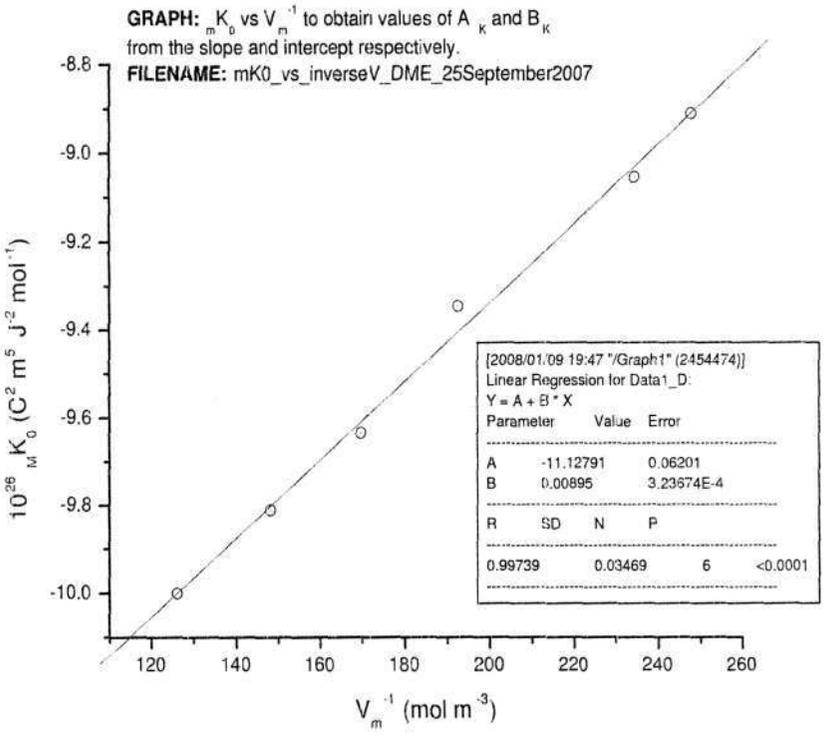

Figure 6.10: Plot of Molar Kerr constant versus inverse molar volume.

Results for $(CH_3)_2O$ at 332.71 K

T (K)	V_m^{-1} (mol m^{-3})	$10^{27}\ {}_mK_0$ ($C^2m^5J^{-2}mol^{-1}$)
332.83	427.98	-7.311
332.73	258.63	-8.271
332.84	226.31	-8.491
332.64	154.89	-8.853
332.55	117.24	-9.094
332.67	79.35	-9.357

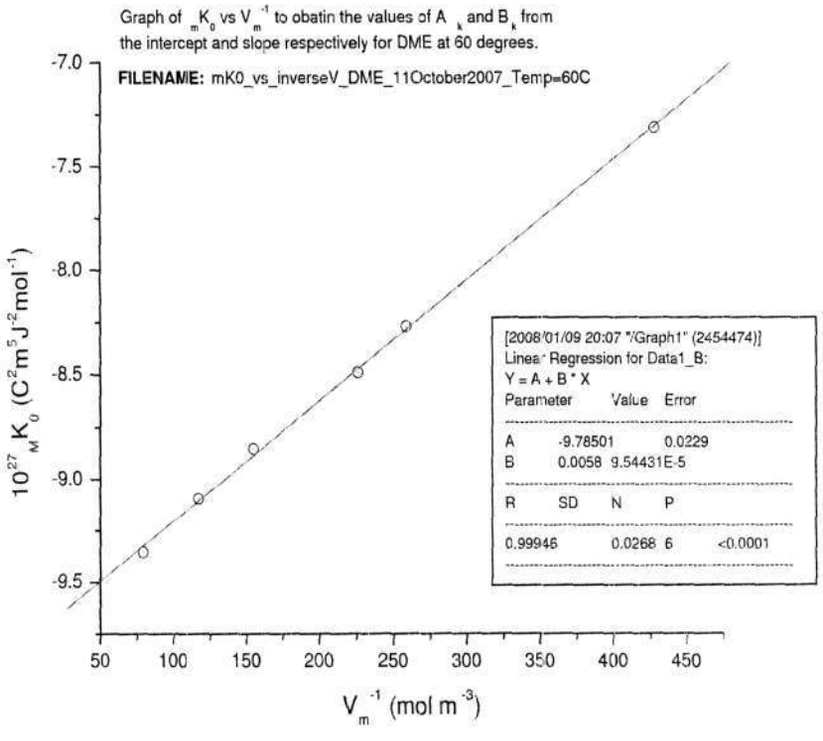

Figure 6.11: Plot of Molar Kerr constant versus inverse molar volume.

Results for $(CH_3)_2O$ at 362.34 K

T (K)	V_m^{-1} (mol m^{-3})	$10^{27}\ {}_mK_0$ ($C^2m^5J^{-2}mol^{-1}$)
362.39	315.09	-6.591
362.31	295.68	-6.688
362.32	276.43	-6.818
362.37	243.61	-6.911
362.35	206.62	-7.053
362.30	178.63	-7.176
362.35	145.05	-7.344
362.36	113.50	-7.466

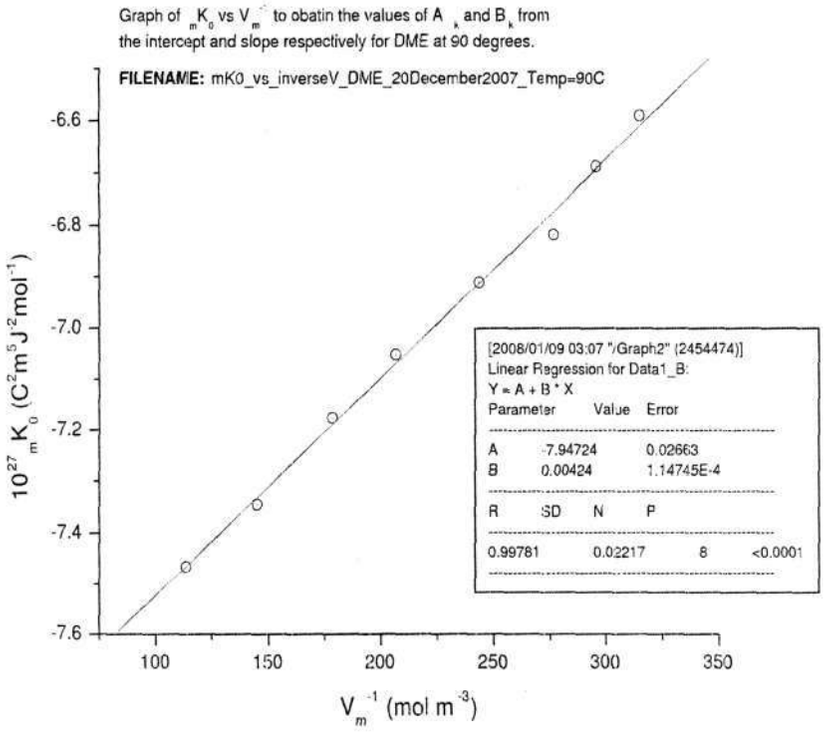

Figure 6.12: Plot of Molar Kerr constant versus inverse molar volume.

Results for $(CH_3)_2O$ at 393.01 K

T (K)	V_m^{-1} (mol m^{-3})	$10^{27}\ {}_mK_0$ ($C^2m^5J^{-2}mol^{-1}$)
393.03	441.29	-4.995
393.05	315.97	-5.456
392.99	283.14	-5.552
393.04	221.22	-5.809
392.99	183.59	-5.945
393.02	138.77	-6.082
392.98	89.26	-6.280

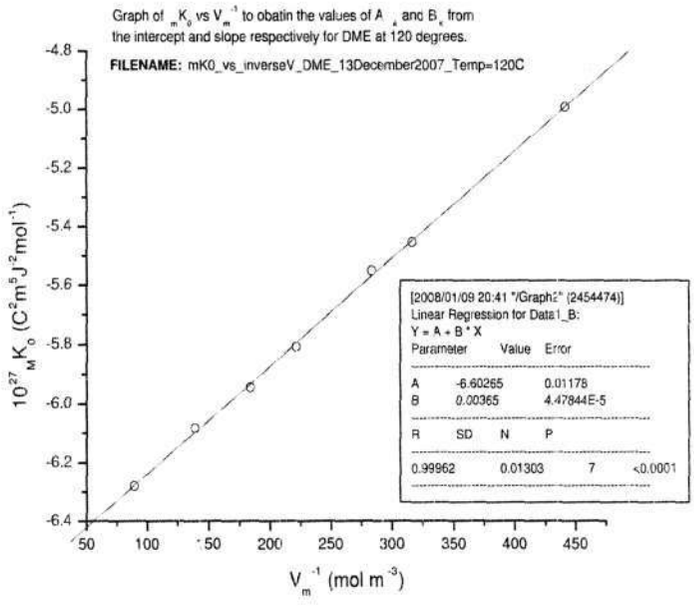

Figure 6.13: Plot of Molar Kerr constant versus inverse molar volume.

Results for $(CH_3)_2O$ at 434.89 K

T (K)	V_m^{-1} (mol m^{-3})	$10^{27}\ {}_mK_0$ (C^{2}m^{5}J^{-2}mol^{-1})
433.37	434.34	-3.996
435.03	396.34	-4.127
435.17	365.54	-4.221
435.17	333.01	-4.308
435.18	294.22	-4.429
434.95	227.43	-4.597
434.94	171.16	-4.800
434.91	126.72	-4.896
435.10	96.33	-5.029
435.05	71.25	-5.138

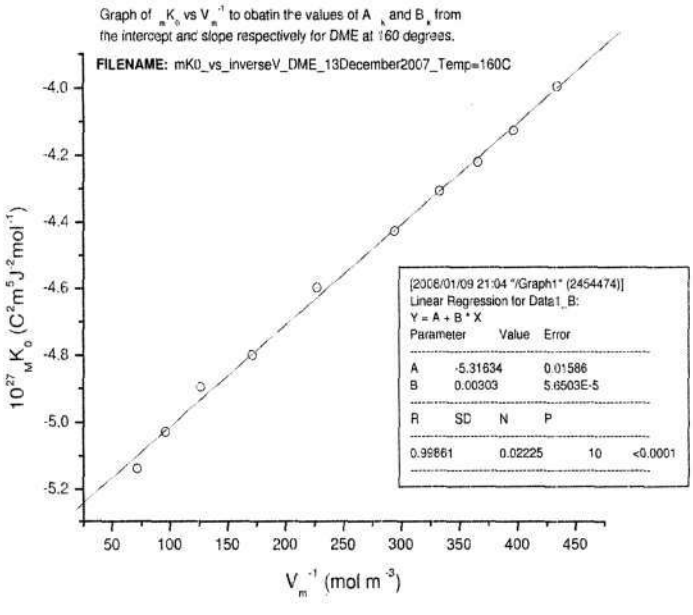

Figure 6.14: Plot of Molar Kerr constant versus inverse molar volume.

Results for $(CH_3)_2O$ at 470.06 K

T (K)	V_m^{-1} (mol m^{-3})	$10^{27}\ {}_mK_0$ ($C^2m^5J^{-2}mol^{-1}$)
470.97	518.86	-2.839
469.31	480.59	-2.922
469.26	425.22	-3.123
470.83	369.80	-3.266
469.11	311.18	-3.453
470.86	252.98	-3.623
469.38	210.67	-3.744
470.14	165.83	-3.842
470.39	130.02	-3.965
470.32	69.05	-4.161

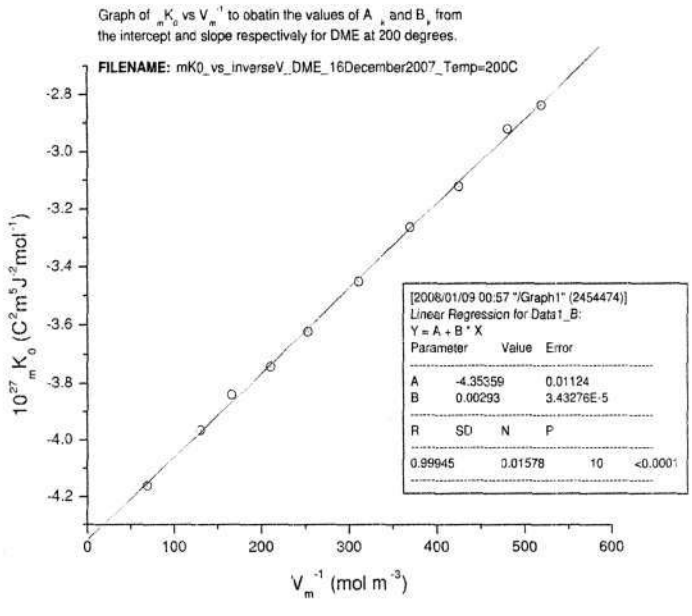

Figure 6.15: Plot of Molar Kerr constant versus inverse molar volume.

Tabulated data to be used in plotting the graph of $(A_K\text{-}\frac{N_A}{\epsilon_0}\gamma)T$ versus T^{-1} for $(CH_3)_2O$ is now given. Here, γ^K for $(CH_3)_2O$ is 0.737×10^{-60} $C^4m^4J^{-3}$.[11]

$\overline{T}$ (K)	$\overline{T^{-1}}$ (K^{-1})	10^{27} Slope ($C^2m^5J^{-2}mol^{-1}$)	10^{30} B_K ($C^2m^5J^{-2}mol^{-1}$)	10^{27} Intercept, A_K ($C^2m^5J^{-2}mol^{-1}$)	$10^{24}(A_K\text{-}\frac{N_A}{81\epsilon_0}\gamma)T$ ($C^2m^5J^{-2}mol^{-1}K$)
307.18	0.0032554	0.00895	9.95±0.36	-11.128±0.062	-3.608
332.71	0.0030056	0.00580	6.63±0.11	-9.785±0.023	-3.461
362.34	0.0027598	0.00424	4.87±0.13	-7.947±0.027	-3.104
393.01	0.0025444	0.00365	4.15±0.05	-6.603±0.012	-2.838
434.89	0.0022995	0.00303	3.40±0.06	-5.316±0.016	-2.581
470.06	0.0021274	0.00293	3.22±0.04	-4.354±0.011	-2.337

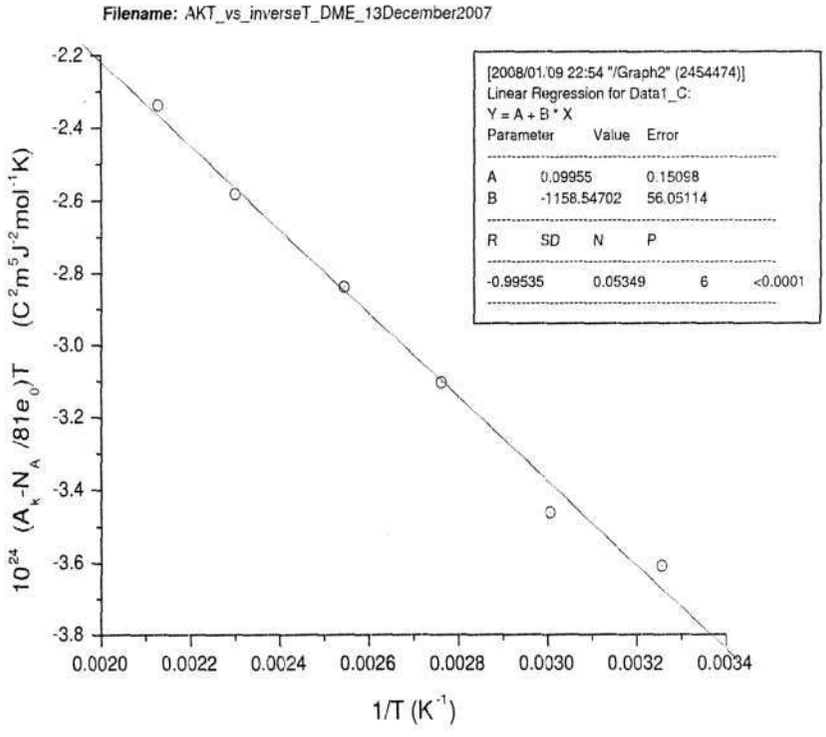

Figure 6.16: Plot of $A_k T$ versus inverse absolute temperature.

6.3.5 Results for CHF_3

The measured Kerr-effect data for trifluoromethane over a range of temperature are now presented. For each experimental temperature a tabulation of V_m^{-1} and ${}_mK_0$ is presented, followed by a plot of ${}_mK_0$ versus V_m^{-1} from which A_K and B_K are extracted. The tabulated molar Kerr constants ${}_mK_0$ have already been adjusted for the field integral correction factor established by the H_2 calibration.

Results for CHF_3 at 307.14 K

T (K)	V_m^{-1} (mol m^{-3})	$10^{27}\ {}_mK_0$ ($C^2m^5J^{-2}mol^{-1}$)
307.19	408.513	-4.893
307.13	378.644	-4.937
307.13	334.616	-5.068
307.18	289.725	-5.175
307.17	244.471	-5.319
307.12	202.596	-5.434
307.07	163.441	-5.536
307.10	122.175	-5.606

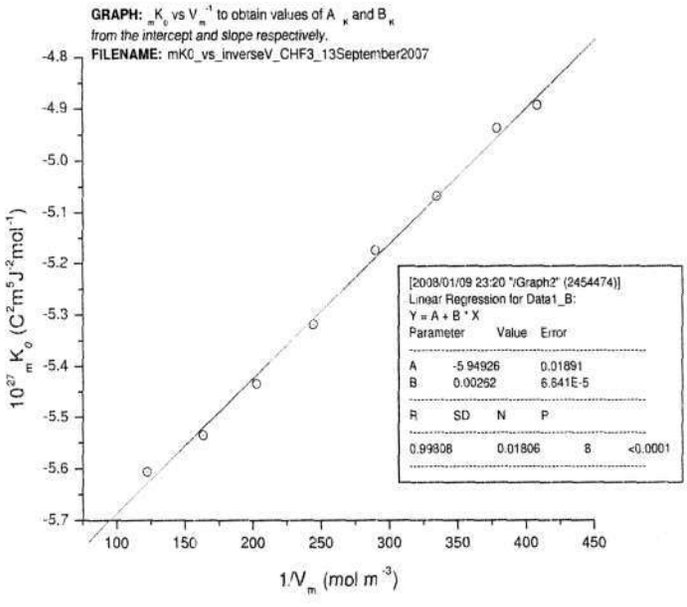

Figure 6.17: Plot of Molar Kerr constant versus inverse molar volume.

Results for CHF_3 at 362.40 K

T (K)	V_m^{-1} (mol m^{-3})	$10^{27}\ {}_mK_0$ ($C^2m^5J^{-2}mol^{-1}$)
362.44	411.343	-3.484
362.43	379.620	-3.505
362.41	349.370	-3.580
362.42	316.820	-3.625
362.39	282.345	-3.680
362.40	247.926	-3.737
362.41	211.635	-3.798
362.52	143.717	-3.892
362.22	75.714	-3.996

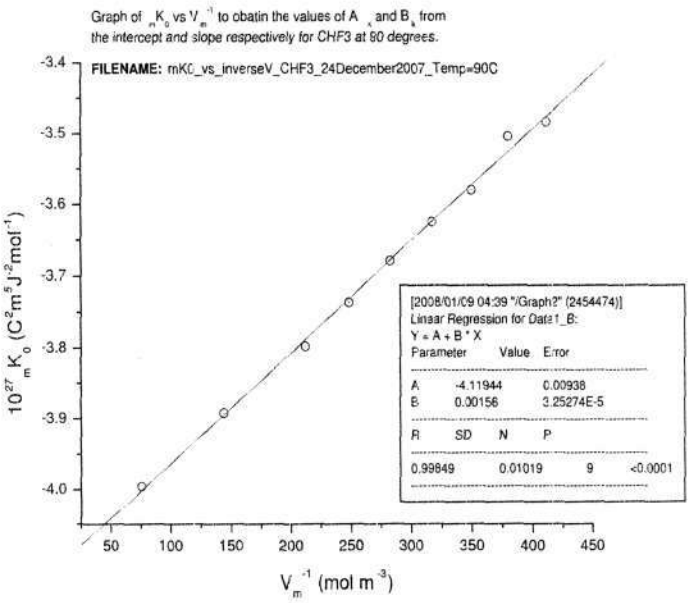

Figure 6.18: Plot of Molar Kerr constant versus inverse molar volume.

Results for CHF_3 at 391.91 K

T (K)	V_m^{-1} (mol m^{-3})	$10^{27}\ {}_mK_0$ ($C^2m^5J^{-2}mol^{-1}$)
392.00	407.051	-3.055
391.95	381.289	-3.082
391.96	348.558	-3.107
391.91	321.244	-3.128
391.87	284.501	-3.157
391.87	249.777	-3.175
391.80	220.279	-3.192

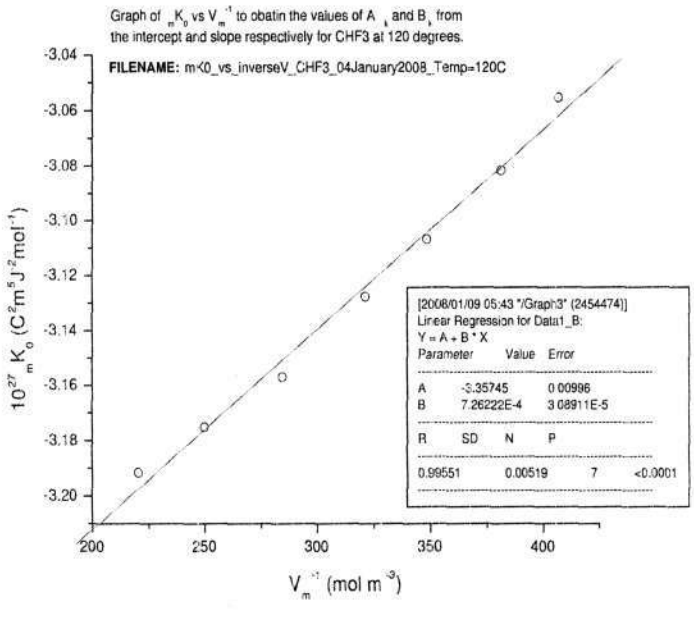

Figure 6.19: Plot of Molar Kerr constant versus inverse molar volume.

Results for CHF_3 at 430.98 K

T (K)	V_m^{-1} (mol m^{-3})	$10^{27}\ {}_mK_0$ ($C^2m^5J^{-2}mol^{-1}$)
431.05	377.361	-2.625
431.10	352.397	-2.645
430.95	324.082	-2.657
430.86	285.670	-2.674
430.94	261.954	-2.684
430.97	230.289	-2.698
430.98	205.371	-2.709

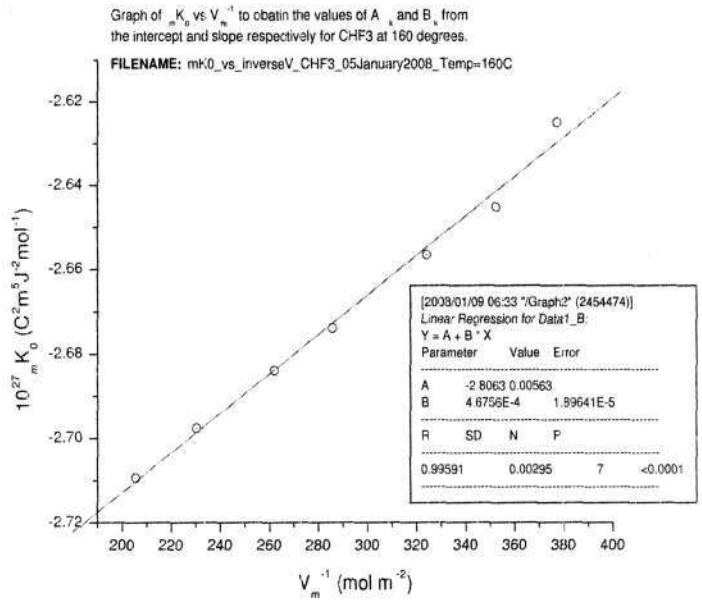

Figure 6.20: Plot of Molar Kerr constant versus inverse molar volume.

Results for CHF_3 at 465.79 K

T (K)	V_m^{-1} (mol m^{-3})	$10^{27}\ {}_mK_0$ ($C^2m^5J^{-2}mol^{-1}$)
465.70	341.322	-2.249
465.81	330.490	-2.255
465.65	324.909	-2.256
465.34	267.504	-2.266
465.70	235.914	-2.273
465.92	214.374	-2.276
466.20	194.510	-2.275
465.99	168.917	-2.285

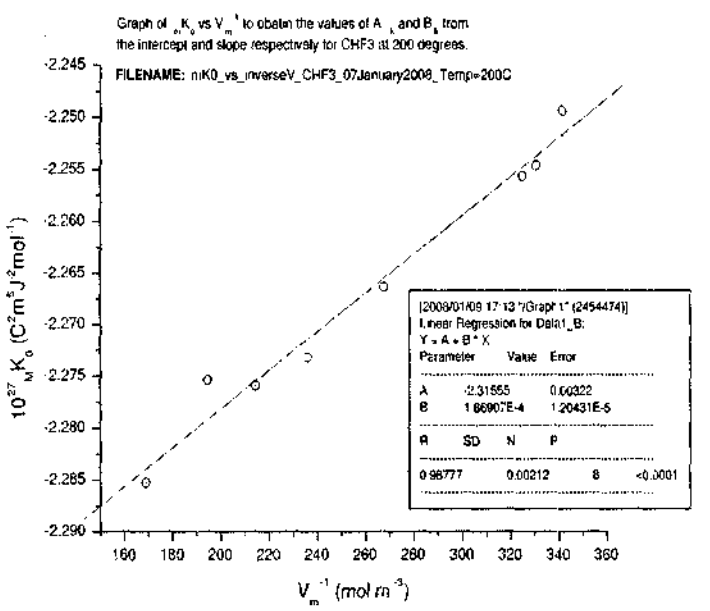

Figure 6.21: Plot of Molar Kerr constant versus inverse molar volume.

Tabulated data to be used in plotting the graph of $(A_K\text{-}\frac{N_A}{\epsilon_0}\gamma)T$ versus T^{-1} for CHF_3 is now given. Here, γ^K for CHF_3 is 0.114×10^{-60} $C^4m^4J^{-3}$.[12]

$\overline{T}$ (K)	$\overline{T^{-1}}$ (K^{-1})	10^{27} Slope ($C^2m^5J^{-2}mol^{-1}$)	10^{30} B_K ($C^2m^5J^{-2}mol^{-1}$)	10^{27} Intercept, A_K ($C^2m^5J^{-2}mol^{-1}$)	$10^{24}(A_K\text{-}\frac{N_A}{81\epsilon_0}\gamma)T$ ($C^2m^5J^{-2}mol^{-1}K$)
307.14	0.0032559	0.00262	3.35±0.08	-5.949±0.019	-1.857
362.40	0.0027594	0.00156	1.99±0.04	-4.119±0.009	-1.528
391.91	0.0025516	0.000726	1.06±0.05	-3.357±0.010	-1.353
430.98	0.0023203	0.000468	0.72±0.03	-2.806±0.006	-1.251
465.79	0.0021469	0.000187	0.38±0.03	-2.316±0.003	-1.123

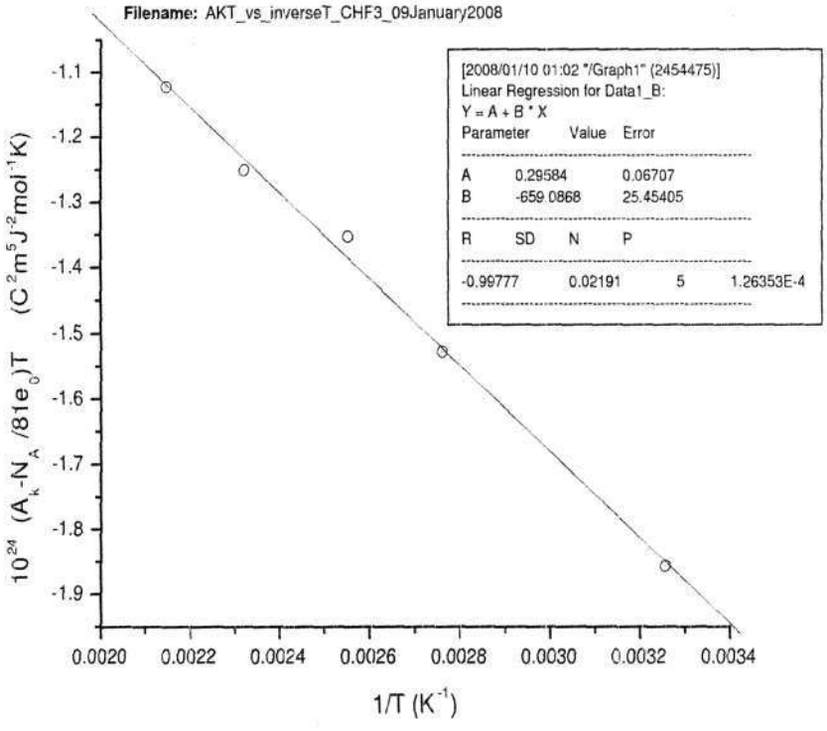

Figure 6.22: Plot of $A_K T$ versus inverse asolute temperature.

6.4 Graphical Analysis of the Results

The first and second virial coefficients have been extracted from the intercepts and slopes of the $(CH_3)_2O$ and CHF_3 graphs using equation 5.10, which we reproduce here.

$$ {}_mK_0 = A_K + [B_K + A_K(2A_\epsilon + \frac{1}{2}A_R)]V_m^{-1}. \tag{6.7} $$

The A_K values extracted from the intercepts can be used to obtain the polarizability anisotropy and hyperpolarizability of the two molecules. This is

are compared with those of other experimentalists, as well as with values computed using the molecular-tensor theory developed in Chapter 4, in the following graphs.

Graph of the temperature dependence of B_K for $(CH_3)_2O$. The solid curve gives B_K calculated for $R_0 = 0.47$ nm, $\epsilon/k = 290.0$ K, D_1 = -0.04926 and D_2 = 0.29666; while for comparative purposes, the dashed curve is for the parameter set $R_0 = 0.48$ nm, $\epsilon/k = 300.0$ K, D_1 = -0.04443 and $D_2 = 0.29760$.[7] Experimental points are represented by circles (this work) and diamonds.[7] There is good agreement between experiment and theory over the entire temperature range.

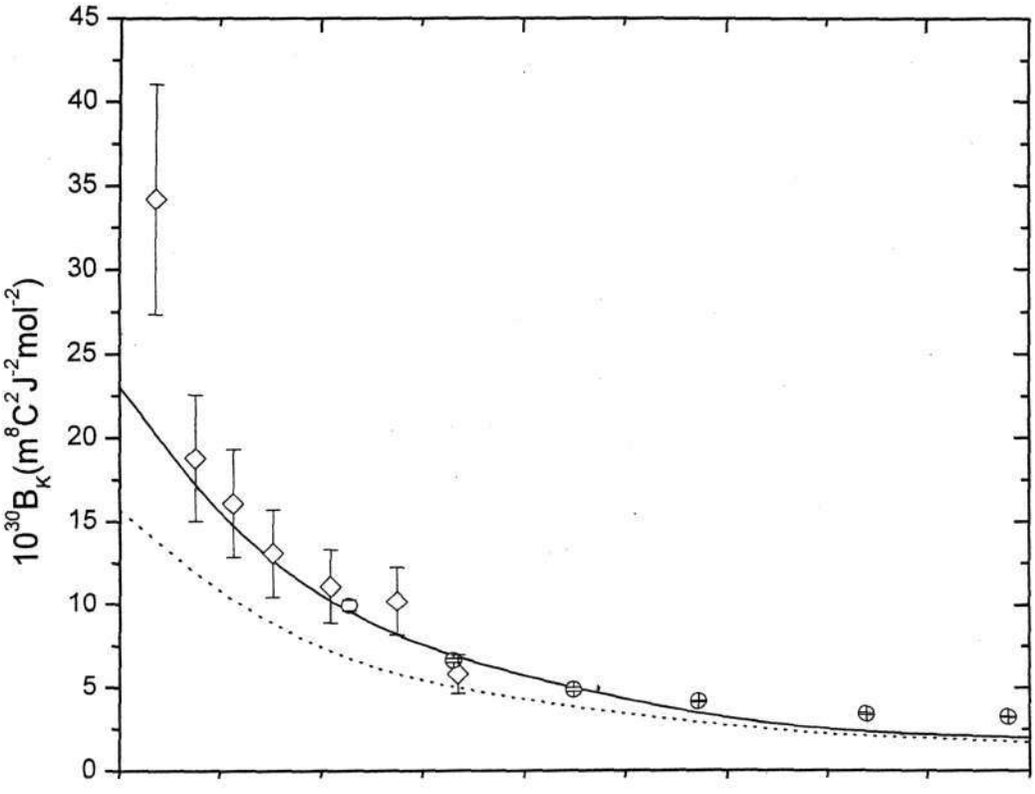

Graph of the temperature dependence of B_K for CHF_3. The solid curve gives B_K calculated for R_0 = 0.440 nm, ϵ/k = 178.5 K and D = -0.050.[4] Experimental points are represented by circles (this work) and diamonds.[7] There is reasonable agreement between experiment and theory over higher temperatures, with the lower temperature values being somewhat discrepant. Note the greatly improved precision of our measured B_K values over the earlier measurements.

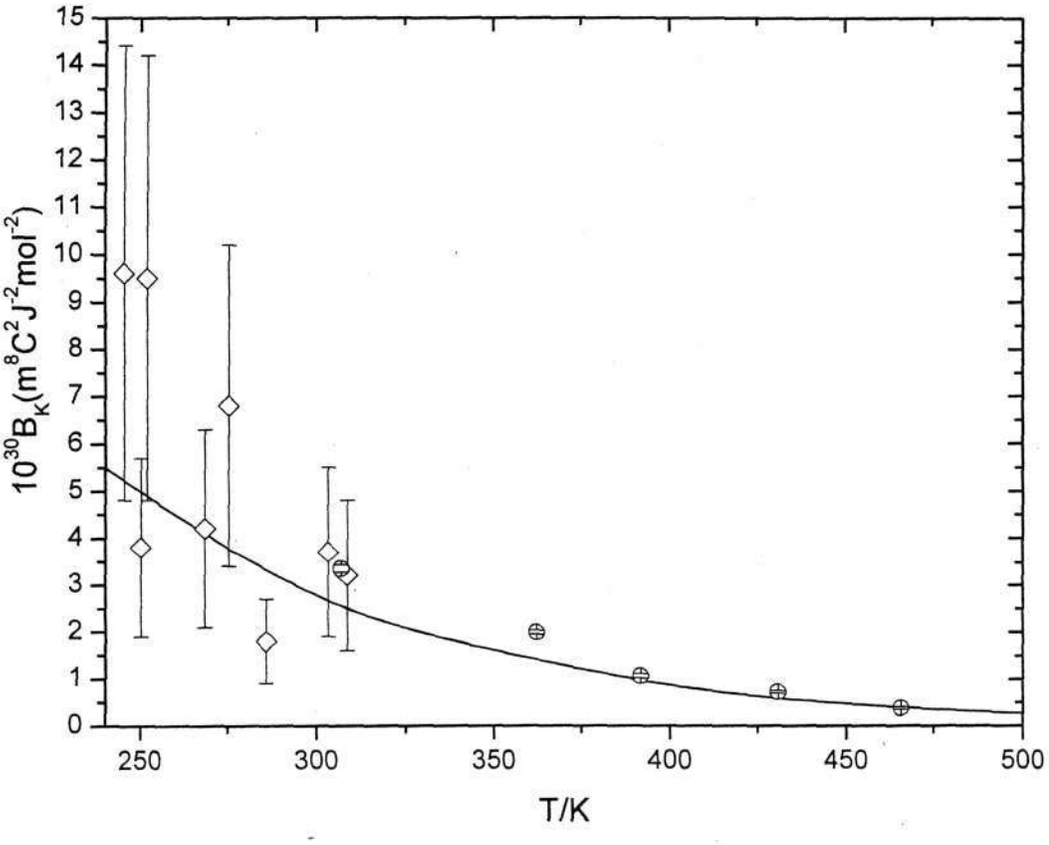

6.5 Conclusion

This investigation of the Kerr effect in dimethyl ether and trifluoromethane has yielded precise new values of the polarizability anisotropy, as well as estimates of the first Kerr hyperpolarizability, for these molecules. In addition, precise second Kerr-effect virial coefficients have been obtained, and compare favourably with values computed using a molecular-tensor theory of the second Kerr-effect virial coefficient B_K.

6.6 References

1. Landolt-Bornstein, Inorganic Compounds, Ammonia
2. G. L. D. Ritchie and E. W. Blanch, *J. Phys. Chem. A*, 2003, **107**, 2096.
3. G. H. F. Diercksen and A. J. Sadlej, *Molecular Physics*, 1986, **57**, 518.
4. V. W. Couling, PhD thesis, University of Natal, 1994.
5. A. D, Buckingham, *Proc. Phys. Soc. A*, 1955, **68**, 910.
6. R. Tammer and W. Huttner, *Chem. Phys.*, 1990, textbf146, 155.
7. R. Tammer, K. Loblein, K. H. Peting and W. Huttner, *Chem. Phys.*, 1992, textbf168, 151.
8. T. J. Sono, MSc thesis, University of Natal, 2003.
9. A. Singh, MSc thesis, University of KwaZulu-Natal, 2005.
10. I. R. Gentle, D. R. Laver and G. L. D. Ritchie, *J. Phys. Chem.*, 1989, textbf93, 3035.
11. V. W. Couling and D. P. Shelton, unpublished work.
12. A. D. Buckingham and B. J. Orr, *Trans. Farad. Soc.*, 1969, **65**, 673.
13. M. P. Bogaard, A. D. Buckingham and G. L. D. Ritchie, *J. Chem. Soc., Faraday Trans. 2*, 1981, **77**, 1550.